Circuits and Systems
Mekelweg 4,
2628 CD Delft
The Netherlands
http://ens.ewi.tudelft.nl/

CAS-2018-10

M.Sc. Thesis

Frequency selection for indoor ranging using compressive sensing

Jinzi Qi

Abstract

Nowadays, indoor ranging and localization have become necessary in daily life. Due to the multi-path propagation and noise in the indoor environment, phase domain ranging method using multi-frequency has been proposed which achieves accurate estimation of indoor target. However, as the indoor communication is usually carried on Bluetooth Low Energy (BLE) or Zigbee, high efficiency is indispensable in the face of limited bandwidth and measuring time. Thus, in this thesis, we aim to reduce the number of frequencies used in the ranging while keeping an acceptable estimation accuracy. We at first build the signal model and study the ambiguity range of the problem. Then based on the estimation theory and the concept of compressive sensing (CS) theory, we take the Cramer Rao Lower Bound (CRLB) and the matrix coherence as the criteria and select the optimal subset on given tone set. To test the performance of selected subset, we utilize gridless reconstruction algorithms, noiseless global matched filter (NL-GMF) and atomic norm minimization (ANM), to estimate target distance with the subset in both simulated data and real data and provide the mean square error (MSE), the estimation probability and the successful estimation probability in various estimation conditions.

Frequency selection for indoor ranging using compressive sensing

Thesis

submitted in partial fulfillment of the
requirements for the degree of

Master of Science

in

Computer Engineering

by

Jinzi Qi
born in Henan, China

This work was performed in:

Circuits and Systems Group
Department of Microelectronics & Computer Engineering
Faculty of Electrical Engineering, Mathematics and Computer Science
Delft University of Technology

Delft University of Technology

Copyright © 2018 Circuits and Systems Group
All rights reserved.

Delft University of Technology
Department of
Microelectronics & Computer Engineering

The undersigned hereby certify that they have read and recommend to the Faculty of Electrical Engineering, Mathematics and Computer Science for acceptance a thesis entitled **"Frequency selection for indoor ranging using compressive sensing"** by **Jinzi Qi** in partial fulfillment of the requirements for the degree of **Master of Science**.

Dated: October 18, 2018

Chairman: _____
prof.dr.ir. Geert Leus

Advisor: _____
prof.dr.ir. Jac Romme

Committee Members: _____
dr. Furak Uysal

_____

Abstract

Nowadays, indoor ranging and localization have become necessary in daily life. Due to the multi-path propagation and noise in the indoor environment, phase domain ranging method using multi-frequency has been proposed which achieves accurate estimation of indoor target. However, as the indoor communication is usually carried on Bluetooth Low Energy (BLE) or Zigbee, high efficiency is indispensable in the face of limited bandwidth and measuring time. Thus, in this thesis, we aim to reduce the number of frequencies used in the ranging while keeping an acceptable estimation accuracy. We at first build the signal model and study the ambiguity range of the problem. Then based on the estimation theory and the concept of compressive sensing (CS) theory, we take the Cramer Rao Lower Bound (CRLB) and the matrix coherence as the criteria and select the optimal subset on given tone set. To test the performance of selected subset, we utilize gridless reconstruction algorithms, noiseless global matched filter (NL-GMF) and atomic norm minimization (ANM), to estimate target distance with the subset in both simulated data and real data and provide the mean square error (MSE), the estimation probability and the successful estimation probability in various estimation conditions.

Acknowledgments

First of all, I would like to thank my supervisor prof. dr. ir. Geert Leus and dr. ir. Jac Romme for their assistance, advice and patience. This thesis would not be possible without their guidance.

Also I am highly indebted to all professors in EEMCS, from whose enlightening lectures I have benefited a lot.

Special thanks to all my friends who have accompanied me, helped me and made my life in Delft full of sunshine.

Finally, I would like to thank my parents and my partner for their continuous support and encouragement all through these years.

Jinzi Qi
Delft, The Netherlands
October 18, 2018

Contents

List of Figures

List of Tables

List of Algorithms

1 Introduction

The informatization and intelligentization of the industry requires the development of the Internet of Things (IoT). As a key technique of the IoT, ranging and localization becomes an increasingly important research field in recent years. In terms of the measurement range, the ranging and localization systems can be classified into the indoor ones and the outdoor ones.

Indeed, the use of the satellites has greatly improved the performance of the outdoor localization systems, so that the outdoor localization can work on a global scale with a deviation of only a few meters, such as the global navigation satellite systems (GNSS). In the GNSS systems, the receiver receives the signals broadcast from the satellites and calculates the location of the receiver based on these signals. Currently, the receivers are not expensive that they can be widely used.

However, in the indoor situation, ranging quality such as high efficiency, low cost and good accuracy are required[2]. Due to the request of low cost, the indoor communication process is usually achieved by means of Bluetooth Low Energy (BLE)[3] or Zigbee[4] in Industrial Scientific Medical band (ISM band) which makes the available bandwidth limited. And within a building, the multi-path propagation should also be considered because of the reflection of transmitted signals against walls[5][6]. Due to these characteristics of indoor ranging, the system GNSS for outdoor localization is not suitable anymore.

Thus, instead of GNSS, the wireless sensor network (WSN)[7] are always used for indoor localization which enables high accuracy at low cost. In the WSN, the location is estimated by measuring the distance between the target and each anchor, where the anchor represents a network node with known location. The distance measurements are mainly carried out in three domains, the time domain, the power domain and the phase domain. In the time domain, the distance can be estimated by measuring the time of flight (ToF) or the time difference of arrival (TDoA). Using the time information, Ultra Wide Band (UWB) can achieve high accuracy in ranging[8][9] but the Non line of sight paths will cause great impact on the estimation result[10]. Chirped spread spectrum(CSS) can also be used in the estimation and it utilizes the ISM band[11]. But to achieve a good accuracy it has to occupy the whole ISM band which may cause conflict with other methods. Except the time information, power information of the received signal can also be used in the distance measurement because the power of the received signal strength(RSS) decreases with increasing distance. Received signal strength indicator(RSSI) are often used in the ranging of power domain[12][13] but the measurement of RSSI is sensitive to the multi-path propagation in the indoor situation[14].

Consequently, although the indoor ranging can be achieved by methods measuring ToF or RSS as shown in the above, the estimation may not be accurate enough due to multi-path propagation or band limit. To achieve good accuracy in limited bandwidth

and in multi-path propagation situation, in 2012, a method which uses signal phase information with multiple frequencies is implemented[1][15]. The ranging procedure is presented in the figure 1.1. As shown, to obtain the distance between device A and device B, the carrier signal is sent after each other in multiple tones from device A. The two devices have their own clock references which are not synchronized. So the device B needs to send the received carrier signal back to correct the error caused by the clocks. Then the device A receives the signal which contains phase difference information and is able to calculate the distance between two devices.

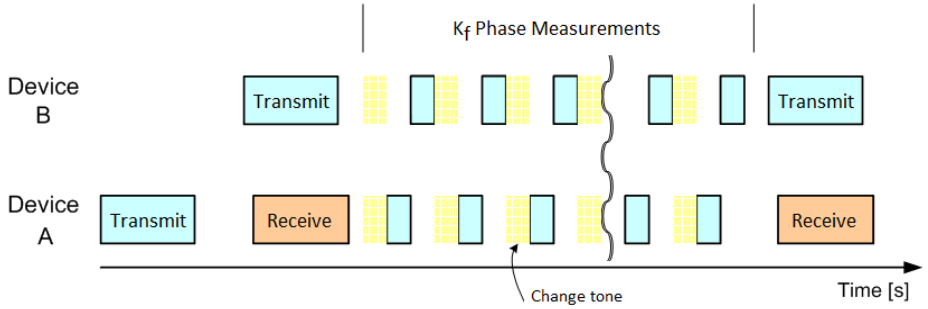

Figure 1.1: Sketch of multiple frequency ranging procedure.[1]

The carrier signal used here is a pure sinusoidal tone which is unmodulated and has constant envelope, so the impact of the radio channel on the carrier signal for one tone f and a free space connection can be expressed by:

$$h(f, r) = a(r)e^{-j2\pi fr/c} \tag{1.1}$$

where f is the radio channel frequency, r is the distance between devices, c is the propagation velocity and $a(r)$ is the absolute amplitude of the signal which also contains distance information. The device A receives K_f measurements of the channel impact thus the equation (1.1) can be extended into case of multiple tones $f_0, f_1, ..., f_{K_f-1}$ where K_f is the number of tones used in the ranging procedure:

$$\begin{bmatrix} h(f_0, r) \\ h(f_1, r) \\ \vdots \\ h(f_{K_f-1}, r) \end{bmatrix} = a(r) \begin{bmatrix} 1 \\ z(\tau) \\ z(\tau)^2 \\ \vdots \\ z(\tau)^{K_f-1} \end{bmatrix} = a(r)\mathbf{z}_{K_f}(\tau) \tag{1.2}$$

In the equation (1.2), $z(\tau) = e^{-j2\pi\Delta f\tau}$ and its phase slope contains information of the distance, $\tau = \frac{r}{c}$, Δf is the frequency step size between tones, $f_n = n\Delta f$, $n = 0, 1, ..., K_f - 1$.

In addition, the indoor scenario contains multi-path propagation which means the carrier signal received by the device A is not only from the line-of-sight (LOS) direction but also from the non-line-of-sight (NLOS) directions. If we represent those distances between two devices in multi-path case by $\mathbf{r}_N = [r_0, r_1, ..., r_{N-1}]$ where we assume

$r_0 < r_n$, $n = 1, 2, ..., N-1$, r_0 will be in LOS and the others are in NLOS. Then the final received carrier signal can be obtained by extending equation (1.2):

$$\begin{aligned}\begin{bmatrix} h(f_0, \boldsymbol{r}_N) \\ h(f_1, \boldsymbol{r}_N) \\ \vdots \\ h(f_{K_f-1}, \boldsymbol{r}_N) \end{bmatrix} &= \begin{bmatrix} 1 & 1 & \cdots & 1 \\ z(\tau_0) & z(\tau_1) & \cdots & z(\tau_{N-1}) \\ z(\tau_0)^2 & z(\tau_1)^2 & \cdots & z(\tau_{N-1})^2 \\ \vdots & \vdots & \ddots & \vdots \\ z(\tau_0)^{K_f-1} & z(\tau_1)^{K_f-1} & \cdots & z(\tau_{N-1})^{K_f-1} \end{bmatrix} \begin{bmatrix} a(r_0) \\ a(r_1) \\ \vdots \\ a(r_{N-1}) \end{bmatrix} \\ &= \begin{bmatrix} \mathbf{z}_{K_f}(\tau_0) & \mathbf{z}_{K_f}(\tau_1) & \cdots & \mathbf{z}_{K_f}(\tau_{N-1}) \end{bmatrix} \mathbf{a}(\mathbf{r}_N) \end{aligned} \tag{1.3}$$

where r_n and τ_n are the distance and time delay between two devices in the n-th path, $\tau_n = \frac{r_n}{c}$, $\mathbf{r}_N = [r_0, r_1, ..., r_{N-1}]$, $\boldsymbol{\tau}_N = [\tau_0, \tau_1, ..., \tau_{N-1}]$, $z(\tau_n) = e^{-j2\pi\Delta f \tau_n}$, $n = 0, ..., N-1$. N is the number of paths in the indoor condition. In a noisy environment, the signal model can also be written as:

$$\mathbf{h}_{K_f} = \begin{bmatrix} \mathbf{z}_{K_f}(\tau_0) & \mathbf{z}_{K_f}(\tau_1) & \cdots & \mathbf{z}_{K_f}(\tau_{N-1}) \end{bmatrix} \mathbf{a}(\mathbf{r}_N) + \mathbf{n} = \mathbf{Z}_{K_f}\mathbf{a}(\mathbf{r}_N) + \mathbf{n} \tag{1.4}$$

where $\mathbf{n}$ is the environment noise. For simplicity, we regard the noise $\mathbf{n}$ as white Gaussian noise and present its intensity by variance σ^2. The signal-to-noise ratio (SNR) is calculated by $SNR = \frac{E_s}{\sigma^2}$ where E_s is the carrier signal power in each path. Then generally, in this multi-path condition, each element in the final received signal vector is the superposition of all the multi-path components according to the equation (1.3). And each ray is assumed to have a constant magnitude for the frequency band of interest. The line of sight (LOS) component always has the smallest delay and, in general, the largest amplitude.

The ranging method utilized phase information with multiple frequencies has good accuracy and low cost and is easy to implement[15]. However, the bandwidth is limited and if we use small Δf, there will be many tones used to communicate. Since the carrier signal is sent and measured sequentially by device A, this will be a long procedure which is against the requirement of high efficiency. Thus, to save time, we would like to reduce the number of tones used while keeping estimation accuracy available. To be clear, we explain our scheme in the model. As introduced, in the original method, K_f tones are selected uniformly on the given bandwidth from f_0 to f_{K_f-1} and are used to measure. Then the unique index set of tones can be expressed by $C_{K_f} = [0, 1, \cdots, K_f - 1]$ and is called full set in our report. If we reduce the number of tones used, only M tones in C_{K_f} are employed for example, we need to select a subset of C_{K_f} with M elements, which can be expressed by $M \ll K_f$, $C_M \subset C_{K_f}$. Then the whole ranging and localization process will be improved in both efficiency and cost. But the subset of C_{K_f} with M elements is not unique. How to decide the number M, how to choose the optimal subset C_M among all subsets of C_{K_f} with M elements and what evaluation criterion of the selection we should use are the topics to study in the thesis. Mathematically, the goal

of our study can be formulated as an optimization problem:

$$\begin{aligned} &\min\ M \\ &\text{s.t. } G(C_M) \leq G_{Tr} \\ &\text{given } G(C_{K_f}) < G_{Tr} \end{aligned} \tag{1.5}$$

where $G(\cdot)$ is the evaluation function of subset, $G(C_{K_f})$ is the evaluation of full set C_{K_f} and G_{Tr} is the evaluation threshold. With various evaluation criterion, the function $G(\cdot)$ and its threshold can be different.

In this report, the equation (1.5) can be solved in two ways. From the perspective of estimation theory, we would like to reduce the estimation error in the ranging procedure and the criterion Cramer-Rao Lower Bound (CRLB) can indicate variance of estimation error in a specific model. CRLB is the easiest criterion to determine in estimation and is high relative to the data model[16]. In our case, the data model depends on the tone selection C_M. Thus we can use this characteristic of CRLB to select the optimal selection which has the minimal number of elements and meets the desired CRLB. The optimal subset C_M is searched by a greedy algorithm with certain CRLB threshold, $G_{CRLB-Tr}$ and the CRLB of subset C_M is presented by evaluation function $G_{CRLB}(C_M)$ in our report.

Apart from the viewpoint of estimation theory, the accuracy of the distance information extraction from fewer measurements should also be considered. To make sure the estimation result is exact enough for practical use, the compressive sensing (CS) method[17] [18] is used in the tone selection process. The selection can be regarded as the construction of dictionary matrix which is an essential point in reconstruction procedure and low coherence among matrix columns is required to guarantee the reconstruction accuracy. Therefore, the matrix coherence can be chosen as a criterion in subset selection and is written as $G_{Co}(\cdot)$. Because CRLB and coherence are two different criteria and have their own calculation method, there will be a new threshold for the criterion coherence which is written as G_{Co-Tr}. And for different criteria, the optimal subset selected will also be different theoretically.

To test the reliability of these selected subsets, we use them in estimation procedure and use CS reconstruction algorithms to do the estimation in different conditions. The classical CS reconstruction approach used to solve linear atom decomposition problem with finite atom candidates, where the atoms are the columns in the dictionary matrix. By decomposing the received signal with these atoms linearly, we are able to get a amplitude vector which is the signal we would like to recover. If the received signal can not be decomposed by these finite atoms, the error would be caused which is also called atom grid[19]. The first algorithm to solve the grid problem is presented in [20] and several more useful algorithms are proposed since 2011[21][22]. In this study, the gridless reconstruction algorithms used to test subset performance are noiseless global matched filter (NL-GMF) [19] and atomic norm minimization (ANM) [23].

The thesis is organized as follows; Chapter 2 provides the Distance information extraction process with full tones and influence of parameters; Chapter 3 and Chapter 4 propose the criteria, CRLB and matrix coherence, respectively to solve the tone selection problem and simulation results and comparison are provided as well; in Chapter

5, the selected optimal tone subsets based on different criteria are tested and compared by CS gridless reconstruction algorithms with both simulated data and real data. The conclusions of the study are provided in the Chapter 6.

Distance information extraction with MUSIC algorithm

2

To extract the distance information accurately in the multi-path environment, multiple tones are used as the communication channel and estimation algorithm is applied to deal with the measurements. The most frequently used estimation algorithm is MUltiple SIgnal Characterization (MUSIC) algorithm[24]. In this section, MUSIC algorithm is introduced and applied in full tone measurements which can be regarded as a comparison with the follow-up study. And some critical parameters in the estimation process are studied to determine the ambiguity range.

2.1 MUSIC algorithm

The MUSIC algorithm is one of the most used algorithms to determine unknown parameters based on measurements received at antenna array. It is an unbiased estimator and can asymptotically estimate the number of received signals, the direction of arrival, the noise strength and so on[24]. In our case, we use the MUSIC algorithm to extract the delay information in received measurements. To introduce the MUSIC algorithm, we at first provide the covariance matrix $\mathbf{S}$ of our received vector $\mathbf{h}_{K_f}$ in full set tones:

$$\mathbf{S} = E\{\mathbf{h}_{K_f}\mathbf{h}_{K_f}^H\} = E\{\mathbf{Z}_{K_f}\mathbf{a}(\mathbf{r}_N)\mathbf{a}^H(\mathbf{r}_N)\mathbf{Z}_{K_f}^H\} + E\{\mathbf{n}\mathbf{n}^H\} \tag{2.1}$$

We assume that the incident signals and the white Gaussian noise are uncorrelated and the noise has zero mean. Because $\mathbf{Z}_{K_f}$ is deterministic, the above equation can be written by:

$$\mathbf{S} = \mathbf{Z}_{K_f}E\{\mathbf{a}(\mathbf{r}_N)\mathbf{a}^H(\mathbf{r}_N)\}\mathbf{Z}_{K_f}^H + E\{\mathbf{n}\mathbf{n}^H\} = \mathbf{Z}_{K_f}\mathbf{P}\mathbf{Z}_{K_f}^H + \sigma^2\mathbf{I} \tag{2.2}$$

where $P = E\{\mathbf{a}(\mathbf{r}_N)\mathbf{a}^H(\mathbf{r}_N)\}$, σ^2 is the covariance of the noise signal, $\mathbf{I}$ is the $K_f \times K_f$ unit matrix. The eigenvalues λ_i and eigenvectors $\mathbf{v}_i$ of $\mathbf{S}$ can be expressed by:

$$\mathbf{S}\mathbf{v}_i = \lambda_i\mathbf{v}_i, \text{for} \quad i = 1, 2, ..., K_f \tag{2.3}$$

where the eigenvalue is ranked by their values, λ_1 is the largest eigenvalue and $\mathbf{v}_1$ is the eigenvector corresponding to λ_1. Then there is:

$$\mathbf{Z}_{K_f}\mathbf{P}\mathbf{Z}_{K_f}^H\mathbf{v}_i = \lambda_i\mathbf{v}_i - \sigma^2\mathbf{I}\mathbf{v}_i = (\lambda_i - \sigma^2)\mathbf{v}_i, \text{for} \quad i = 1, 2, ..., K_f \tag{2.4}$$

In classical MUSIC algorithm, the rank of $\mathbf{P}$ is equal to the number of incident signals N and there exists $\lambda_i = \sigma^2$ for $i = 1, 2, ..., N$ which makes $\mathbf{Z}_{K_f}\mathbf{P}\mathbf{Z}_{K_f}^H\mathbf{v}_i = 0$ or $\mathbf{Z}_{K_f}^H\mathbf{v}_i = 0$. Then the eigenvectors $\mathbf{v}_i$ for $i = 1, 2, ..., N$ are orthogonal to the space spanned by the columns of matrix $\mathbf{Z}_{K_f}$ and these N dimensional subspace spanned

by the incident signal is called signal subspace and the $K_f - N$ dimensional subspace spanned by the noise vector is called noise subspace or null-subspace.

However, in our case, $\mathbf{h}_{K_f}$ is a vector and each element of it is a linear combination of all the multi-path components. Although we have signals from multiple paths, we only have one snapshot of the measurement and the rank of $\mathbf{Z}_{K_f}\mathbf{a}(\mathbf{r}_N)\mathbf{a}^H(\mathbf{r}_N)\mathbf{Z}_{K_f}^H$ is always 1, given equation (2.1). With unknown number of paths, i.e. N is unknown, we are not able to estimation the target distance through classical MUSIC algorithm.

To solve this problem, we reformulate the single snapshot model to multiple measurements model by forming a Hankel matrix based on the approach in [25]:

$$\mathbf{H}_{K_f} = \begin{bmatrix} h(f_0, \boldsymbol{r}_N) & h(f_1, \boldsymbol{r}_N) & \cdots & h(f_L, \boldsymbol{r}_N) \\ h(f_1, \mathbf{r}_N) & h(f_2, \boldsymbol{r}_N) & \cdots & h(f_{L+1}, \boldsymbol{r}_N) \\ \vdots & \vdots & \ddots & \vdots \\ h(f_{K_f-L-1}, \boldsymbol{r}_N) & h(f_{K_f-L}, \boldsymbol{r}_N) & \cdots & h(f_{K_f-1}, \boldsymbol{r}_N) \end{bmatrix} \tag{2.5}$$

where $L \approx K_f/3$. Then covariance matrix of $\mathbf{H}_{K_f}$ is $\hat{\mathbf{S}}$ of size $(K_f - L) \times (K_f - L)$. When the signal $\mathbf{h}_{K_f}$ is noiseless i.e. σ is 0, the rank of $\hat{\mathbf{S}}$ will be N. The so-called null-subspace $\hat{\mathbf{V}}_n$ will be formed by $(K_f - L - N)$ eigenvectors $\mathbf{v}_i$, $i = N, N+1, ..., (K_f - L - 1)$ and the size of $\hat{\mathbf{V}}_n$ is $(K_f - L) \times (K_f - L - N)$.

By calculating the MUSIC cost function of a series of time delay τ:

$$J_{MUSIC}(\tau) = \frac{\mathbf{z}_{K_f}^H(\tau)\mathbf{z}_{K_f}(\tau)}{\mathbf{z}_{K_f}^H(\tau)\hat{\mathbf{V}}_n\hat{\mathbf{V}}_n^H\mathbf{z}_{K_f}(\tau)} \tag{2.6}$$

where $\mathbf{z}_{K_f}(\tau)$ is a steering vector of delay τ, we can obtain the relationship between cost function value and delay τ which is called inverse pseudo spectrum.

In the inverse pseudo spectrum, the orthogonality between null-subspace and steering vector at each τ value is shown. Higher cost function value shows that the steering vector is more orthogonal with the null-subspace and vice versa. The corresponding delays of peaks in the inverse pseudo spectrum represent the delays in each path. The peak corresponding to the minimum delay is in the LOS direction and is the one we need. Then the indoor ranging will be achieved by calculate the distance with the minimum delay.

However, in practice, it is not easy for us to know the number of paths, i.e. N. So we will use the latter half of the eigenvalues to construct the null-subspace. And the whole procedure of the MUSIC algorithm is provided in the algorithm 1.

2.2 Simulation results

In this section, we will do simulations on the MUSIC algorithm and study the impact of some critical parameters. The ambiguity range of the model will also be calculated. As the parameters in the model is complex, we will start with simple case using normalized Bandwidth.

Algorithm 1 MUSIC algorithm

Input: Step size and range of steering vector $\mathbf{z}_{K_f}(\tau)$, frequency step size Δf, tone set C_{K_f}, received signal $\mathbf{h}_{K_f}$, L

Output: Estimated time delay τ_0

1: Construct the Hankel matrix $\mathbf{H}_{K_f}$ by $\mathbf{h}_{K_f}$ and calculate its covariance matrix $\hat{\mathbf{S}}$.
2: Calculate the eigenvectors $\mathbf{v}_i$ of the covariance matrix for $i = 1, 2, ..., K_f - L$. Construct the null-subspace matrix $\hat{\mathbf{V}}_n$ by $\lfloor \frac{K_f - L}{2} \rfloor$ eigenvectors $\mathbf{v}_i$, $i = \lfloor \frac{K_f - L}{2} \rfloor + 1, \lfloor \frac{K_f - L}{2} \rfloor + 2, ..., K_f - L$.
3: Calculate the cost function $J_{MUSIC}(\tau)$ and find the maximum in the inverse pseudo spectrum $J_{MUSIC-max}$.
4: Choose peaks with magnitude larger than $0.6 \times J_{MUSIC-max}$ as the candidates. Select the candidate with the smallest delay as the final result and output the delay which is τ_0

2.2.1 Normalized frequency

To make the study simple, normalized frequency is used in the preliminary simulation. The available bandwidth in our case is $80MHz$ and by doing Min-Max Normalization[26], the frequency $80MHz$ is transformed into unit 1 and the frequency step size becomes a number between 0 and 1, i.e. $\Delta f \in (0, 1]$. The bandwidth with the normalized frequency will be calculated by $BW = K_f \times \Delta f$.

In this simulation, we set $\Delta f = 0.0001$, number of tones used is $K_f = 10000$, the delays $\boldsymbol{\tau}_N$ are set as $[3, 3.1, 3.2, 3.3]s$ and the amplitude of the n-th ray is set $a(r_n) = e^{-n}$, $n \in [0, 1, 2, 3]$, the search range of MUSIC algorithm is $[0, 10]s$ and the delay step size of steering vector is $0.01s$. When using additional Gaussian white noise with $\sigma^2 = -100dB$, the inverse pseudo spectrum is shown in Figure 2.1. Select the local maximal values that are larger than $0.6 \times J_{MUSIC-max}$ as candidates and choose the one with smallest delay among the candidates, where $J_{MUSIC-max}$ is the global maximum in the search range. Then as shown, the final estimated delay in LOS is $3s$ which is very exact.

i) Frequency step size

If we only change the frequency step size to $\Delta f = 1$, there will be $BW = K_f \times \Delta f = 10000$. Keep the other parameters fixed and the result of MUSIC algorithm is presented in Figure 2.2.

As shown in the figure 2.2, although we use bandwidth much more than available, the estimation result is still inaccurate because of the ambiguity. The delay is calculated by $\tau = \frac{r}{c} = \frac{1}{2\pi\Delta f} \mod \frac{1}{\Delta f}$, given equation(1.1) thus the unambiguous scope is $\tau_{unam} = \frac{1}{\Delta f}$. In the figure 2.1 when $\Delta f = 0.0001$, the unambiguous scope is $\tau_{unam} = \frac{1}{\Delta f} = 10000s$ and the set delays $[3, 3.1, 3.2, 3.3]s$ are in the scope. In the figure 2.2, the unambiguous scope is $\tau_{unam} = \frac{1}{\Delta f} = 1s$ for $\Delta f = 1$ and the set delays are obviously beyond the scope which caused an ambiguous result. Thus we can conclude that the unambiguous scope depends on the frequency step size and in unambiguous condition the frequency step size may not influence the estimation result.

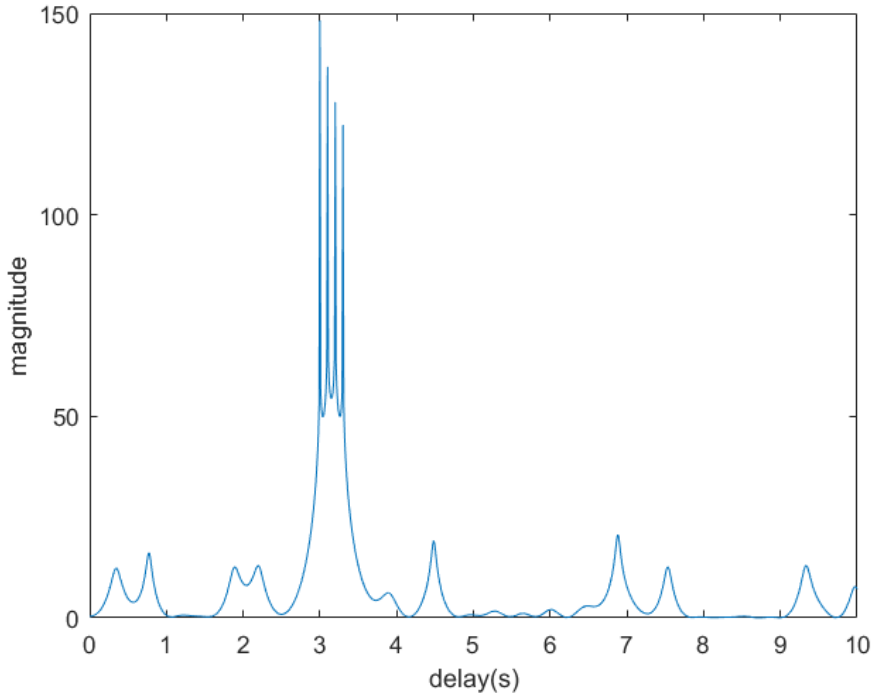

Figure 2.1: Inverse pseudo spectrum for $K_f = 10000$, $\Delta f = 0.0001$, $\sigma^2 = -100dB$, $\boldsymbol{\tau}_N = [3, 3.1, 3.2, 3.3]s$.

ii) Delay interval

If we only change the set delays to $[3, 3.0001, 3.0002, 3.3]s$, there will be $BW = K_f \times \Delta f = 1$. Keep the other parameters fixed, the inverse pseudo spectrum of MUSIC algorithm is provided in Figure 2.3. The final estimated τ_0 is $3s$ which is correct but we can see that the inverse pseudo spectrum can not show all the paths. It is because the difference between set delays are smaller than the step size of the steering vector in MUSIC algorithm, i.e. the resolution of the MUSIC algorithm.

If we reduce the delay step size of the steering vector and keep the search range of the MUSIC algorithm the same, the calculation load will increase rapidly. If we reduce the delay step size and the search range together, the calculation load can be acceptable but the new search range may not cover all useful information in the measurement date. Thus, to have an accurate result and a reasonable calculation load, these two parameters, the delay step size in steering vector and the search range, should be set properly according to the prior information.

It is also noteworthy that the estimation result is still accurate because we only choose the local maximum larger or equal to $0.6 \times J_{MUSIC-max}$. If we only choose the local maximum with smallest delay the estimation will no long be correct which shows that the method we used to choose estimated delay is more robust.

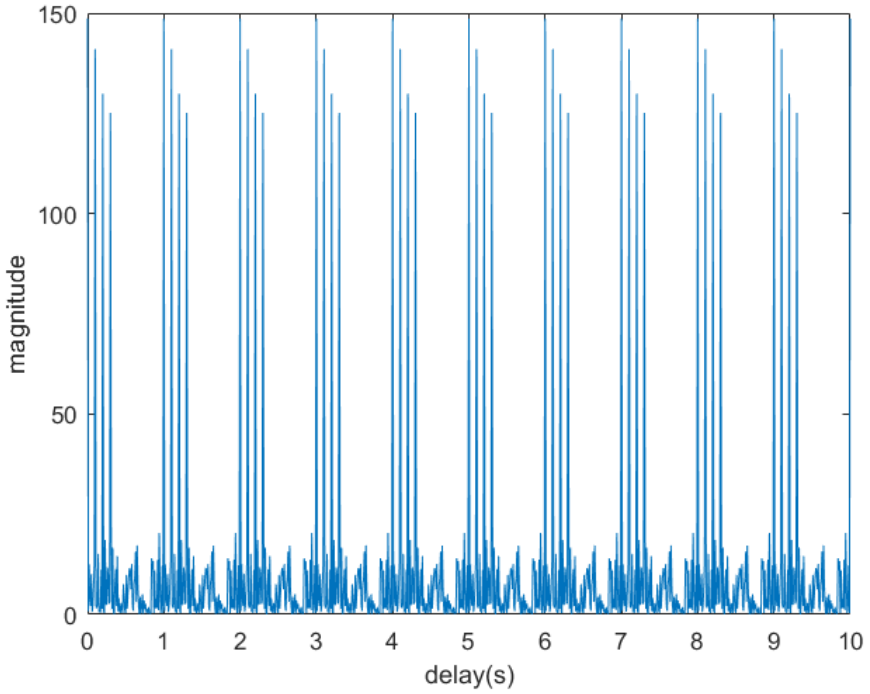

Figure 2.2: Inverse pseudo spectrum for $K_f = 10000$, $\Delta f = 1$, $\sigma^2 = -100dB$, $\boldsymbol{\tau}_N = [3, 3.1, 3.2, 3.3]s$.

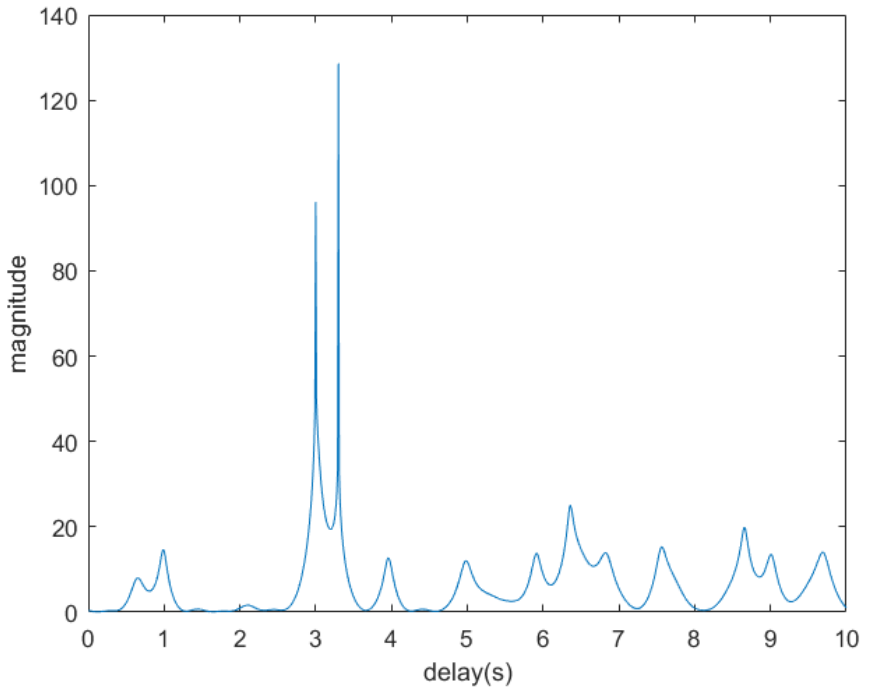

Figure 2.3: Inverse pseudo spectrum for $K_f = 10000$, $\Delta f = 0.0001$, $\sigma^2 = -100dB$, $\boldsymbol{\tau}_N = [3, 3.0001, 3.0002, 3.3]s$.

iii) Noise variance

If we change the noise variance σ^2 while keeping the other parameters fixed, we can get the result of mean delay error in Figure 2.4. The σ^2 is set as $20dB, 15dB, ..., -100dB$ and for each σ^2 value the estimation procedure is run 10 times. The mean delay error is the absolute difference between the set LOS delay $3s$ and the mean among 10 estimated delays for each σ^2.

As shown in the Figure 2.4, we can see that the estimation accuracy is highly correlated to the noise condition. When the noise variance is higher than $0dB$, the mean error decreases while the σ^2 decreases. But for $\sigma^2 < 0dB$, the mean error is always close to zero. Thus we can conclude that the noise has negative relationship with the estimation accuracy in high σ^2 values. And MUSIC algorithm is a good method to do the ranging in good environment condition.

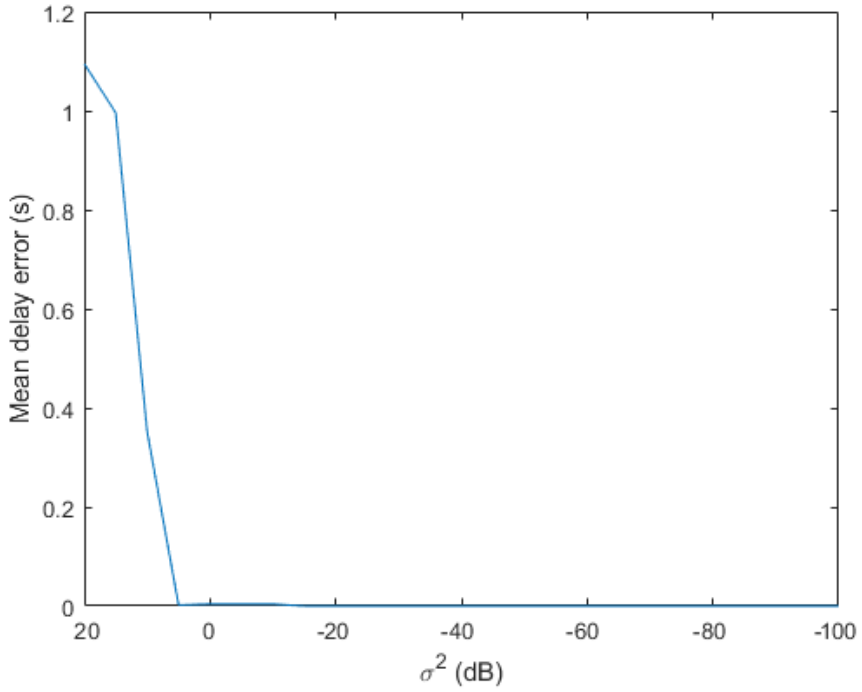

Figure 2.4: Mean delay error for various σ^2, $\Delta f = 0.0001$, $\boldsymbol{\tau}_N = [3, 3.1, 3.2, 3.3]s$.

2.2.2 Practical frequency

In this part, we start to consider the tone selection problem by using practical frequency. The frequency band we can use is $2.4GHz - 2.48GHz$ and the bandwidth is $80MHz$. Assume there are three propagation paths and the distances between the two devices over each path are $\mathbf{r}_N = [0.9, 3, 5]m$. With the propagation speed $c = 3 \times 10^8$m/s, the delay over each path is calculated by $\boldsymbol{\tau}_N = \frac{\mathbf{r}_N}{c} = [3, 10, 16.7] \times 10^{-9}s$. And the devices are placed in a environment with Additional Gaussian white noise. The noise is zero mean and has variance σ^2.

Except the above numbers, a proper frequency step size Δf should be chosen to avoid ambiguity. If the range of K_f is the interval $(1, 10000]$, we have $\Delta f = \frac{Bandwidth}{K_f} \in (8 \times 10^3 Hz, 8 \times 10^7]Hz$ and the unambiguous scope is $\tau_{unam} = \frac{1}{\Delta f} \in [1.25^{-8}, 1.25 \times 10^{-4})s$. Thus in this simulation, the result will not be ambiguous if we use $K_f \in (1, 10000]$. The relationships between accuracy of estimation result and different parameters are discussed below.

i) Fixed frequency step

If we keep the frequency step size at $\Delta f = 8 \times 10^3 Hz$, we have $K_f = 10000$. To use less tones in the ranging, we can take first M elements in the full set $C_{K_f} = [0, 1, ..., 9999]$ and study the influence of the number M. In the simulation, the M is changed from 100 to 10000 with step size 100 and estimation procedure is run 10 times for each M. The delay step size of steering vector in MUSIC algorithm is $\frac{0.01m}{c}$ and the search range of the MUSIC algorithm is $[\frac{0m}{c}, \frac{10m}{c}]$. Set $\sigma^2 = -100dB$. The mean distance error of each M is the absolute difference between the set LOS distance $0.9m$ and the mean among 10 estimated distances. The relation ship between M and the mean distance error is provided in the figure 2.5.

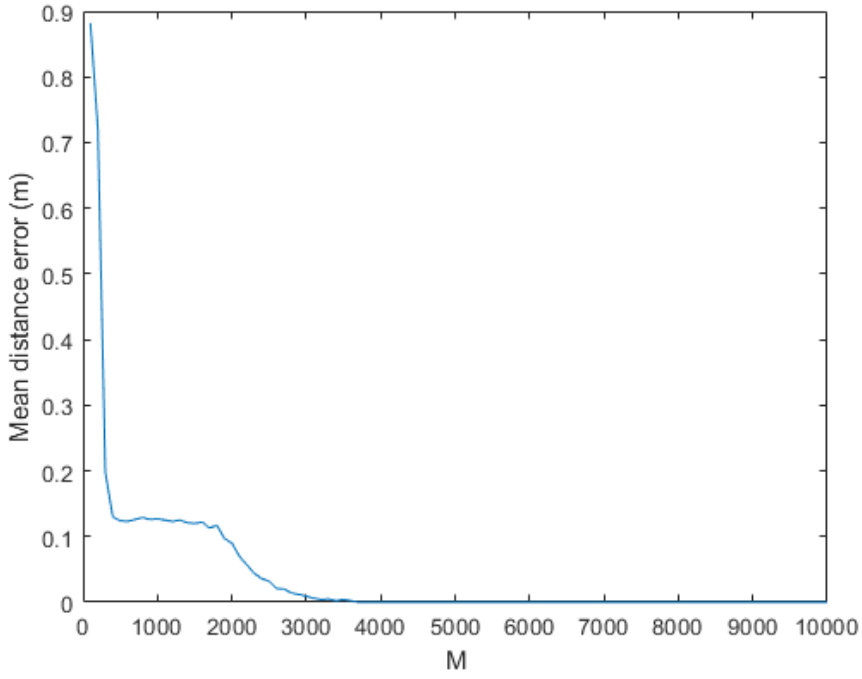

Figure 2.5: Mean distance error for $\sigma^2 = -100dB$, various M, $K_f = 10000$, $\Delta f = 8 \times 10^3 Hz$, $\mathbf{r}_N = [0.9, 3, 5]m$.

As we can see in the figure 2.5, the mean square error decreases when the number M increases. The reason is that with fixed Δf, the bandwidth depends on M by $BW = M \times \Delta f$. And the estimation accuracy of distance is relative to the bandwidth by

$d_{accuracy} = \frac{c}{2BW}$[27]. With wider bandwidth, $d_{accuracy}$ will be lower and the estimation accuracy will be improved. And in the figure, there is a floor between $M = 0$ and $M = 2000$. The reason of this floor may be that we do not have enough bandwidth in low M value and the MUSIC algorithm can only estimate 2 peaks instead of 3 which causes a deviation in the estimation.

ii) Fixed bandwidth

In the above part, we choose first M frequencies in the given bandwidth with fixed Δf. In this part, we fix the bandwidth and change the number K_f from 100 to 10000 with step size 100. So the frequency step size is also changed and the full set is always used here. In this condition, the bandwidth is constant and the tones are chosen uniformly over the band, so Δf should be calculated by $\Delta f = \frac{bandwidth}{K_f}$. Set $\sigma^2 = -50dB$. Keeping the other parameters the same, we have the relationship between mean distance error and the number K_f in figure 2.6.

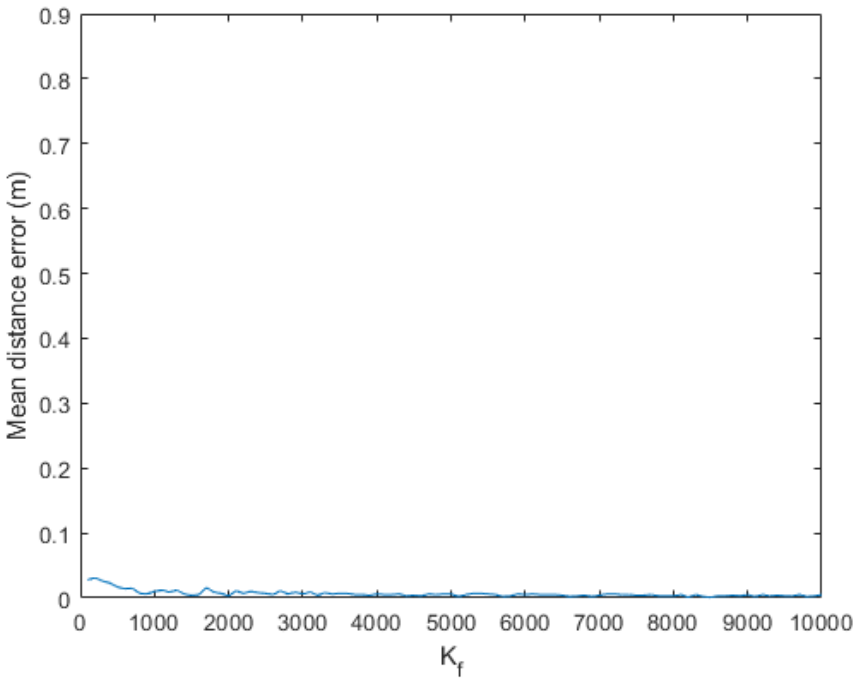

Figure 2.6: Mean distance error for $\sigma^2 = -50dB$, various K_f, $\Delta f = \frac{8\times10^7}{K_f}Hz$, $\mathbf{r}_N = [0.9, 3, 5]m$.

Figure 2.6 shows that the mean distance error is not related to the K_f value and with higher σ^2, the error is even lower compared to the figure 2.5. It is because we always use whole bandwidth in this condition which makes the estimation accuracy good. Consequently, in unambiguous range, the bandwidth is the key point to get the correct estimation result.

iii) Fixed frequency step and fixed bandwidth

With fixed bandwidth $BW = 80MHz$ and fixed Δf, the K_f will always be 10000. If we do not take first M elements in the full set $C_{K_f} = [0, 1, ..., 9999]$, instead, we randomly select M elements in the full set, we can obtain a relation ship between the mean distance error an the number M. The random selection is achieved by the *randperm* function in Matlab. The M is changed from 100 to 10000 with step size 100 and estimation procedure is run 10 times for each M. Keeping the other parameters the same, the result is provided in the figure 2.7.

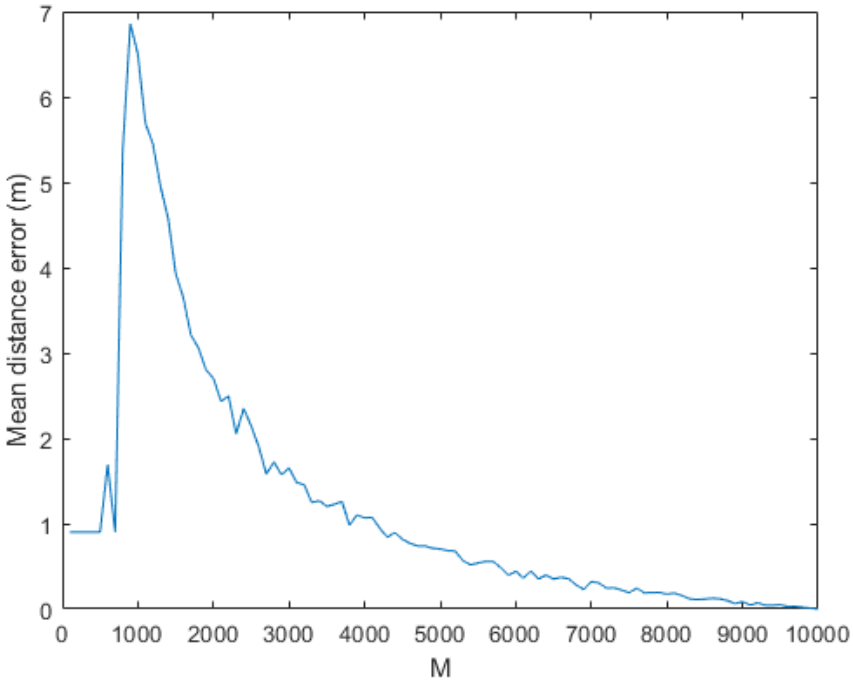

Figure 2.7: Mean distance error for various M, $\sigma^2 = -100dB$, $\Delta f = 8 \times 10^3 Hz$, $\mathbf{r}_N = [0.9, 3, 5]m$, $K_f = 10000$.

As we can see, the result becomes accurate with increasing K_f but is still much worse compared to Figure 2.5 and 2.6. The reason is that the random selection may destroy the data structure and increase the rank of Hankel matrix. In noiseless condition, when we uniformly select the tones, the interval between tones are equal and more than N columns in Hankel matrix are linearly dependent. Then the rank of the Hankel matrix is N which is equal to the number of paths. If we randomly select the tones, the interval between each tones are not equal and the columns in Hankel matrix are not linearly dependent which may increase the rank of Hankel matrix. MUSIC algorithm need to utilized the rank of the Hankel matrix to estimate N path delays. Thus for random selection, MUSIC algorithm is not suitable anymore and new methods should be considered. Also we can see that below $M = 1000$ the mean error is low. It is because below $M = 1000$, MUSIC algorithm do not have any output, so we set the

estimated distance to $0m$ in this case which makes the mean error around $0.9m$.

2.3 Conclusion

This chapter mainly introduces the frequently used estimation algorithm, MUSIC algorithm, and provides simulation results of parameter study.

With normalized bandwidth $80MHz$, we study the impact of the frequency step size Δf, the delay interval and the noise variance. The unambiguous range depends on the frequency step size by $\tau_{unam} = \frac{1}{\Delta f}$ and the noise variance has positive relation with the estimation accuracy. The delay step size of the steering vector in MUSIC algorithm also has influence in the estimation and the computational load. To balance the accuracy and computational load, it is better to have some prior information which can be helpful in parameter setting.

When using practical bandwidth $80MHz$, we consider the tone selection problem roughly in unambiguous range. If the used tones are selected uniformly on the available bandwidth, wider bandwidth is essential for accurate estimation. If we randomly select tones on the given full set, the estimation will have large error even whole bandwidth is used. Because random selection will destroy the data structure while uniform selection will not and the data structure has influence on the MUSIC algorithm.

Based on the conclusions above, the optimal tone selection methods and criteria are studied and new methods of data reconstruction and range estimation will be used in the following chapters.

Optimal tone selection with CRLB

3

As mentioned in the introduction, the indoor ranging problem based on the signal model (3) is a typical estimation problem and in the estimation theory, the CRLB is the easiest criterion to calculate. The CRLB is able to indicate possible estimation error which can be a criterion to the problem. Thus in this chapter, we use the criterion CRLB to determine the number of elements in the subset and to choose the optimal tone subset C_M. We at first introduce the CRLB and its derivation, then provide its calculation method and do the selection simulations.

3.1 Cramer Rao Lower Bound

Cramer-Rao lower bound was proposed by Harald Cramer and Calyampudi Radakrishna Rao in about 1945[28][29]. It is a lower bound of the estimation error variance in an estimation problem. To be more clear, as an evaluation metric of estimation problem, CRLB can indicate how accurate we can estimate a parameter in a given data model[30][31][32][16]. With high CRLB, the variance of the estimation error is high and the estimation result is more possible to have large error. For the indoor ranging problem, it is essential that we do the distance measurement accurately which means CRLB can be a suitable criterion for our case.

In our model, we are interested in the LOS path delay τ_0 and we regard the delays in other paths as the nuisance parameters. So the general unknown targets will be the delay vector $\boldsymbol{\tau}_N$ and the measurement vector is $\mathbf{h}_{K_f}$ of the full set C_{K_f}. As the data are all complex value and the noise in the model is the white Gaussian noise, we can write the probability density function (PDF) of the delay vector $\boldsymbol{\tau}_N$ when the measurements $\mathbf{h}_{K_f}$ is given:

$$p(\boldsymbol{\tau}_N|\mathbf{h}_{K_f}) = \frac{1}{(\pi\sigma^2)^{K_f}} \exp\left[-\frac{1}{\sigma^2}(\mathbf{h}_{K_f} - \mathbf{Z}_{K_f}\mathbf{a}(\mathbf{r}_N))^H((\mathbf{h}_{K_f} - \mathbf{Z}_{K_f}\mathbf{a}(\mathbf{r}_N)))\right] \tag{3.1}$$

where σ^2 is the known noise variance and the amplitude $\mathbf{a}(\mathbf{r}_N)$ is also known. The PDF $p(\boldsymbol{\tau}_N|\mathbf{h}_{K_f})$ specify the probability of $\boldsymbol{\tau}_N$ value falling within a particular range of values when given $\mathbf{h}_{K_f}$. The PDF is also called likelihood function. If we take the logarithm of the PDF, we will obtain the log-likelihood function $s(\boldsymbol{\tau}_N|\mathbf{h}_{K_f})$ is:

$$\mathbf{s}(\boldsymbol{\tau}_N|\mathbf{h}_{K_f}) = \frac{\partial \ln p(\boldsymbol{\tau}_N|\mathbf{h}_{K_f})}{\partial \boldsymbol{\tau}_N} \tag{3.2}$$

The variance of the log-likelihood function is called the Fisher information:

$$\mathbf{I}_{K_f}(\boldsymbol{\tau}_N|\mathbf{h}_{K_f}) = -\mathrm{E}\left[\frac{\partial^2 \ln p(\boldsymbol{\tau}_N|\mathbf{h}_{K_f})}{\partial \boldsymbol{\tau}_N \partial \boldsymbol{\tau}_N^H}\right] = \mathrm{E}\left[\frac{\partial \ln p(\boldsymbol{\tau}_N|\mathbf{h}_{K_f})}{\partial \boldsymbol{\tau}_N}\frac{\partial \ln p(\boldsymbol{\tau}_N|\mathbf{h}_{K_f})}{\partial \boldsymbol{\tau}_N^H}\right] \tag{3.3}$$

which is a $N \times N$ matrix. And the Fisher matrix is non-negative and additive for independent measurements.

If assume the PDF $p(\boldsymbol{\tau}_N|\mathbf{h}_{K_f})$ satisfies the regularity condition, i.e.

$$\mathrm{E}\left[\frac{\partial \ln(\boldsymbol{\tau}_N|\mathbf{h}_{K_f})}{\partial \boldsymbol{\tau}_N}\right] = 0, \text{for all } \boldsymbol{\tau}_N \tag{3.4}$$

then the variance of any unbiased estimated parameter $\hat{\boldsymbol{\tau}}_N$ satisfies:

$$\mathrm{var}_{K_f}(\hat{\boldsymbol{\tau}}_N|\mathbf{h}_{K_f}) \geq \frac{1}{-\mathrm{E}\left[\frac{\partial^2 \ln p(\boldsymbol{\tau}_N|\mathbf{h}_{K_f})}{\partial \boldsymbol{\tau}_N \partial \boldsymbol{\tau}_N^H}\right]} = \frac{1}{\mathrm{E}\left[\frac{\partial \ln p(\boldsymbol{\tau}_N|\mathbf{h}_{K_f})}{\partial \boldsymbol{\tau}_N}\frac{\partial \ln p(\boldsymbol{\tau}_N|\mathbf{h}_{K_f})}{\partial \boldsymbol{\tau}_N^H}\right]} = \frac{1}{\mathbf{I}_{K_f}(\boldsymbol{\tau}_N|\mathbf{h}_{K_f})} \tag{3.5}$$

And the lower bound in the above equation is called Cramer-Rao lower bound of full set C_{K_f}. Thus, with known noise variance and amplitude vector, the evaluation function of criterion CRLB can be expressed as follows:

$$\mathbf{G}_{CRLB}(\hat{\boldsymbol{\tau}}_N|\mathbf{h}_{K_f}) = \frac{1}{\mathbf{I}_{K_f}(\boldsymbol{\tau}_N|\mathbf{h}_{K_f})} \tag{3.6}$$

3.1.1 CRLB calculation for single path

To calculate the CRLB of single path, we at first introduce the close-form solution of CRLB in [31]. For multi-path case, if the amplitudes $\mathbf{a}(\mathbf{r}_N)$, the noise variance σ^2 and the structure of the matrix $\mathbf{Z}_{K_f}$ are known, we can have the following close form solution of CRLB in full set C_{K_f}:

$$\mathbf{G}_{CRLB}(\hat{\boldsymbol{\tau}}_N|\mathbf{h}_{K_f}) = \frac{\sigma^2}{2}\{Re[\boldsymbol{\Lambda}^H \mathbf{D}^H (\mathbf{I} - \mathbf{Z}_{K_f}(\mathbf{Z}_{K_f}^H \mathbf{Z}_{K_f})^{-1}\mathbf{Z}_{K_f}^H)\mathbf{D}\boldsymbol{\Lambda}]\}^{-1} \tag{3.7}$$

where

$$\boldsymbol{\Lambda} = \begin{bmatrix} a(r_0) & 0 & \cdots & 0 \\ 0 & a(r_1) & \cdots & 0 \\ \vdots & \vdots & \ddots & \vdots \\ 0 & 0 & \cdots & a(r_{N-1}) \end{bmatrix} \tag{3.8}$$

$$\mathbf{D} = \begin{bmatrix} \boldsymbol{\zeta}_{K_f}(\tau_0) & \boldsymbol{\zeta}_{K_f}(\tau_1) & \cdots & \boldsymbol{\zeta}_{K_f}(\tau_{N-1}) \end{bmatrix} \tag{3.9}$$

$$\boldsymbol{\zeta}_{K_f}(\tau_n) = \frac{\partial \mathbf{z}_{K_f}(\tau_n)}{\partial \tau_n} \tag{3.10}$$

In the equation (3.7), $\mathbf{G}_{CRLB}(\hat{\boldsymbol{\tau}}_N|\mathbf{h}_{K_f})$ indicates the estimation accuracy when the delay vector is $\boldsymbol{\tau}_N$ and is a $N \times N$ matrix. The $n-th$ element in its diagonal is the variance of error when estimating $n-th$ path delay, i.e. the first diagonal elements is the error variance in LOS direction.

Then, in the analysis of CRLB, it is easier to start with the single path case, which means there is only one path in the indoor environment and $N = 1$. In this case, the delay vector $\boldsymbol{\tau}_N$ can be any delay scalar τ_n. In this report, we assume that if $N = 1$, we only have the LOS path and $\boldsymbol{\tau}_N = \tau_0$. Take the CRLB of full set C_{K_f} as an example, we have:

$$\boldsymbol{\Lambda} = a(r_0) \tag{3.11}$$

$$\mathbf{Z}_{K_f} = \mathbf{z}_{K_f}(\tau_0) = \begin{bmatrix} 1 & e^{l\tau_0} & e^{2l\tau_0} & \cdots & e^{(K_f-1)l\tau_0} \end{bmatrix}^T \tag{3.12}$$

$$\mathbf{D} = \boldsymbol{\zeta}_{K_f}(\tau_0) = \begin{bmatrix} 0 & le^{l\tau_0} & 2le^{2l\tau_0} & \cdots & (K_f-1)le^{(K_f-1)l\tau_0} \end{bmatrix}^T \tag{3.13}$$

where $l = (-j2\pi\Delta f)$. Thus, the CRLB for single path and full set is:

$$\begin{aligned}
\mathbf{G}_{CRLB}(\hat{\tau}_0|\mathbf{h}_{K_f}) &= \frac{\sigma^2}{2}\{Re[\boldsymbol{\Lambda}^H\mathbf{D}^H(\mathbf{I} - \mathbf{Z}_{K_f}(\mathbf{Z}_{K_f}^H\mathbf{Z}_{K_f})^{-1}\mathbf{Z}_{K_f}^H)\mathbf{D}\boldsymbol{\Lambda}]\}^{-1} \\
&= \frac{\sigma^2}{2}\{Re[a^2(r_0)\mathbf{D}^H\mathbf{D} - a^2(r_0)\mathbf{D}^H\mathbf{Z}_{K_f}(\mathbf{Z}_{K_f}^H\mathbf{Z}_{K_f})^{-1}\mathbf{Z}_{K_f}^H\mathbf{D}\}^{-1}] \\
&= \frac{\sigma^2}{2}[a^2(r_0)4\pi^2\Delta f^2\frac{K_f(K_f-1)(2K_f-1)}{6} - a^2(r_0)4\pi^2\Delta f^2\frac{K_f(K_f-1)^2}{4} \\
&= \frac{\sigma^2}{2}[(a^2(r_0)4\pi^2\Delta f^2)\frac{K_f^3 - K_f}{12}]^{-1} \\
&= \frac{3\sigma^2}{2(a^2(r_0)\pi^2\Delta f^2)(K_f^3 - K_f)}
\end{aligned} \tag{3.14}$$

where

$$\begin{aligned}
\mathbf{D}^H\mathbf{D} &= -(l^2 + 4l^2 + ... + (K_f-1)^2l^2) = -l^2(1 + 2^2 + ... + (K_f-1)^2) \\
&= -l^2\frac{K_f(K_f-1)(2K_f-1)}{6} = 4\pi^2\Delta f^2\frac{K_f(K_f-1)(2K_f-1)}{6}
\end{aligned} \tag{3.15}$$

$$\mathbf{Z}_{K_f}^H\mathbf{Z}_{K_f} = K_f \tag{3.16}$$

$$\mathbf{D}^H\mathbf{Z}_{K_f} = -l - 2l - ... - (K_f-1)l = -l\frac{K_f(K_f-1)}{2} = j2\pi\Delta f\frac{K_f(K_f-1)}{2} \tag{3.17}$$

In the equation (3.15) to (3.17), we substitute l by $(-j2\pi\Delta f)$ and use the sum equation of number series: $1 + 2 + ... + (K_f - 1) = \frac{K_f(K_f-1)}{2}$, the sum equation of square number series: $l^2 + 4l^2 + ... + (K_f-1)^2l^2 = \frac{K_f(K_f-1)(2K_f-1)}{6}$.

Consequently, with known signal amplitude, noise variance and frequency step, the CRLB for the single path case and full set is only relative to the tone number K_f in full set. But if subset C_M is used instead of the full set, the CRLB value for the single path will not depend on the number of elements M in the subset, but depend on the element distribution. It is because equation (3.15) to (3.17) are simplified based on the sum of the square number series which is only available in full set. For subset C_M, the value of $\mathbf{D}^H\mathbf{D}$, $\mathbf{Z}_{K_f}^H\mathbf{Z}_{K_f}$ and $\mathbf{D}^H\mathbf{Z}_{K_f}$ will be decided by the subset element distribution. Thus for the subsets with the same M and different element distribution, the CRLB values will be different. This conclusion provides us the opportunity to choose the best one with minimal CRLB among all subsets of C_{K_f}.

3.1.2 CRLB calculation for two paths

Although the multi-path propagation environment contains N delays, we only need to focus on the delay in LOS direction, i.e. the smallest delay which is assumed τ_0, to achieve ranging. To estimate the smallest delay τ_0 more accurate, it is necessary to obtain a low CRLB on the estimated delay τ_0.

As proven in [33], compared with using the CRLB of one target, it is more robust and accurate to use the CRLB of two targets as the performance metric in the subset selection problem. Thus, in this section, calculation of the CRLB of two paths is provided.

In two-path case, we have $N = 2$. Assume $\boldsymbol{\tau}_N = [\tau_0, \tau_1]$ and take the full set as an example, we have:

$$\mathbf{\Lambda} = \begin{bmatrix} a(r_0) & 0 \\ 0 & a(r_1) \end{bmatrix} \tag{3.18}$$

$$\mathbf{Z}_{K_f} = \begin{bmatrix} \mathbf{z}_{K_f}(\tau_0) & \mathbf{z}_{K_f}(\tau_1) \end{bmatrix} = \begin{bmatrix} 1 & e^{l\tau_0} & e^{2l\tau_0} & \cdots & e^{(K_f-1)l\tau_0} \\ 1 & e^{l\tau_1} & e^{2l\tau_1} & \cdots & e^{(K_f-1)l\tau_1} \end{bmatrix}^T \tag{3.19}$$

$$\mathbf{D} = \begin{bmatrix} \boldsymbol{\zeta}_{K_f}(\tau_0) & \boldsymbol{\zeta}_{K_f}(\tau_1) \end{bmatrix} = \begin{bmatrix} 0 & le^{l\tau_0} & 2le^{2l\tau_0} & \cdots & (K_f-1)le^{(K_f-1)l\tau_0} \\ 0 & le^{l\tau_1} & 2le^{2l\tau_1} & \cdots & (K_f-1)le^{(K_f-1)l\tau_1} \end{bmatrix}^T \tag{3.20}$$

where $l = (-j2\pi\Delta f)$. Then the CRLB of two path case is a 2×2 matrix which can be calculated following the equation:

$$\begin{aligned} \mathbf{G}_{CRLB}(\hat{\tau}_0, \hat{\tau}_1 | \mathbf{h}_{K_f}) &= \frac{\sigma^2}{2}\{Re[\mathbf{\Lambda}^H\mathbf{D}^H(\mathbf{I} - \mathbf{Z}_{K_f}(\mathbf{Z}_{K_f}^H\mathbf{Z}_{K_f})^{-1}\mathbf{Z}_{K_f}^H)\mathbf{D}\mathbf{\Lambda}]\}^{-1} \\ &= \frac{\sigma^2}{2}\{Re[\Lambda^H\mathbf{D}^H\mathbf{D}\Lambda - \Lambda^H\mathbf{D}^H\mathbf{Z}_{K_f}(\mathbf{Z}_{K_f}^H\mathbf{Z}_{K_f})^{-1}\mathbf{Z}_{K_f}^H\mathbf{D}\Lambda]\}^{-1} \end{aligned} \tag{3.21}$$

where

$$\mathbf{D}^H\mathbf{D} = \begin{bmatrix} -l^2\frac{K_f(K_f-1)(2K_f-1)}{6} & -l^2e^{l\Delta\tau_{10}}\frac{K_f(K_f-1)(2K_f-1)}{6} \\ -l^2e^{-l\Delta\tau_{10}}\frac{K_f(K_f-1)(2K_f-1)}{6} & -l^2\frac{K_f(K_f-1)(2K_f-1)}{6} \end{bmatrix} \tag{3.22}$$

$$\mathbf{Z}_{K_f}^H\mathbf{Z}_{K_f} = \begin{bmatrix} K_f & \frac{1-e^{K_f l\Delta\tau_{10}}}{1-e^{l\Delta\tau_{10}}} \\ \frac{1-e^{-K_f l\Delta\tau_{10}}}{1-e^{-l\Delta\tau_{10}}} & K_f \end{bmatrix} \tag{3.23}$$

$$\mathbf{D}^H\mathbf{Z}_{K_f} = \begin{bmatrix} -l\frac{K_f(K_f-1)}{2} & -l(\frac{e^{l\Delta\tau_{10}}-K_f e^{K_f l\Delta\tau_{10}}+(K_f-1)e^{(K_f+1)l\Delta\tau_{10}}}{(1-e^{l\Delta\tau_{10}})^2}) \\ -l(\frac{e^{-l\Delta\tau_{10}}-K_f e^{-K_f l\Delta\tau_{10}}+(K_f-1)e^{-(K_f+1)l\Delta\tau_{10}}}{(1-e^{-l\Delta\tau_{10}})^2}) & -l\frac{K_f(K_f-1)}{2} \end{bmatrix} \tag{3.24}$$

and $\Delta\tau_{10} = \tau_1 - \tau_0$.

Then the first element in the diagonal of $\mathbf{G}_{CRLB}(\hat{\tau}_0, \hat{\tau}_1|\mathbf{h}_{K_f})$ becomes the lower bound of the variance of estimated LOS delay:

$$\text{var}_{K_f}(\hat{\tau}_0|\mathbf{h}_{K_f}) \geq G_{CRLB,11}(\hat{\tau}_0, \hat{\tau}_1|\mathbf{h}_{K_f}) \tag{3.25}$$

where $G_{CRLB,11}(\hat{\tau}_0, \hat{\tau}_1|\mathbf{h}_{K_f})$ is the first diagonal elements of $\mathbf{G}_{CRLB}(\hat{\tau}_0, \hat{\tau}_1|\mathbf{h}_{K_f})$. As we can see from the equation (3.21)-(3.24), the CRLB of the LOS direction delay mainly depends on the time difference $\Delta\tau_{10}$ between two paths instead of the path delays τ_0, τ_1. Also, the tone set has great influence on the CRLB of 2-path case. So in the following part, we will use this feature of CRLB to select the optimal tone subset.

3.2 Optimal tone selection

As discussed in the above section, to ranging a target in the multi-path situation, we only need to estimate the smallest delay, τ_0. But the other paths will have impacts on the LOS path which may cause ambiguity or inaccurate estimation. CRLB can indicate the possible estimation error in the ranging. Thus it is necessary to minimize the CRLB of τ_0 in multi-path case which is helpful in increasing the estimation accuracy.

As mentioned, the LOS path delay is easily influenced by the other path and the path nearest to the LOS path has the greatest impact on it. In this report, we name the nearest path by the $2nd$ path. Thus, to simplify the CRLB calculation in multi-path case, we concentrate on the estimation accuracy of the LOS path and the $2nd$ path. We calculate the CRLB of these two path with changed delay difference between them. By doing so, we try to increase the estimation accuracy of LOS path no matter how far the $2nd$ path is. To achieve the goal, we set a delay grid vector $\boldsymbol{\tau}_{grid} = [\tau_{g1}, \tau_{g2}, \tau_{g3}, ...]$ which contains the possible delay of the $2nd$ path. By calculating the CRLB of τ_0 and τ_{gn}, where $n \geq 1$, we can minimize the weighted mean among the first diagonal elements of CRLB matrix, which can be expressed by:

$$\begin{aligned} &G_{CRLB,11}(\hat{\tau}_0, \hat{\boldsymbol{\tau}_{grid}}|\mathbf{h}_M) \\ &= F(G_{CRLB,11}(\hat{\tau}_0, \hat{\tau_{g1}}|\mathbf{h}_M), G_{CRLB,11}(\hat{\tau}_0, \hat{\tau_{g2}}|\mathbf{h}_M), G_{CRLB,11}(\hat{\tau}_0, \hat{\tau_{g3}}|\mathbf{h}_M), ...) \end{aligned} \tag{3.26}$$

where $F(\cdot)$ is a function calculating the weighted mean among the CRLBs values.

3.2.1 Weighted mean function

The Weighted mean function $F(\cdot)$ can be various and in this study, three different $F(\cdot)$s will be utilized. To show the influences of different weights in $F(\cdot)$s, in figure 3.1, we provide the relationship between $\Delta\boldsymbol{\tau}_{gn0}$ and the $G_{CRLB,11}(\hat{\tau}_0, \hat{\tau_{gn}}|\mathbf{h}_{K_f})$, $n \geq 1$ of full set

C_{K_f} using simulation parameters: $K_f = 400$, $c = 3 \times 10^8 m/s$, $\Delta f = 200kHz$, $\tau_0 = 0$, grid vector $\boldsymbol{\tau}_{grid} = [\tau_{g1}, \tau_{g2}, \tau_{g3}, ...] = \frac{0.1,0.2,...,10.0]meter}{c}$, $\sigma^2 = 20dB$.

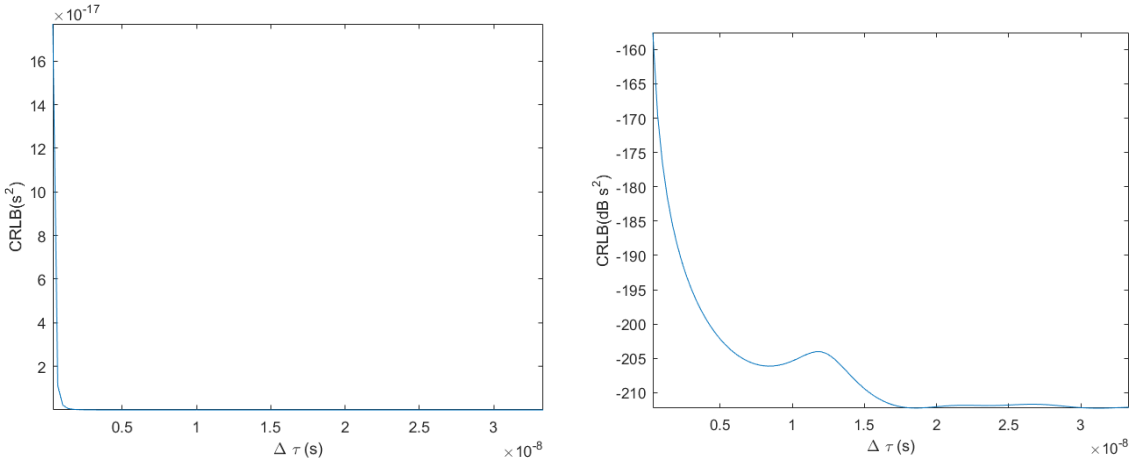

(a) CRLBs in s^2 (b) CRLBs in dBs^2

Figure 3.1: relationship between $\Delta\boldsymbol{\tau}_{gn0}$ and the $G_{CRLB,11}(\hat{\tau}_0, \hat{\tau_{gn}}|\mathbf{h}_{K_f})$, $n \geq 1$ of full set.

i) mean value

The most simple and general way to calculate the CRLB of multi-path environment is to take the mean value which can be expressed as follows:

$$\begin{aligned} &F_{mean}(G_{CRLB,11}(\hat{\tau}_0, \hat{\tau_{g1}}|\mathbf{h}_M), G_{CRLB,11}(\hat{\tau}_0, \hat{\tau_{g2}}|\mathbf{h}_M), G_{CRLB,11}(\hat{\tau}_0, \hat{\tau_{g3}}|\mathbf{h}_M), ...) \\ &= \frac{1}{N_{grid} - 1} \sum_{n=1}^{Ngrid} G_{CRLB,11}(\hat{\tau}_0, \hat{\tau_{gn}}|\mathbf{h}_M) \end{aligned} \tag{3.27}$$

where N_{grid} is the number of elements in the delay grid vector. The weights in the F_{mean} are uniform and CRLB of each $\Delta\tau$ shows same effect in the calculated CRLB of τ_0. Using the data in figure 3.1a, the CRLB of 2-path case with full set and F_{mean} is $1.9194 \times 10^{-18} s^2$.

ii) logarithmic mean value

Except taking the mean to calculate the CRLB of multi-path environment, as introduced in [33], we can also average the logarithmic determinant of the matrix. As the CRLB matrix in 2-path case is a symmetric matrix, in this report we use the logarithms of the first elements of CRLB matrix to obtain the weighted mean value which can be expressed by the following equation:

$$\begin{aligned} &F_{log-mean}(G_{CRLB,11}(\hat{\tau}_0, \hat{\tau_{g1}}|\mathbf{h}_M), G_{CRLB,11}(\hat{\tau}_0, \hat{\tau_{g2}}|\mathbf{h}_M), G_{CRLB,11}(\hat{\tau}_0, \hat{\tau_{g3}}|\mathbf{h}_M), ...) \\ &= 10^{\frac{1}{10(N_{grid}-1)} \sum_{n=1}^{Ngrid} log_{10}(G_{CRLB,11}(\hat{\tau}_0, \hat{\tau_{gn}}|\mathbf{h}_M))} \end{aligned} \tag{3.28}$$

Compared to the original CRLB data in figure 3.1a, the logarithmic CRLBs in figure 3.1b have smaller difference with each other. By taking the logarithm of the CRLB,

the small CRLB values play more important role in the averaging progress. Generally, the large values are suppressed and small values are encouraged in the contribution of the final logarithmic mean. Thus, using the data in figure 3.1b, the logarithmic mean value of the CRLB is $2.2186 \times 10^{-21} s^2$, which is much smaller than the mean value.

iii) expectation with probability of $\Delta\tau_{gn0}$

The mean and the logarithmic mean value of the CRLB both do not consider the prior information in the subset selection procedure. To include the prior information in the selection, we would like to use the probability distribution of $\Delta\tau_n$ and calculate the expectation of the CRLB value rather than the simple mean value. The calculation can be written as:

$$\begin{aligned} &F_{expectation}(G_{CRLB,11}(\hat{\tau}_0, \hat{\tau_{g1}}|\mathbf{h}_M), G_{CRLB,11}(\hat{\tau}_0, \hat{\tau_{g2}}|\mathbf{h}_M), G_{CRLB,11}(\hat{\tau}_0, \hat{\tau_{g3}}|\mathbf{h}_M), ...) \\ &= \frac{1}{\sum_{n=1}^{Ngrid} p_{\Delta\tau}(\Delta\tau_{gn0})} \sum_{n=1}^{Ngrid} G_{CRLB,11}(\hat{\tau}_0, \hat{\tau_{gn}}|\mathbf{h}_M) \times p_{\Delta\tau}(\Delta\tau_{gn0}) \end{aligned} \tag{3.29}$$

where $\Delta\tau_{gn0} = \tau_{gn} - \tau_0$, $p_{\Delta\tau}(\Delta\tau_{gn0})$ is the probability that the $2-th$ path delay τ_{gn} has time difference $\Delta\tau_{gn0}$ compared to LOS direction delay τ_0 in multi-path propagation environment. Based on the results in [34], the probability distribution of $\Delta\tau_{gn0}$ is close to the exponential distribution. Thus we can write the following expression:

$$p_{\Delta\tau}(\Delta\tau_{gn0}) = \eta e^{-\eta\Delta\tau_{gn0}}, \tau_{gn0} \geq 0 \tag{3.30}$$

where η is called ray arrival rate and can be set equal to the value of operational bandwidth[34]. Thus we can have the figure 3.2 of $p_{\Delta\tau}(\Delta\tau_{gn0})$ with simulation parameters: $Bandwidth = 80MHz$ and $\boldsymbol{\tau}_{grid} = \frac{[0,0.1,0.2,...,10.0]meter}{c}$.

We can see that compared to the mean value, the expectation would concentrate more on the paths closer to the LOS path according to the figure 3.2, which make the result more practical. Thus, using the data in figure 3.1b and 3.2, the expectation of CRLB with prior information is $5.4099 \times 10^{-18} s^2$, which is bigger than the mean value and the logarithmic mean value.

3.2.2 Greedy algorithm of optimal tone selection

In the above section, the CRLB of the LOS path delay is calculated by using three weighted mean functions and will be used as the selection criteria in the tone selection problem. To obtain the subset with the smallest number of tones, while ensuring the CRLB is below or equal to the required accuracy, we use the greedy-algorithm as the selection method.

The greedy algorithm chooses the local optimal solution in each stage intending to find the global optimal solution after the whole operation. And in a time long enough, the procedure of greedy algorithm will produce a final result which approximates the global optimal result. By dividing the complex global optimization problem into a combination of simple local optimization problems in each stage, the greedy algorithm can provide a good approximation to the optimal solution for problems that do not

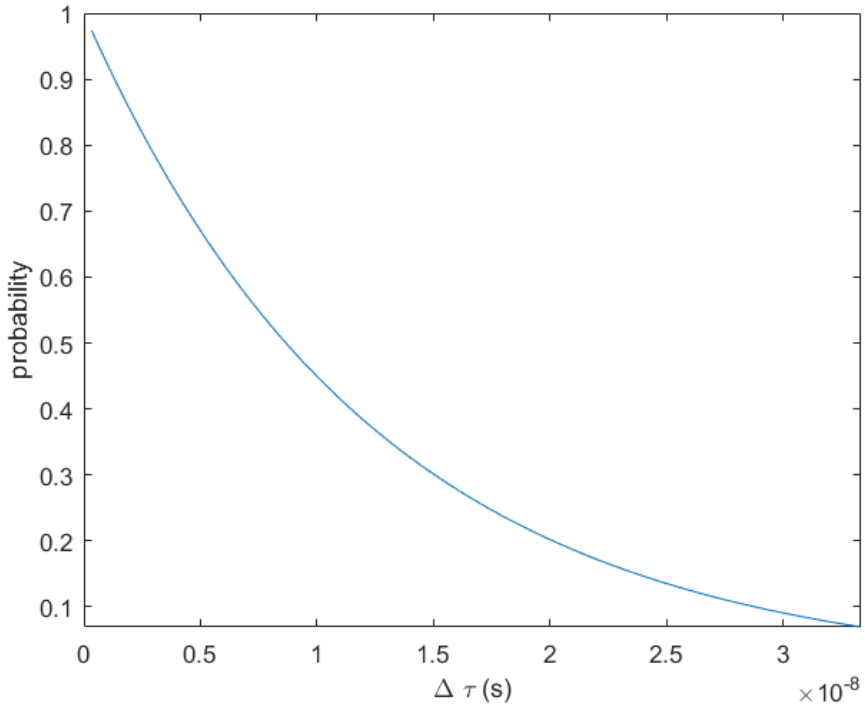

Figure 3.2: $p_{\Delta\tau}(\Delta\tau_{gn0})$ with $Bandwidth = 80MHz$ and $\Delta\boldsymbol{\tau}_{gn0}$, $n \geq 1$.

require much accuracy. Because the available number of tones K_f is large and the subsets of the C_{K_f} will be too many. It is not possible for us to check CRLB of every subsets. And the CRLB is monotonic with the number M, so the greedy algorithm will be efficient and accurate compared to random search algorithm. Thus, for our selection problem, the greedy algorithm is a good choice.

In our case, we can set the square of the disired accuracy as the CRLB threshold, i.e. $G_{CRLB-Tr}$. Then we calculate the CRLBs of τ_0 for all possible subsets $C_{K_f-1} \subset C_{K_f}$ and choose the minimal CRLB among them. If the chosen minimal CRLB is smaller than the $G_{CRLB-Tr}$, the corresponding subset is chosen as the selection results in this step. If not, the selection will end and the superset will be selected eventually. By repeating the above selection procedure, we can finally obtain a subset C_M containing the fewest elements and CRLB of τ_0 smaller than the threshold. The procedure is provided in the algorithm2.

3.3 Simulation results

In the simulation, Matlab is used to calculate the CRLB values and select the optimal tone subset. The results are in three parts: the optimal tone subset selected according to the CRLB of τ_0 in single path case, in two paths with fixed time and in two paths with various time difference respectively.

Algorithm 2 Greedy Algorithm for Optimal Tone Selection Using Criterion CRLB

Input: original set element number K_f, step size and range of delay grid vector, frequency step size Δf, noise variance σ^2, CRLB threshold $G_{CRLB-Tr}$, stage number $w = K_f$

Output: Optimal tone subset C_M, $G_{CRLB,11}(\hat{\tau}_0, \hat{\boldsymbol{\tau}_{grid}}|\mathbf{h}_M)$

1: In stage w, if the set C_w has less than 3 elements, end the algorithm and out put the final selection $C_M = C_w$. Else, calculate $G_{CRLB,11}(\hat{\tau}_0, \hat{\boldsymbol{\tau}_{grid}}|\mathbf{h}_{w-1})$s for all possible subsets $C_{w-1} \subset C_w$ using one weighted mean function $F(\cdot)$.

2: Choose the minimal CRLB value $\min(G_{CRLB,11}(\hat{\tau}_0, \hat{\boldsymbol{\tau}_{grid}}|\mathbf{h}_{w-1}))$ and its corresponding subset $C_{(w-1)-\min}$. If there are more than one minimum, choose the first one.

3: If the $\min(G_{CRLB,11}(\hat{\tau}_0, \hat{\boldsymbol{\tau}_{grid}}|\mathbf{h}_{w-1}))$ is smaller than the threshold $G_{CRLB-Tr}$, $w = w-1$, $C_w = C_{(w-1)-\min}$ and go to step 1.

4: If not, end the algorithm and output the final selection $C_M = C_w$ and its corresponding $G_{CRLB,11}(\hat{\tau}_0, \hat{\boldsymbol{\tau}_{grid}}|\mathbf{h}_w)$

3.3.1 Single path case

In single path case, the CRLB of LOS direction delay τ_0 can be calculated by equation 3.14 in full set. Using subset C_M, we can also calculate the CRLB and the selection is carried out by greedy algorithm. In the simulation, the signal energy is set as $E_s = 1$, thus the SNR can be calculated by $SNR = 10log_{10}(\frac{1}{\sigma^2})$ where σ^2 is the noise variance. $K_f = 400$, $\tau_0 = \frac{4m}{c} = 1.33 \times 10^{-8}s$, $\Delta f = 200kHz$, $SNR = [0, 5, 10, 15, 20, 25, 30]dB$ and the required distance accuracy is $0.1m$, thus $G_{CRLB-Tr} = (\frac{0.1m}{c})^2 = 1.1111 \times 10^{-19}s^2$. With $\Delta f = 200kHz$, there will not be ambiguity in the estimation. Then we can have the following result:

SNR(dB)	0	5	10	15	20	25	30
Number of subset elements	90	24	8	3	3	3	3
CRLB value ($10^{-19}s^2$)	1.1107	1.1081	1.0095	0.9458	0.2991	0.0946	0.0300

Table 3.1: Results of optimal tone subset selection for different SNRs using CRLB of τ_0 in single path case as the criterion.

To show the trend and the distribution of the selected tones more directly, we show the above data and the distribution of the selected subset in figure 3.3 and 3.4.

As we can see from figure 3.3, with higher SNR value, the tones needed for distance estimation become fewer. That is because the CRLB value of the single path and the SNR value has linear dependence. Thus in low noise variance (high SNR) environment, the CRLB value is much lower and in the selection procedure, we can discard more tones.

In figure 3.4. the selected tones distribute in both ends because wide bandwidth is essential to the result accuracy which has been proved in Chapter 2. To maintain a maximal bandwidth and reach the desired accuracy, the tones have to be located in both ends. Also it can be noticed that the selected tones are located in two blocks. Maybe it is because in the single path case, the tones are used to estimate one target

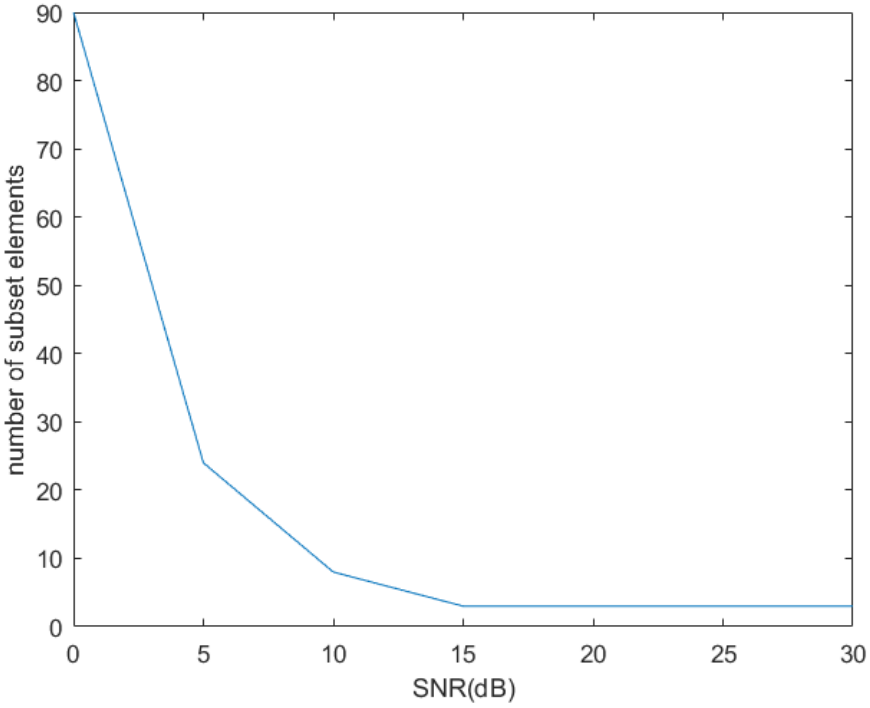

Figure 3.3: Number of elements in selected subset for different SNRs in single path case.

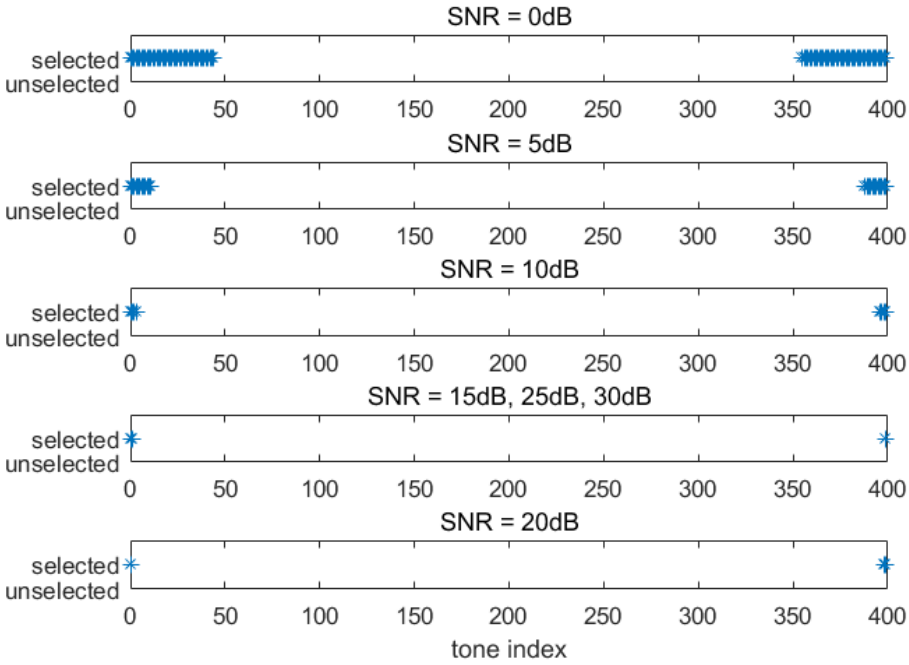

Figure 3.4: Distribution of selected tone for different SNRs in single path case.

and two blocks are considered enough for the estimation.

3.3.2 Two paths with fixed time difference

If we use the CRLB in two paths case with fixed delay difference, we can set $\tau_0 = \frac{4m}{c} = 1.33 \times 10^{-8}s$, $\tau_1 = \frac{9m}{c} = 3 \times 10^{-8}s$, $\Delta\tau_{10} = 1.67 \times 10^{-8}s$. The signal energy in both path are assumed 1, and the other parameters are set the same as in section 3.3.1. The results are provided in the following table3.2:

SNR(dB)	0	5	10	15	20	25	30
Number of subset elements	129	40	13	5	3	3	3
CRLB value ($10^{-19}s^2$)	1.1082	1.0997	1.0632	0.9448	0.6191	0.1958	0.0619

Table 3.2: Results of optimal tone selection for different SNRs using CRLB in two paths with fixed time difference.

To show the data more directly, we have figure 3.5 and 3.6. As shown, the SNR still has influence on the tone selection result and high SNR can reduce the number of tones used conspicuously. But the distribution of the selected tones are different. Although the tones still tend to locate at the both end of the bandwidth, they are divided into more than 3 blocks. This may be because in this case, the path is two and we need more than 3 blocks to estimate these 2 delays.

3.3.3 Two paths with various time differences

In this part, we start to select the optimal tone subset in case that is more close to multi-path environment. We calculate the CRLB in multi-path case by averaging the CRLBs in 2-path case with various time differences. Then we select the optimal subset C_M with minimal $G_{CRLB,11}(\hat{\tau}_0, \hat{\boldsymbol{\tau}_{grid}}|\mathbf{h}_M)$. In the simulation, we study the results under different thresholds(range accuracy), noise variances, weighted mean functions and step sizes of delay grid vector to see their impacts. The step size of delay grid vector is presented by distance step size Δd in the figures for convenience. The range of the grid vector is $[0, 10]m$. The signal energy is set as $E_s = 1$ in all path, thus the SNR is $SNR = 10log_{10}(\frac{1}{\sigma^2})$. $K_f = 400$, $\Delta f = 200kHz$.The results of selected tone numbers are provided in the figure 3.7-3.9. And the distributions of the subsets are provided in the Appendix A.

As shown, high SNR value will lead to a smaller number of tones in the subsets. In the same SNR case, we have the following conclusions: if better accuracy is desired, more tones needs to be selected in general to have more measurement data. And when using weighted mean function $F_{log-mean}(\cdot)$, fewer tones are selected compared to results using other function. This is because $F_{log-mean}(\cdot)$ tends to make the CRLB of τ_0 smaller than other functions do, which makes the CRLB more possible to be lower than the CRLB threshold and we can do more iterations in the greedy algorithm. When using function $F_{expectation}(\cdot)$, we usually choose more tones because the probability of small

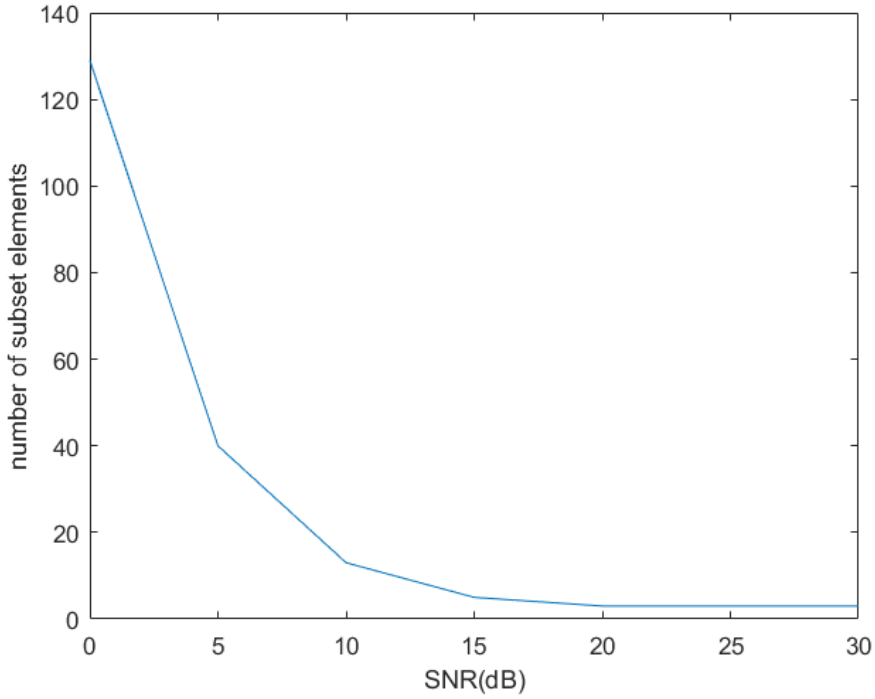

Figure 3.5: Number of elements in selected subset for different SNRs in two paths with fixed time difference.

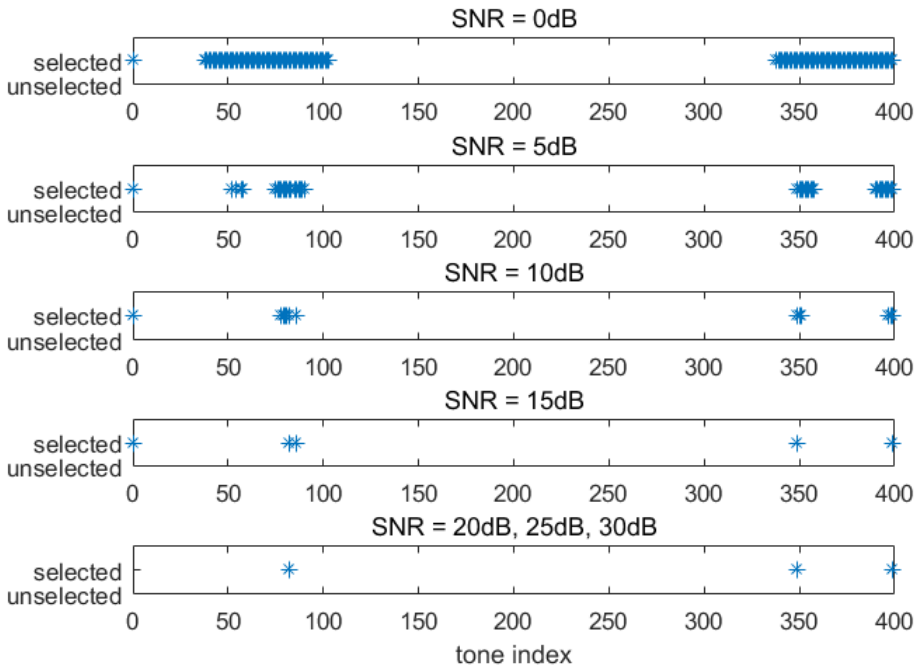

Figure 3.6: Distribution of selected tone for different SNRs in two paths with fixed time difference.

delay difference is higher. So when calculate the expectation of CRLB among range of delay difference, the CRLB in small delay difference is encouraged and makes the final CRLB value larger. With larger CRLB, the greedy algorithm tends to do fewer iterations and the number of tones selected will be larger.

In addition, the number of tones selected decreases while the distance step size increases. The reason is that the CRLB value is higher in small delay difference and when the Δd increases and the sampling rate decreases, the high CRLB value is not always sampled. Thus the calculated $G_{CRLB,11}(\hat{\tau}_0, \hat{\boldsymbol{\tau}_{grid}}|\mathbf{h}_M)$ becomes smaller and more tones will be discarded in selection procedure due to more iterations.

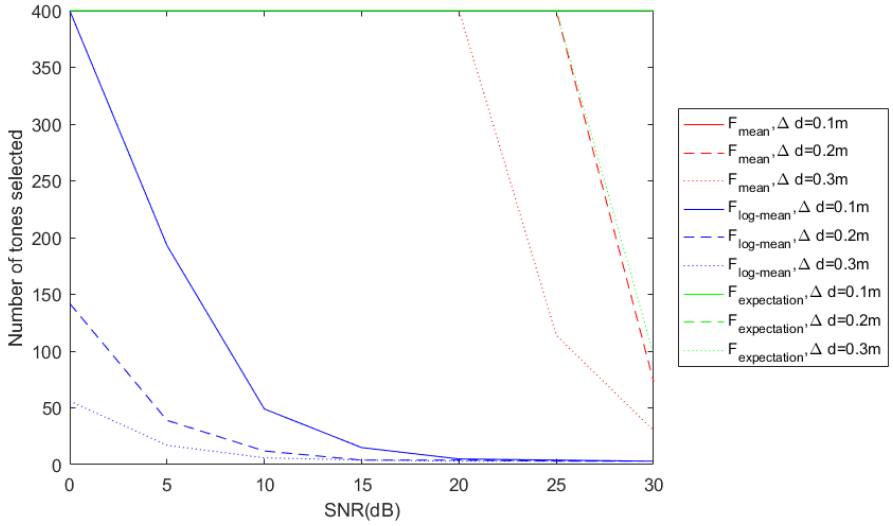

Figure 3.7: Number of elements in selected subset in two paths with various time difference for different SNRs, weighted mean functions, Δds with desired range accuracy $0.1 meter$.

Moreover, if we imagine that the subset selected is an antenna array, we can show the receiving characteristic of the subset. The beam pattern provides the receiving characteristics of the subset which is formed by the coherence calculated on the grid delay vector. (The coherence will be introduced in the Chapter 4.) Here we only use the subset selected in $SNR = 20dB$ and compare them with the full set C_{K_f} and subsets selected in the the single path and 2-path cases. The Beam patterns are provided in figure 3.10-3.13.

We can see that, the beam patterns provide the gain of each delay value in the receiving procedure. Compared to full set beam pattern, the beam patterns of all selected subsets has narrow main lobe and higher side lobes. Narrow main lobe will make the ranging process more accurate and has higher resolution in the scope of main lobe. But the high side lobes will make the estimated result erroneous in side lobe scope. For the single path case, 2-path case and $G_{CRLB,11}(\hat{\tau}_0, \hat{\boldsymbol{\tau}_{grid}}|\mathbf{h}_M)$ with $F_{log-mean}(\cdot)$, the first side lobe of their beam pattern is more close to the main lobe which may make the estimated results inaccurate if there exists non-LOS path with smaller $\Delta\tau$ in the environment. On the contrary, for $G_{CRLB,11}(\hat{\tau}_0, \hat{\boldsymbol{\tau}_{grid}}|\mathbf{h}_M)$ with $F_{mean}(\cdot)$ and $F_{expectation}(\cdot)$, their main lobe and side lobes are more separated. As a consequence, the

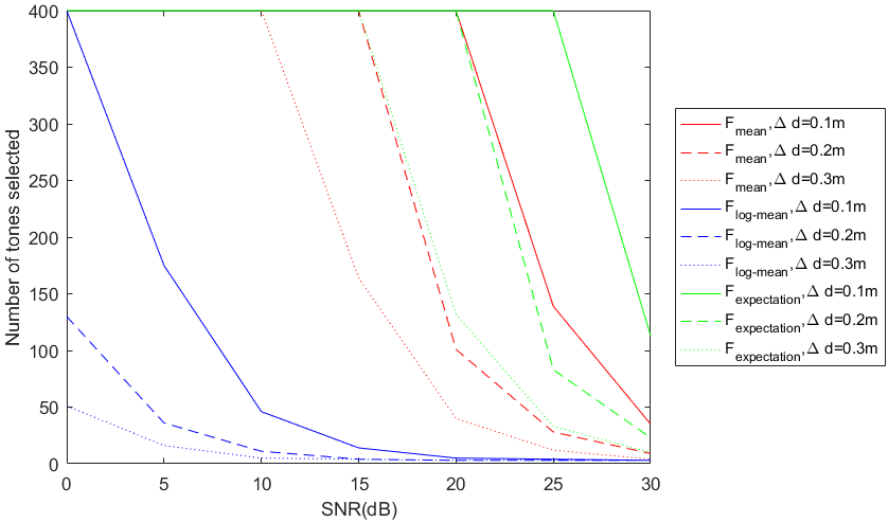

Figure 3.8: Number of elements in selected subset in two paths with various time difference for different SNRs, weighted mean functions, Δds with desired range accuracy $0.2meter$.

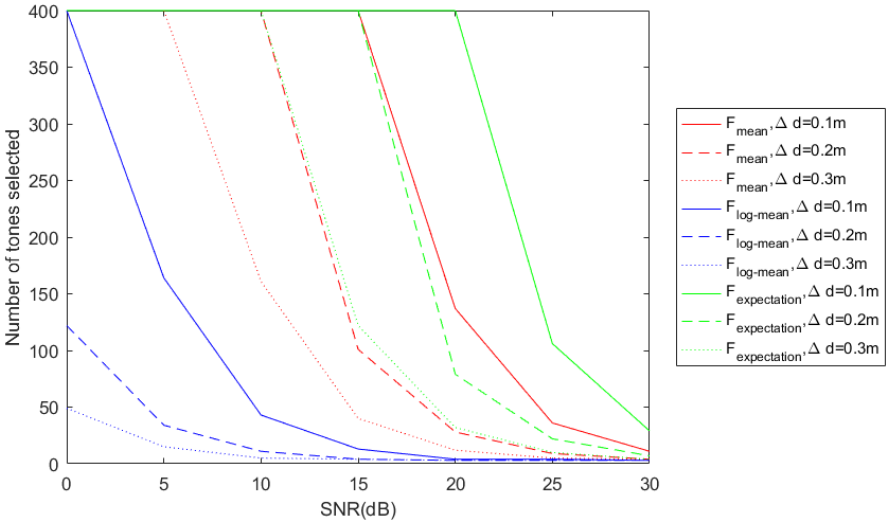

Figure 3.9: Number of elements in selected subset in two paths with various time difference for different SNRs, weighted mean functions, Δds with desired range accuracy $0.3meter$.

results will be inferential with existence of large delay difference in the environment.

3.4 Conclusion

In this chapter, we introduce the expression of Cramer-Rao lower bound and derive its calculation equation for single path case and 2-path case. Then we simplify the CRLB calculation of τ_0 in multiple paths environment to 2-path case with various time

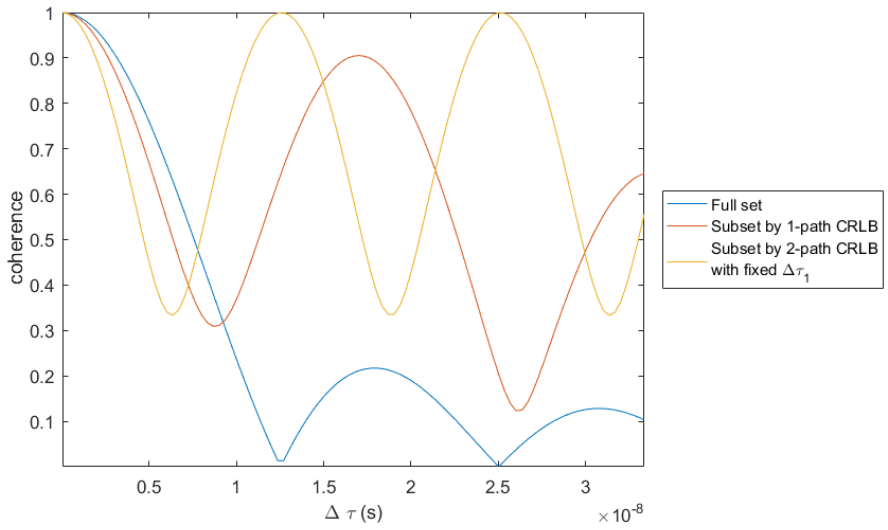

Figure 3.10: Beampattern comparison between full set and subsets selected with single path CRLB and 2-path CRLB with fixed delay difference.

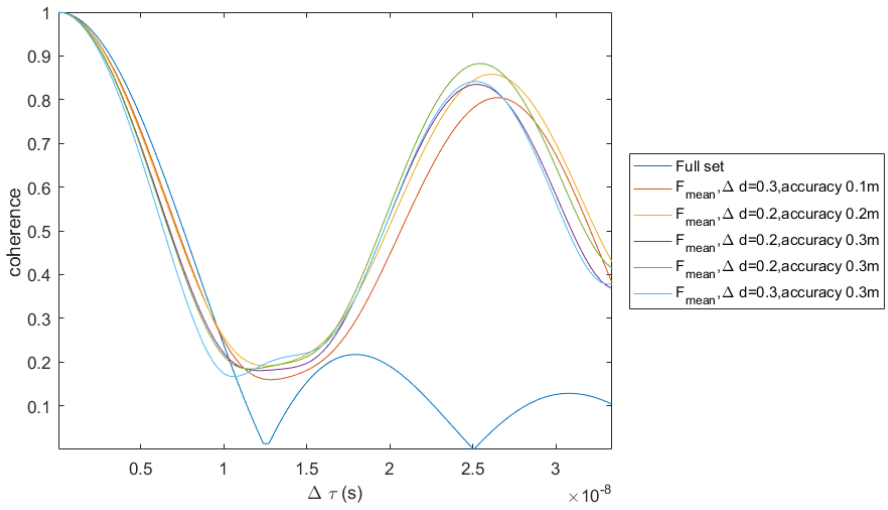

Figure 3.11: Beampattern comparison between full set and subsets selected with 2-path CRLB for $F_{mean}(\cdot)$, various delay difference and accuracy.

differences $\Delta\tau_{n0}$. By regarding the CRLB of τ_0 as the evaluation criterion, we are finally able to select the optimal tone subset using the greedy algorithm.

In the simulation, we get the following observation and analysis:

i) High SNR can reduce the number of tones used and the tones selected tend to distribute at both ends of the bandwidth to achieve the widest bandwidth during the measurement. It is because wide bandwidth is the key point to achieve accurate estimation which has been proved in Chapter 2.

ii) If the threshold is lower, i.e. the desired accuracy value is smaller, then more

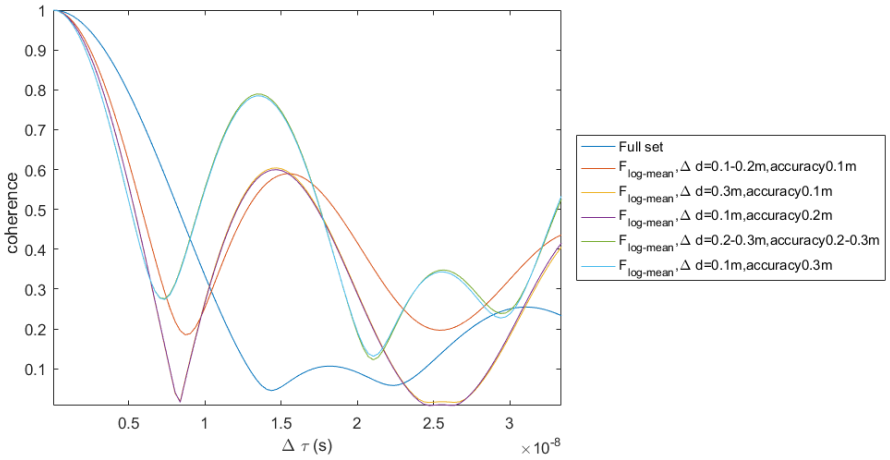

Figure 3.12: Beampattern comparison between full set and subsets selected with 2-path CRLB for $F_{log-mean}(\cdot)$, various delay difference and accuracy.

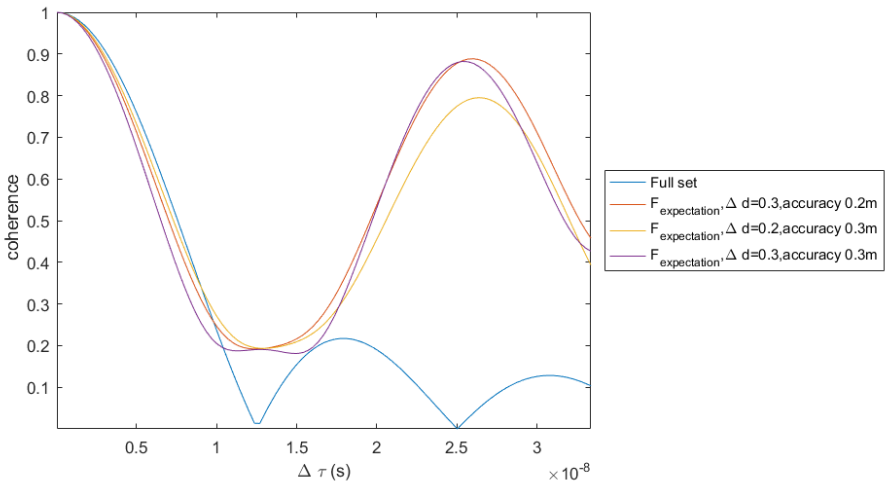

Figure 3.13: Beampattern comparison between full set and subsets selected with 2-path CRLB for $F_{expectation}(\cdot)$, various delay difference and accuracy.

tones need to be selected to receive more data and to reach the accuracy.

iii) If $F_{log-mean}(\cdot)$ is used, then much fewer tones will be selected compared to using $F_{mean}(\cdot)$ or $F_{expectation}(\cdot)$ because the $F_{log-mean}(\cdot)$ tends to make the CRLB of τ_0 smaller which will be more possible to be lower than the threshold. As a result, there will be more iterations of the algorithm and more tones will be discarded.

iv) The step size of grid delay vector during the calculation of the CRLB also influences the tone subset selection and larger step size tends to make the CRLB of τ_0 smaller because the high $G_{CRLB,11}(\hat{\tau}_0, \hat{\boldsymbol{\tau}}_{grid}|\mathbf{h}_M)$ is not always sampled.

v) Compared to the full set, the beam patterns of selected subsets have narrow main lobe and higher sidelobes. For single path case, 2-path case and $G_{CRLB,11}(\hat{\tau}_0, \hat{\boldsymbol{\tau}}_{grid}|\mathbf{h}_M)$ with $F_{log-mean}(\cdot)$, the sidelobes are more close to the mainlobe.

For $G_{CRLB,11}(\hat{\tau}_0, \hat{\boldsymbol{\tau}_{grid}}|\mathbf{h}_M)$ with $F_{mean}(\cdot)$ and with $F_{expectation}(\cdot)$, the mainlobe and the sidelobes are more separated. Based on the analysis of the beampatterns, the estimation procedure may have good resolution but will be influenced by the non-LOS path signal.

Generally speaking, if we want to reduce the number of tones used during multi-frequency ranging in multi-path environment and only consider the CRLB as the criterion, then, theoretically, we should use the $F_{log-mean}(\cdot)$ with large Δd as the function to calculated the CRLB of τ_0, decide a high desired accuracy and place the targets in high SNR environment to reach a better result. In the aspect of beampattern, if non-LOS paths exist and have small time difference with the LOS path, we should consider $G_{CRLB,11}(\hat{\tau}_0, \hat{\boldsymbol{\tau}_{grid}}|\mathbf{h}_M)$ with $F_{log-mean}(\cdot)$ as the selected criterion. If the non-LOS path has large $\Delta\tau$ compared to the τ_0 path, $G_{CRLB,11}(\hat{\tau}_0, \hat{\boldsymbol{\tau}_{grid}}|\mathbf{h}_M)$ with $F_{mean}(\cdot)$ and with $F_{expectation}(\cdot)$ should be used.

However, the subsets selected above are based on the 2-path CRLB while in our case, the ranging condition is multi-path. So the criterion, 2-path CRLB, may be not so efficient for practical use. Also, the beam pattern of the selected subsets are not good enough due to the high side lobes. As a consequence, in the next chapter, we are going to use another criterion, the matrix coherence to select the tone subset and in the Chapter 5, we will test the subsets' performance in real estimation procedure.

Optimal tone selection with matrix coherence

4

In the chapter 3, we utilize the CRLB as the evaluation criterion to solve the optimal tone selection problem as the target equation (1.5) is a typical estimation problem. But consider the solution in another point of view, reducing the number of tones used can be regarded as the dictionary construction problem in a compressive sensing (CS) procedure. Thus, in this chapter, we introduce the concept of CS theory, the dictionary matrix and the Restricted Isometry Property(RIP) at first. Then we use the matrix coherence to indicate the dictionary RIP and to construct the optimal dictionary matrix. The simulation results and conclusions are also provided.

4.1 Compressive sensing theory

Usually, when we sample a signal and want to recover it accurately through the samples, we need to follow the Nyquist rate, i.e. the sampling rate must not be lower than twice the maximum frequency in the signal. If we use fewer samples, the reconstruction problem will become an underdetermined linear system which do not have a unique solution. However, with the concept of compressive sensing, we are able to recover the signal from far few samples that transitional methods use. This is because CS utilizes the sparsity of the signal and is able to find a sparse solution of the underdetermined linear system which is unique. The detailed information of CS theory is provided below.

In classical compressive sensing theory, the final compressed signal $\mathbf{y}$ in received terminal can be expressed by:

$$\mathbf{y} = \mathbf{R}(C_m)\Phi\mathbf{f} \tag{4.1}$$

where $\mathbf{f}$ is a $q \times 1$ transmitted signal vector, Φ is the $q \times q$ measurement matrix. $m \times q$ selecting matrix $\mathbf{R}(C_m)$ extract samples according to the coordinates C_m to construct the final compressed signal $\mathbf{y}$ which has size $m \times 1$ and C_m is a subset of $\{0, 1, \cdots, q-1\}$. Clearly, $m < q$ and the sampling rate is lower than the Nyquist rate which make the equation (4.1) a underdetermined linear system having infinite solutions.

To be sure that we can find a unique solution of equation (4.1) by CS technology, the following fundamental premises must exist: [17][18]:

i) The signal $\mathbf{f}$ is sparse in some domain which can be expressed by:

$$\mathbf{f} = \Psi\mathbf{x} \tag{4.2}$$

where Ψ is a $q \times p$ sparse base and $\mathbf{x}$ is a $p \times 1$ $k - sparse$ signal which means $\mathbf{x}$ only has k non-zero elements, $k \leq m < q \leq p$.

Then equation (4.1) ran be rewritten as:

$$\mathbf{y} = \mathbf{R}(C_m)\Phi\mathbf{f} = \mathbf{R}(C_m)\Phi\Psi\mathbf{x} = \mathbf{R}(C_m)\mathbf{A}\mathbf{x} = \mathbf{A'}(C_m)\mathbf{x} \tag{4.3}$$

where $\mathbf{A}$ is the full dictionary with size $q \times p$ and $\mathbf{A'}(C_m) = \mathbf{R}(C_m)\mathbf{A} = \mathbf{R}(C_m)\Phi\Psi$ is the compressed dictionary with size $m \times p$.

ii) The compressed dictionary must have enough Restricted Isometry Property (RIP) to make sure its columns have incoherence.

If the above requirements are meet, then after receiving $\mathbf{y}$, reconstruction methods will be used to recover sparse signal $\mathbf{x}$ uniquely and original data $\mathbf{f}$ can be obtained via equation (4.2).

To apply the compressive sensing method to the multi-frequency ranging case, we can assume the measurement matrix Φ is a unit matrix and regard the $\mathbf{h}_{K_f}$ as $\mathbf{f}$ in equation (4.2). Then $\mathbf{h}_{K_f}$ should be sparse in a domain, so we regard the $\mathbf{a}(\mathbf{r}_N)$ and $\mathbf{Z}_{K_f}$ in equation (4) as the $\mathbf{x}$ and Ψ in equation (4.2) respectively. But the $\mathbf{x}$ is a sparse vector while $\mathbf{a}(\mathbf{r}_N)$ is not. To build a sparse vector, we can set a grid vector of distance $\mathbf{r}_{grid} = [r_{g1}, r_{g2}, r_{g3}, ...]$ and $\mathbf{a}(\mathbf{r}_{grid})$ contains amplitudes of paths at grid points. Multi-path distance $\mathbf{r}_N$ are all at the grid point and the corresponding amplitudes in $\mathbf{a}(\mathbf{r}_{grid})$ are non-zero while the other elements in $\mathbf{a}(\mathbf{r}_{grid})$ are zeros.For example, if the paths are $\mathbf{r}_N = [4, 9, 17]m$ in the multi-path condition, the $\mathbf{a}(\mathbf{r}_{grid})$ will be:

$$\mathbf{a}(\mathbf{r}_{grid}) = \begin{bmatrix} 0 & ... & 0 & a(4) & 0 & ... & 0 & a(9) & 0 & ... & 0 & a(17) & 0 & ... \end{bmatrix}^T \tag{4.4}$$

Thus the new grid amplitude vector $\mathbf{a}(\mathbf{r}_{grid})$ is sparse and meets the requirement of compressive sensing. The grid dictionary $\mathbf{Z}'_{K_f}$ can be expressed by:

$$\mathbf{Z}'_{K_f} = \begin{bmatrix} \mathbf{z}_{K_f}(\tau_{g0}) & \mathbf{z}_{K_f}(\tau_{g1}) & \mathbf{z}_{K_f}(\tau_{g2}) & ... \end{bmatrix} \tag{4.5}$$

where $\boldsymbol{\tau}_{grid} = [\tau_{g1}, \tau_{g2}, \tau_{g3}, ...] = \frac{\mathbf{r}_{grid}}{c}$. And the final vector $\mathbf{h}_{K_f}$ will not be influenced by the zeros:

$$\mathbf{h}_{K_f} = \mathbf{Z}_{K_f}\mathbf{a}(\mathbf{r}_N) + \mathbf{n} = \mathbf{Z}'_{K_f}\mathbf{a}(\mathbf{r}_{grid}) + \mathbf{n} \tag{4.6}$$

The compressed received signal $\mathbf{h}_M$ can be regarded as $\mathbf{y}$ in the equation (4.3) and is written by:

$$\begin{aligned} \mathbf{h}_M &= \mathbf{R}(C_M)\Phi\mathbf{h}_{K_f} + \mathbf{n} \\ &= \mathbf{R}(C_M)\mathbf{Z}'_{K_f}\mathbf{a}(\mathbf{r}_{grid}) + \mathbf{n} \\ &= \mathbf{Z}'_M\mathbf{a}(\mathbf{r}_{grid}) + \mathbf{n} \end{aligned} \tag{4.7}$$

where matrix $\mathbf{R}(C_M)$ extracts rows in full dictionary $\mathbf{Z}'_{K_f}$ according to the sampled coordinate information in C_M, C_M has been introduced in the introduction which is a subset of $\{0, 1, \cdots, K_f - 1\}$, noise vector $\mathbf{n}$ has size $M \times 1$, $\mathbf{Z}'_M = \mathbf{R}(C_M)\mathbf{Z}'_{K_f}$ is the compressed grid dictionary matrix. Then, in our case, the distance information can be extracted from the estimated $\hat{\mathbf{h}}_{K_f}$ via reconstruction algorithm with known $\mathbf{h}_M$ and $\mathbf{Z}_M$.

As motioned before, to have a unique sparse solution of equation (4.1), one of the requirements is that the compressed dictionary must have enough RIP to make sure its column have incoherence, i.e. its columns have low coherence. Then in the

following, the concept of RIP will be introduced and several criteria that can indicate the coherence of CS dictionary will be provided.

4.2 Optimal dictionary matrix

In real world, the target signal can not always be sparse and there are always noises and perturbations. Thus the robustness of CS is necessary to accurately recover signals from few measurements and noises. As stated in [17], the robustness of CS procedure is based on two fundamental elements: the sparsity of the compressived signal and the RIP of the compressed dictionary. For each integer $k = 1, 2, ...$, the isometry constant δ_k is defined by:

$$(1 - \delta_k)\|\mathbf{x}\|_{\ell_2}^2 \leq \|\mathbf{A'}(C_m)\mathbf{x}\|_{\ell_2}^2 \leq (1 + \delta_k)\|\mathbf{x}\|_{\ell_2}^2 \tag{4.8}$$

where $\mathbf{x}$ is a $k - sparse$ vector.

Then if the constant δ_k is not too close to 1, we can say that the matrix $\mathbf{A'}(C_m)$ obeys RIP loosely. As a consequence, matrix $\mathbf{A'}(C_m)$ can approximately preserve the Euclidean length of the signal $\mathbf{x}$ and $\mathbf{x}$ is not in the null-space of $\mathbf{A'}(C_m)$. Briefly speaking, we can also say that all subsets extracting columns from $\mathbf{A'}(C_m)$ are nearly orthogonal. When it comes to the signal compression and recover, it is proved that if $\mathbf{A'}(C_m)$ has RIP, there exists robust and efficient algorithms to recover the sparse signal from limited CS measurements[17]. Thus, RIP can be a sufficient evaluation metric to our selection problem. As RIP guarantees the incoherence among columns of the compressed dictionary, the coherence of matrix $\mathbf{Z}'_M$ can be a good indicator of the dictionary RIP and low coherence is the goal we want to achieve.

4.2.1 Coherence calculation

Main indicators of the matrix coherence are the mean coherence and the maximal coherence of the matrix.

i) Mean coherence

If we would like to reduce the average coherence among all possible column pairs in the matrix, the $G_{Co-mean}(C_M, \boldsymbol{\tau}_{grid})$ could be used as the criterion to indicate matrix coherence, where $\boldsymbol{\tau}_{grid}$ is the delay grid vector, $\boldsymbol{\tau}_{grid} = [\tau_{g1}, \tau_{g2}, \tau_{g3}, ...]$. The coherence of two columns in the compressed grid dictionary matrix $\mathbf{Z}'_M$ can be calculated by:

$$\mu(C_M, n, n') = |\mathbf{z}'_M(\tau_{gn})^H \mathbf{z}'_M(\tau_{gn'})| \tag{4.9}$$

where $\mathbf{z}'_M(\tau_{gn})$ is the n-th column of matrix $\mathbf{Z}'_M$ and τ_{gn} is the $n - th$ elements in the delay grid vector $\boldsymbol{\tau}_{grid}$, $n, n' \geq 1, n \neq n'$.

As the matrix $\mathbf{Z}'_M$ is constructed as follows:

$$\begin{aligned}\mathbf{Z}'_M &= \begin{bmatrix} z(\tau_{g1})^{b_0} & z(\tau_{g2})^{b_0} & z(\tau_{g3})^{b_0} & ... \\ z(\tau_{g1})^{b_1} & z(\tau_{g2})^{b_1} & z(\tau_{g3})^{b_1} & ... \\ \vdots & \vdots & \ddots & \vdots \\ z(\tau_{g1})^{b_{M-1}} & z(\tau_{g2})^{b_{M-1}} & z(\tau_{g3})^{b_{M-1}} & ... \end{bmatrix} \\ &= \begin{bmatrix} e^{-j2b_0\pi\Delta f\tau_{g1}} & e^{-j2b_0\pi\Delta f\tau_{g2}} & e^{-j2b_0\pi\Delta f\tau_{g3}} & ... \\ e^{-j2b_1\pi\Delta f\tau_{g1}} & e^{-j2b_1\pi\Delta f\tau_{g2}} & e^{-j2b_1\pi\Delta f\tau_{g3}} & ... \\ \vdots & \vdots & \ddots & \vdots \\ e^{-j2b_{M-1}\pi\Delta f\tau_{g1}} & e^{-j2b_{M-1}\pi\Delta f\tau_{g2}} & e^{-j2b_{M-1}\pi\Delta f\tau_{g3}} & ... \end{bmatrix}\end{aligned} \tag{4.10}$$

where $b_0, b_1, ..., b_{M-1} \in C_M$, we can rewrite the equation (4.9):

$$\mu(C_M, n, n') = \sum_{b \in C_M} e^{-j2b\pi\Delta f(\tau_{gn} - \tau_{gn'})} \tag{4.11}$$

which means that the coherence of two columns in the $\mathbf{Z}'_M$ only depends on their time difference $\tau_{gn} - \tau_{gn'}$ and the subset C_M which is similar to the CRLB calculation of two paths. So we also use $\Delta\tau_{gn} = \tau_{gn} - \tau_{g1}$ to denote the time difference between the first column and the other column, $n \geq 1$. Then we have:

$$\mu(C_M, \Delta\tau_{gn}) = \sum_{b \in C_M} e^{-j2b\pi\Delta f\Delta\tau_{gn}} \tag{4.12}$$

and the mean value of the coherence of the compressed dictionary matrix can be written as:

$$G_{Co-mean}(C_M, \boldsymbol{\tau}_{grid}) = \frac{1}{N_{grid} - 1} \sum_{\Delta\tau_{gn}} \mu(C_M, \Delta\tau_{gn}) = \frac{1}{N_{grid} - 1} \sum_{\Delta\tau_{gn}} \sum_{b \in C_M} e^{-j2b\pi\Delta f\Delta\tau_{gn}} \tag{4.13}$$

where N_{grid} is the number of elements in the delay grid vector $\boldsymbol{\tau}_{grid}$.

ii) Maximal coherence

If we would like to reduce the maximum of the matrix coherence, the maximal coherence could be used as the criterion which is calculated by:

$$G_{Co-max}(C_M, \boldsymbol{\tau}_{grid}) = \max_{n,n' \geq 1, n \neq n'} |\mathbf{z}_M(\tau_{gn})^H \mathbf{z}_M(\tau_{gn'})| \tag{4.14}$$

There also exists following lower bound of $G_{Co-max}(C_M, \boldsymbol{\tau}_{grid})$ for matrix $\mathbf{Z}'_M$ with $N_{grid} \geq M$ [35]:

$$G_{Co-max}(C_M, \boldsymbol{\tau}_{grid}) \geq \sqrt{\frac{N_{grid} - M}{(N_{grid} - 1)M}} \tag{4.15}$$

with equality if and only if $\sum_{\tau_{gn}} \mathbf{z}_M(\tau_{gn}) \mathbf{z}_M(\tau_{gn})^H = \frac{N_{grid}}{M}\mathbf{I}$, i.e. coherence among all possible column pairs are equal.

The above bounds are known as the Welch lower bound which is more useful for small N_{grid}. For large N_{grid}, a tighter composite lower bound on $G_{Co-max}(C_M, \boldsymbol{\tau}_{grid})$ is proposed in [36]:

$$G_{Co-max}(C_M, \boldsymbol{\tau}_{grid}) \geq \max(\sqrt{\frac{N_{grid} - M}{(N_{grid} - 1)M}}, 1 - 2N_{grid}^{-\frac{1}{M-1}}) \tag{4.16}$$

In addition, [36] has proved that if the full dictionary $\mathbf{Z}'_{K_f}$ is a complete FFT matrix, difference set can be used as the subset C_M and the matrix $\mathbf{Z}'_M$ will reach the Welch bound. The difference set is defined as follows: If $M(M-1)$ differences $p - p'$ take all possible values $1, 2, ..., N_d - 1$ for λ times, then the subset $C_M \subset C_{K_f}$ is called a (N_d, M, λ) difference set. With proper delay step size, we can guarantee that the matrix $\mathbf{Z}'_{K_f}$ is complete and has orthogonality. Then we can apply the difference set in our optimal dictionary construction.

4.2.2 Selection algorithm for optimal dictionary construction

In the optimal dictionary construction, if we use the mean coherence $G_{Co-mean}(C_M, \boldsymbol{\tau}_{grid})$ as the evaluation criterion, we can see that the coherence of the matrix is not monotonic with the number of elements in C_M. So it is not possible to use the greedy algorithm here. And if we use the exhaust search to find the subset with minimal $G_{Co-mean}(C_M, \boldsymbol{\tau}_{grid})$, the subsets of the full set C_{K_f} will be too many and the time used to test all these subsets is unacceptable. Thus we have to use the random search algorithm to find a sub-optimal solution and we need to change the target optimization function (5) to fit this case:

$$\min G_{Co-mean}(C_M, \boldsymbol{\tau}_{grid}) \tag{4.17}$$

The random search algorithm for subset selection based on $G_{Co-mean}(C_M, \boldsymbol{\tau}_{grid})$ is provided in Algorithm 3.

Algorithm 3 Greedy algorithm for optimal dictionary construction using criterion $G_{Co-mean}(C_M)$

Input: original full set C_{K_f}, range and step size of delay grid vector $\boldsymbol{\tau}_{grid}$), frequency step size Δf, stage number $w = 1$, $G_{Co-mean-tres} = 1$

Output: Optimal subset C_M

1: In stage w, choose a subset $C_w \subset C_{K_f}$ randomly which has more than 4 elements and calculate the $G_{Co-mean}(C_w, \boldsymbol{\tau}_{grid})$.
2: If $G_{Co-mean}(C_w, \boldsymbol{\tau}_{grid})$ is smaller than $G_{Co-mean-tres}$, set $G_{Co-mean-tres} = G_{Co-mean}(C_w, \boldsymbol{\tau}_{grid})$ and $C_M = C_w$, $w = w + 1$;
3: If not, $w = w + 1$.
4: If $w > 10^8$, end the algorithm and out put the final selection C_M. If not, go to step 1.

As for the other metric, the maximal coherence, we can use existing difference set as the dictionary index which can reach the Welch bound. The maximal number of

frequencies used in our report is 400, so we find a difference set $(400, 57, 8)$ which meets our requirement and can be used in the following simulations. It is noteworthy that there exist multiple difference sets with $N_d = 400$ theoretically but only the difference set $(400, 57, 8)$ is known. That is reason why we only use difference set $(400, 57, 8)$ in the simulation here.

4.3 Simulation Result

In the simulation, we still use Matlab as the simulation software and use criteria $G_{Co-mean}(C_M, \boldsymbol{\tau}_{grid})$ and $G_{Co-max}(C_M, \boldsymbol{\tau}_{grid})$ as the evaluation metrics. The selection results are provided in this section.

At first, we set the delay grid vector $\boldsymbol{\tau}_{grid} = \frac{[0,0.1,...,10.0]m}{c}$ where $c = 3 \times 10^8 m/s$. Then we provide the beam pattern of full set matrix $\mathbf{Z}'_{K_f}$ in figure 4.1:

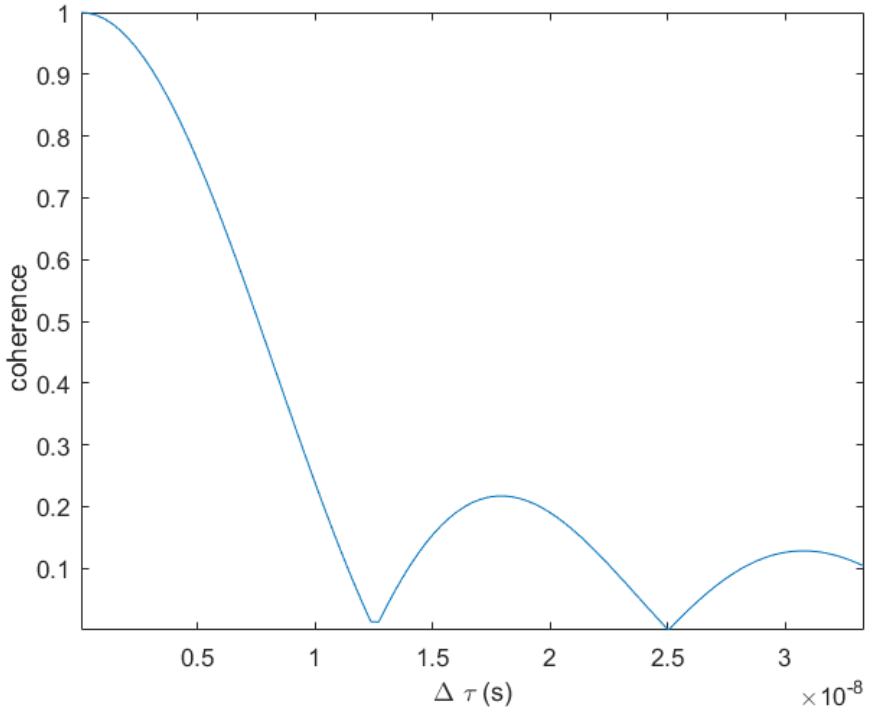

Figure 4.1: Beampattern of full set matrix $\mathbf{Z}'_{K_f}$ in grid step size $\frac{0.1m}{c}$.

For $G_{Co-mean}(C_M, \boldsymbol{\tau}_{grid})$, with $K_f = 400$, $\Delta f = 200kHz$, we can obtain a sub-optimal selection of tones using random search algorithm and the selected subset has 9 elements. The distribution of the subset is shown in figure 4.2.

For $G_{Co-max}(C_M, \boldsymbol{\tau}_{grid})$, to reach the Welch bound, we need to construct a complete FFT dictionary matrix. Thus the delay grid vector should have step size $\frac{1}{Bandwidth} = 1.25 \times 10^{-8} s$, so we have $\boldsymbol{\tau}_{grid} = [0, 1.25, 2.50, ..., 498.75] \times 10^{-8} s$. The different set used as the C_M here is $(400, 57, 8)$. With $K_f = 400$, $c = 3 \times 10^8 m/s$, $\Delta f = 200kHz$, the C_M element distribution and beam-pattern are presented in figure 4.3 and 4.4. As we can

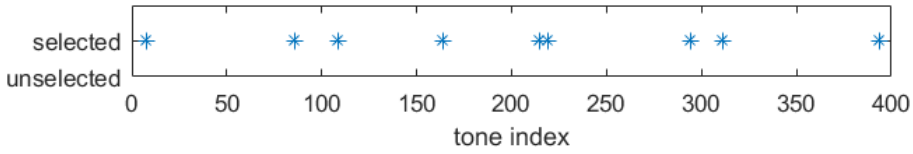

Figure 4.2: Distribution of elements in selected subset using criterion $G_{Co-mean}(C_M, \boldsymbol{\tau}_{grid})$.

see in figure 4.4, the beam-pattern of difference set $(400, 57, 8)$ conforms to the analysis in the above section that the $\mu(C_M, n, n')$ for all possible (n, n') pairs are equal.

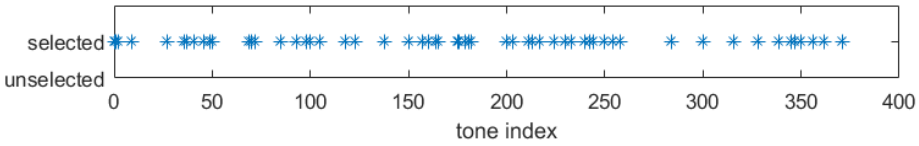

Figure 4.3: Distribution of elements in difference set $(400, 57, 8)$.

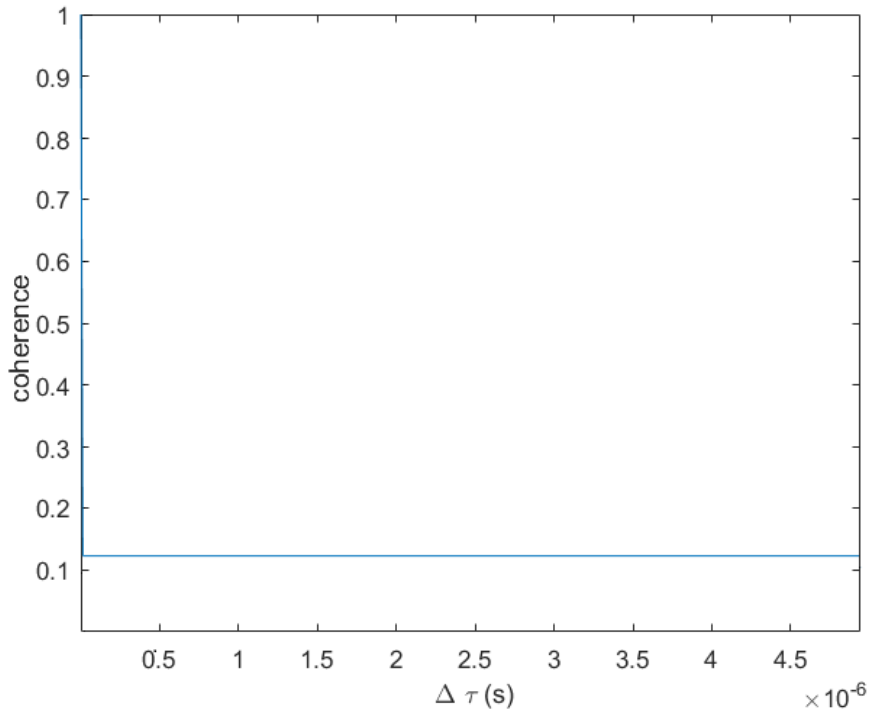

Figure 4.4: Beampattern of matrix $\mathbf{Z}'_M$ using difference set $(400, 57, 8)$ in grid step size $\frac{1}{Bandwidth} = 1.25 \times 10^{-8} s$.

The beampattern of full set matrix and subsets selected above are provided in figure 4.5. In the figure, the delay grid step size is $\frac{0.1m}{c}$. As shown, difference set and subset selected by $G_{Co-mean}(C_M, \boldsymbol{\tau}_{grid})$ has wider main lobe and lower side lobes compared

to the full set. The side lobes of subset selected by $G_{Co-mean}(C_M, \boldsymbol{\tau}_{grid})$ is lowest as it needs to reach a low coherence in the whole range. We can also see that the rightmost part of the yellow line seems to be rising outside the grid vector range. It is the $G_{Co-mean}(C_M, \boldsymbol{\tau}_{grid})$ only supress the sidlobes and the whole beam pattern in the grid vector range which is the range of interest. For the part outside our target range, the beampattern may be poor but it is out of our consideration. In addition, compared to the figure 4.2, the beam pattern line of difference set in figure 4.4 is different which is caused by the different delay grid step sizes in grid vector.

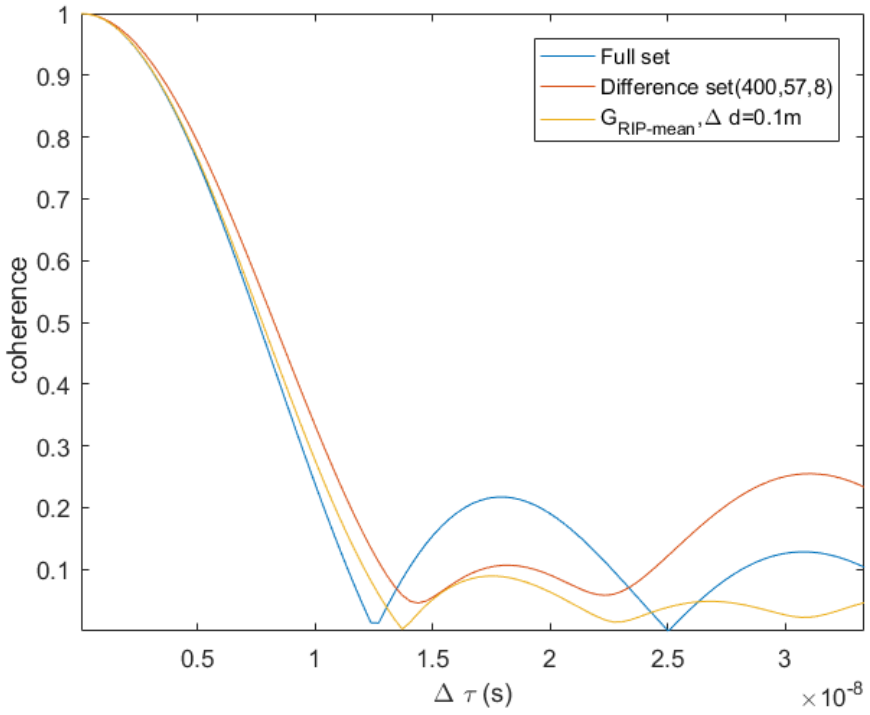

Figure 4.5: Beampatterns of full set and selected subsets using RIP as the criterion.

4.4 Conclusion

In this section, we introduce the theory of compressive sensing and the concept of Restricted Isometry Property of dictionary matrix. Then we use the coherence of matrix to indicate the dictionary RIP and to construct the optimal CS dictionary $\mathbf{Z}'_M$. Based on the criteria, the mean coherence and the maximal coherence, two subsets are obtained.

If we use the $G_{Co-mean}(C_M, \boldsymbol{\tau}_{grid})$ as the criterion, we will obtain a subset with 9 elements by random search algorithm. The beam pattern of the selected subset has wider main lobe and low side lobes in the target range (grid vector range) compared to full set.

If we use the maximal coherence as the evaluation metric, there exists a lower bound

of maximal coherence which is known as Welch bound and we can only reach the Welch bound when using difference set. In this report we use the difference set $(400, 57, 8)$ as the subset C_M and for delay grid step size $\frac{0.1m}{c}$, the beam pattern of difference set has wider main lobe and lower sidelobes compared to the full set beam pattern.

However, the selected subsets based on various criteria are theoretically optimal. Their real performances in data reconstruction procedure is unknown. Thus we will test the performance of the subset in data recover and estimation procedure in the next Chapter.

Optimal subset performance test by gridless compressive sensing

5

To see the performance of the selected subsets, we will use them to construct the dictionary matrix and use the dictionary to recover the original data to achieve indoor ranging. The accuracy of the estimated distance will be the performance indicator. The used reconstruction algorithm will be gridless compressive sensing algorithm which will be introduced in the next section.

5.1 Gridless compressive sensing algorithms

As mentioned in the introduction, the traditional CS reconstruction method deals with the linear atom decomposition problem with finite atom candidates, which may cause atom grid. To offset the possible error and ambiguity caused by the grid, we may increase the sampling rate to make the grid dense enough to meet our accuracy. But the additional computational load will be higher. To solve the grid problem efficiently, some gridless reconstruction algorithms are proposed recently. In this section, 2 typical gridless reconstruction algorithms, NL-GMF and ANM are introduced and implemented.

5.1.1 Noiseless global matched filter

To introduce the Noiseless Global matched filter(NL-GMF) more clearly, we need to introduce its base, the Basis Pursuit (BP) method[37] at first.

Suppose that the compressed received signal $\mathbf{h}_M$ can be decomposed to the column elements $\mathbf{z}_M(\tau_n)$ in matrix $\mathbf{Z}_M$ with amplitudes $\hat{a}(r_0), \hat{a}(r_1), ..., \hat{a}(r_\beta)$, and β can be arbitrary:

$$\mathbf{h}_M = \sum_{n=0}^{\beta} \hat{a}(r_n)\mathbf{z}_M(\tau_n) \tag{5.1}$$

Then if we can not use the atoms (column element) fewer than β to decompose the signal $\mathbf{h}_M$, then the above atomic decomposition is called ideal. And the ideal atomic decomposition of number n or other smaller number is unique if any column subsets of $\mathbf{Z}_M$ with 2β atoms is linearly independent. In our case, the number of columns is finite, $\mathbf{Z}_M = [\mathbf{z}_M(\tau_0), \mathbf{z}_M(\tau_1), ..., \mathbf{z}_M(\tau_{N-1})]$, $\beta = N - 1$, we can only solve the decomposition problem by solving the proximal convex optimization:

$$\begin{aligned} &\min_{\mathbf{a}_N} \sum_{n=1}^{N-1} |\hat{a}(r_n)| \\ &\text{s.t. } \mathbf{h}_M = \mathbf{Z}_M \hat{\mathbf{a}}(\mathbf{r}_N) \end{aligned} \tag{5.2}$$

where $\hat{\mathbf{a}}(\mathbf{r}_N)$ is a $N \times 1$ amplitude vector. And solving the above optimization problem is known as Basis Pursuit method which aims to use few atoms to decompose received signal.

To make sure the BP solution is the ideal decomposition, the dictionary $\mathbf{Z}_M$ with finite number of columns must obey RIP[23] and then we have to face the atom grid problem. Noiseless Global matched filter is proposed then in [23] to solve the atom grid problem in data recover procedure using an equivalent dual form of the BP method. It is proved that the vector $\hat{\mathbf{a}}(\mathbf{r}_N)$ is the optimal solution of equation (5.2) iff $\mathbf{h}_M = \mathbf{Z}_M \hat{\mathbf{a}}(\mathbf{r}_N)$ and there exists a vector $\mathbf{g}$ containing the dual parameters such that:

$$\begin{cases} |\mathbf{z}_M(\tau_n)^H \mathbf{g}| \leq 1, \hat{a}(r_n) = 0 \\ \mathbf{z}_M(\tau_n)^H \mathbf{g} = \gamma_n = \frac{\hat{a}(r_n)}{|\hat{a}(r_n)|}, \hat{a}(r_n) \neq 0 \end{cases} \tag{5.3}$$

for all $n = 0, 1, ..., N-1$ where vector $\mathbf{g}$ has size $M \times 1$. The above conclusion is named by Dual Null Space Property(DNSP) which also applies to dictionary with infinite columns. And the BP method in equation (5.2) can be rewritten as follows using the dual parameter vector:

$$\begin{aligned} &\max_{\mathbf{g}} \ \Re(\mathbf{g}^H \mathbf{h}_M) \\ &\text{s.t. } \forall n, \mathbf{z}_M(\tau_n)^H \mathbf{g}| \leq 1 \end{aligned} \tag{5.4}$$

The above optimization problem is the target function to be solved by NL-GMF method. And the local search algorithm to implement the optimization procedure is provided:

Algorithm 4 NL-GMF

Input: All-zero vector $\mathbf{g}_0$, maximal iteration number w_{max}, iteration index $w = 1$, step size ϵ small enough

Output: Estimated time delay $\tau_0, \tau_1, ...$

1: Calculate the spectrum $J_{NL-GMF}(\tau) = |\mathbf{z}_M(\tau)^H \mathbf{g}_{w-1}|$ and find the peak points in the spectrum.
2: Find the peak points $\tau_0, \tau_1, ...$ that $J_{NL-GMF}(\tau) > 1$.
3: Compute a feasible direction ξ and update the vector $\mathbf{g}_w = \mathbf{g}_{w-1} + \epsilon\xi$. So that the $J_{NL-GMF}(\tau_0), J_{NL-GMF}(\tau_1), ...$ decrease and $\Re(\mathbf{g}^H \mathbf{h}_M)$ increases.
4: $w = w + 1$. If $w > w_{max}$, end the algorithm and output the peaks $\tau_0, \tau_1, ...$ in $J_{NL-GMF}(\tau) = |\mathbf{z}_M(\tau)^H \mathbf{g}_{w-1}|$. If not, go to step one.

But as we can see, the NL-GMF is derived in noiseless condition which may not be so robust in our noisy multi-path environment. So we also use another gridless reconstruction algorithm, atomic norm minimization, as the comparison.

5.1.2 Atomic norm minimization

Except using the concept of dual vector, in [19], the concept of atomic norm is used to solve the gridless reconstruction problem. Similar to the atom concept in NL-GMF

method, here we assume that the dictionary matrix $\mathbf{Z}_{K_f}$ consists of atoms $\mathbf{z}_{K_f}(\tau_n)$ for $n \in \mathcal{N}$ and $\mathbf{h}_{K_f} = \sum_{n=0}^{N-1} \hat{a}(r_n)\mathbf{z}_{K_f}(\tau_n)$. Then the atomic norm of the received signal is defined by:

$$\begin{aligned} \|\mathbf{h}_{K_f}\|_{\mathbf{Z}_{K_f}} &= \inf\{t > 0 : \mathbf{h}_{K_f} \in t\text{conv}(\mathbf{Z}_{K_f}))\} \\ &= \inf_{\hat{a}(r_n)\geq 0} \left\{ \sum_{n=0}^{N-1} \hat{a}(r_n) : \mathbf{h}_{K_f} = \sum_{n=0}^{N-1} \hat{a}(r_n)\mathbf{z}_{K_f}(\tau_n) \right\} \end{aligned} \tag{5.5}$$

The atomic norm forces the matrix $\mathbf{Z}_{K_f}$ to have less elements. Then we can do the semidefinite programming characterization of the atomic norm:

$$\|\mathbf{h}_{K_f}\|_{\mathbf{Z}_{K_f}} = \inf \left\{ \frac{1}{2K_f}\text{trace}(\text{Toep}(\mathbf{u})) + \frac{1}{2}t : \begin{bmatrix} \text{Toep}(\mathbf{u})) & \mathbf{h}_{K_f} \\ \mathbf{h}_{K_f}^H & t \end{bmatrix} \succeq 0 \right\} \tag{5.6}$$

where $\text{Toep}(\mathbf{u})$ denotes the Toeplitz matrix whose first column is the vector $\mathbf{u}$, $\mathbf{u}$ and t are intermediate variables.

To compress the received the received signal vector $\mathbf{h}_{K_f}$ which has K_f elements, we discard $K_f - M$ elements of the signal (actually we do not measure these discarded elements during sensing procedure and the technology is called compressive sensing) and the compressed received signal becomes sparse. The index of the preserved elements is $C_M \subset C_{K_f}$ Then we can utilize the sparsity of the signal and solve the following minimization problem to construct it:

$$\begin{aligned} &\min_{\hat{\mathbf{h}}_{K_f}} \|\hat{\mathbf{h}}_{K_f}\|_{\mathbf{Z}_{K_f}} \\ &\text{s.t. } h_{b_n} = \hat{h}_{b_n}, \text{for all } b_n \in C_M \end{aligned} \tag{5.7}$$

which can also be written as:

$$\begin{aligned} &\min_{\mathbf{u},\hat{\mathbf{h}}_{K_f},t} \frac{1}{2K_f}\text{trace}(\text{Toep}(\mathbf{u})) + \frac{1}{2}t \\ &\text{s.t. } \begin{bmatrix} \text{Toep}(\mathbf{u})) & \hat{\mathbf{h}}_{K_f} \\ \hat{\mathbf{h}}_{K_f}^H & t \end{bmatrix} \succeq 0 \\ &\quad h_{b_n} = \hat{h}_{b_n}, \text{for all } b_n \in C_M \end{aligned} \tag{5.8}$$

After obtaining the recovered signal $\hat{\mathbf{h}}_{K_f}$ we can use the MUSIC algorithm to extract the distance information.

5.2 Test results in simulated data

In the subset performance test, we first use the subsets obtained in the previous Chapters in simulated data. The used subsets are all selected in $SNR = 20dB$. The

algorithms used to test are the NL-GMF and the ANM algorithm which has been introduced above. For convenience, we number the subsets in the appendix B and provide their elements.

i) Selected subset performance in 2-path case and 3-path case

At first, we test the selected subsets by using them to estimate target distance in 2-path environment and 3-path environment. The parameters are set as: $K_f = 400$, $c = 3 \times 10^8 m/s$, $\Delta f = 200kHz$, $\epsilon = 0.0003$, $w_{max} = 1000$. The signal energy $E_s = 1$ for each path and the SNR is $20dB$. The delay step size of steering vector in MUSIC algorithm is $10^{-10}s$ and the search range is $[0, 10^{-7}]s$. The NL-GMF algorithm is repeated 100 times for each subset and ANM algorithm repeats 6 times for each subset. And we take the mean square error (MSE) among the results and count the number of result with error smaller than 0.3m to calculate the successful estimation probability: $P_{suc-est} = \frac{\text{number of results with error less than 0.3m}}{\text{number of all results}}$. We also set $\mathbf{r}_N = [4, 9]m$ and $\mathbf{r}_N = [4, 9, 17]m$ respectively to see the influence of environment condition. The table 5.1 provides the MSE and successful estimation probability of the estimated distance with 2-path environment and the table 5.2 provides the MSE and successful estimation probability of the estimated distance with 3-path environment.

Set number	M	NL-GMF		ANM	
		MSE(m^2)	$P_{suc-est}$	MSE(m^2)	$P_{suc-est}$
Full set	400	0.2156	98%	0.0002	100%
subset1	3	30.6656	0%	33.9424	0%
subset2	3	2.0961	92%	6.8957	0%
subset3	137	0.0005	100%	0.0003	100%
subset4	101	0.0004	100%	0.0003	100%
subset5	28	0.0096	100%	0.0015	100%
subset6	40	0.0058	100%	0.0014	100%
subset7	12	0.0182	100%	0.0089	100%
subset8	79	0.0012	100%	0.0004	100%
subset9	132	0.0004	100%	0.0009	100%
subset10	32	0.0088	100%	0.0019	83%
subset11	5	0.0088	100%	7.7658	0%
subset12	4	0.0257	100%	5.7773	0%
subset13	4	0.0278	100%	5.7111	0%
subset14	3	332.6304	0%	6.0382	0%
subset15	3	253.5876	0%	5.6393	0%
Difference set (400,57,8)	57	0.0007	100%	0.0025	100%
subset16	9	0.0022	100%	0.0095	100%

Table 5.1: Mean square error and successful estimation probability of estimated distance with different algorithms, subsets in $SNR = 20dB$ and $\mathbf{r}_N = [4, 9]m$.

As we can see in the tables, the reconstruction algorithm has essential influence on

Set number	M	NL-GMF		ANM	
		MSE(m^2)	$P_{suc-est}$	MSE(m^2)	$P_{suc-est}$
Full set	400	0.3816	96%	0.0004	100%
subset1	3	16.7412	0%	47.6399	0%
subset2	3	38.8103	0%	3.4935	0%
subset3	137	4.3653	64%	0.0111	100%
subset4	101	6.3003	35%	0.0071	100%
subset5	28	0.0136	100%	0.0095	100%
subset6	40	0.2837	96%	0.0038	100%
subset7	12	0.0414	100%	0.0318	100%
subset8	79	1.9275	79%	0.0035	100%
subset9	132	5.0460	53%	0.0041	100%
subset10	32	0.0574	99%	0.0023	100%
subset11	5	0.4057	0%	0.0940	33%
subset12	4	2.0927	0%	0.1588	0%
subset13	4	0.3725	0%	0.1674	0%
subset14	3	249.7305	0%	220.8214	0%
subset15	3	244.6208	0%	260.8317	0%
Difference set (400,57,8)	57	0.0009	100%	0.0008	100%
subset16	9	0.0051	100%	1.2469	0%

Table 5.2: Mean square error and successful estimation probability of estimated distance with different algorithms, subsets in $SNR = 20dB$ and $\mathbf{r}_N = [4, 9, 17]m$.

the estimated results. For most of the subsets, using the ANM algorithm can obtain a low MSE and for the others NL-GMF is a better choice.

Compared to the others, difference set, the full set, subset3-subset10 and subset16 have good estimation accuracy in target distance in at least one algorithm. Most of them are selected with $\Delta d = 0.2m - 0.3m$, threshold $0.2m - 0.3m$, CRLB with $F_{mean}(\cdot)$ and CRLB with $F_{expectation}(\cdot)$.

Also, compared to the 3-path environment, 2-path environment makes the estimation more accurate when using subset2-subset10. The reason is that those subsets are selected based on the 2-path CRLB which are more suitable for 2-path case. For subset 11-15, their advantages in 2-path case is not obvious because they have too few elements which may not be able to show all of their characteristic.

It is also noteworthy that most of the MSEs of subset1-subset15 obtained by NL-GMF are above the Cramer Rao lower bound of $\mathbf{r}_N = [4, 9, 17]m$ and $\mathbf{r}_N = [4, 9]m$ which meets the estimation theory. But for ANM algorithm, some MSEs are lower than the CRLB because the CRLB is only suitable for unbiased estimator like the global matched filter, and the atomic norm minimization algorithm can be biased which makes the results lower than the CRLB. Also, the amount of the data used to calculate the MSE of ANM algorithm is too few which can also cause the error in result MSE.

Except the MSE, we can also see that the subsets having low MSE also have good estimation probability. And the subsets having large MSE may also have good successful

estimation probability because the large MSE may be caused by some outliers.

Although the results of subset1-subset15 are corresponding to the CRLB theory, the difference set which has larger CRLB has the best estimation accuracy and successful estimation probability in the table. This indicates that the CRLB of 2 paths may not be the optimal metric for our case.

ii) Selected subset performance in resolution

To study the estimation resolution of selected subsets, we test the subsets by setting $\mathbf{r}_N = [4, 4.1, 17]m$ and the obtained results are provided in the table 5.3.

Set number	M	NL-GMF		ANM	
		MSE(m^2)	$P_{suc-est}$	MSE(m^2)	$P_{suc-est}$
Full set	400	0.1758	98%	0.0031	100%
subset1	3	8.6666	0%	11.8508	0%
subset2	3	0.2934	1%	0.9482	0%
subset3	137	0.0030	100%	0.0044	100%
subset4	101	0.0034	100%	0.0031	100%
subset5	28	0.0119	100%	0.0077	100%
subset6	40	0.0039	100%	0.0034	100%
subset7	12	0.0158	100%	0.0044	100%
subset8	79	0.0028	100%	0.0031	100%
subset9	132	0.0032	100%	0.0025	100%
subset10	32	0.0044	100%	0.0031	100%
subset11	5	4.7202	1%	0.5144	0%
subset12	4	3.8658	17%	0.4057	0%
subset13	4	2.0246	59%	0.3471	0%
subset14	3	115.5558	0%	228.4652	0%
subset15	3	111.0166	0%	226.9560	0%
Difference set (400,57,8)	57	0.0024	100%	0.0025	100%
subset16	28	0.0129	100%	0.0053	83%

Table 5.3: Mean square error and successful estimation probability of estimated distance with different algorithms, subsets in $SNR = 20dB$ and $\mathbf{r}_N = [4, 4.1, 17]m$.

As we can see, compared to the results of $\mathbf{r}_N = [4, 9, 17]m$, the MSEs of NL-GMF is lower and the $P_{suc-est}$s is higher in table 5.3 while the result of ANM is not better. It is because the NL-GMF algorithm depends much on the subset's beampattern and ANM does not. As $r_0 = 4m, r_1 = 4.1m$ both lie in the mainlobe of the subsets' beampattern, it is not possible for algorithm to distinguish these two paths and the estimated results would be around $4m$ and $4.1m$. Compared to $r_2 = 9m$, $r_2 = 17m$ will have less interference on the LOS path estimation which leads to a small MSE. But for $\mathbf{r}_N = [4, 9, 17]m$, $r_1 = 9m$ has large probability lying in the first sidelobe and the sidelobe value is high which makes the estimated results erroneous.

iii) Comparison between difference set, 57-element random set and uniform set

As the difference set has the best estimation performance in table 5.1-5.3, is it the optimal result we can obtain? In this section, we would like to compare the difference set with the sets of same number of elements but different distributions to answer the question. We use 30 randomly chosen subsets and 1 uniformly distributed subset as the comparison. $\mathbf{r}_N = [4, 9, 17]m$. The beampatterns of difference set and the uniform distribution set are provided in the figure 5.1 and the MSEs of the estimated target distances with different subsets using NL-GMF are provided in the figure 5.2. The NL-GMF algorithm is repeated 100 times for each subset to obtained the MSE result.

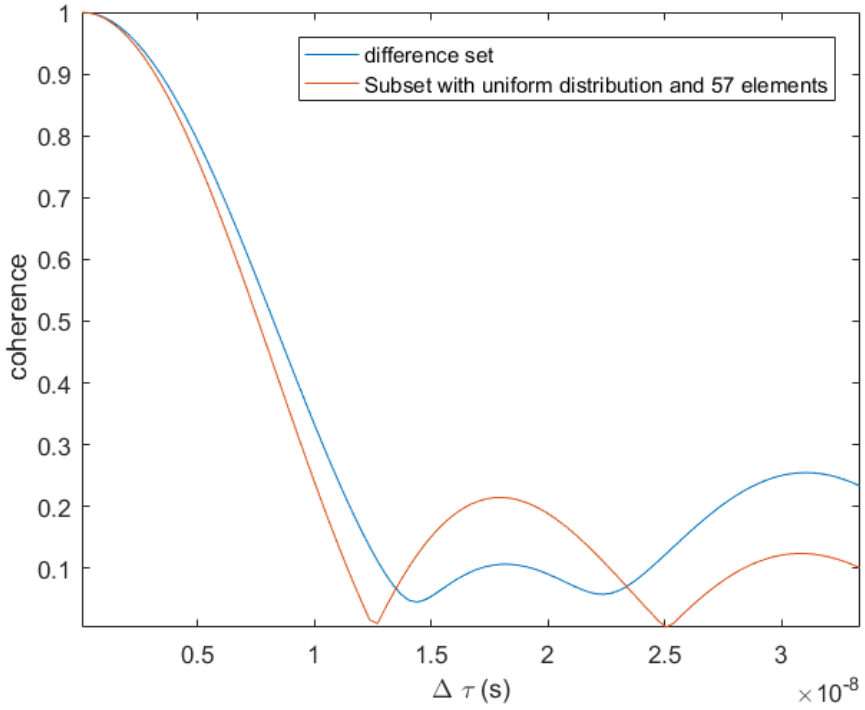

Figure 5.1: Beampattern of uniform distributed subsets with 57 elements and difference set (400,57,8).

As shown in the figure 5.2, the subset with uniform distribution has the best estimation accuracy which indicates that although difference set has good performance in table 5.1 and 5.3, the maximum coherence of the matrix may not be the optimal metric for optimal dictionary construction.

iv) Comparison between subset by random search and uniform set

In the table 5.1 and 5.2, the subset16 which is selected by random search algorithm based on the minimal average coherence has both low estimation error in most cases and few number of elements. So is the minimal average coherence the best metric for our case? To figure this out, we select a uniform distributed subset with 9 elements and

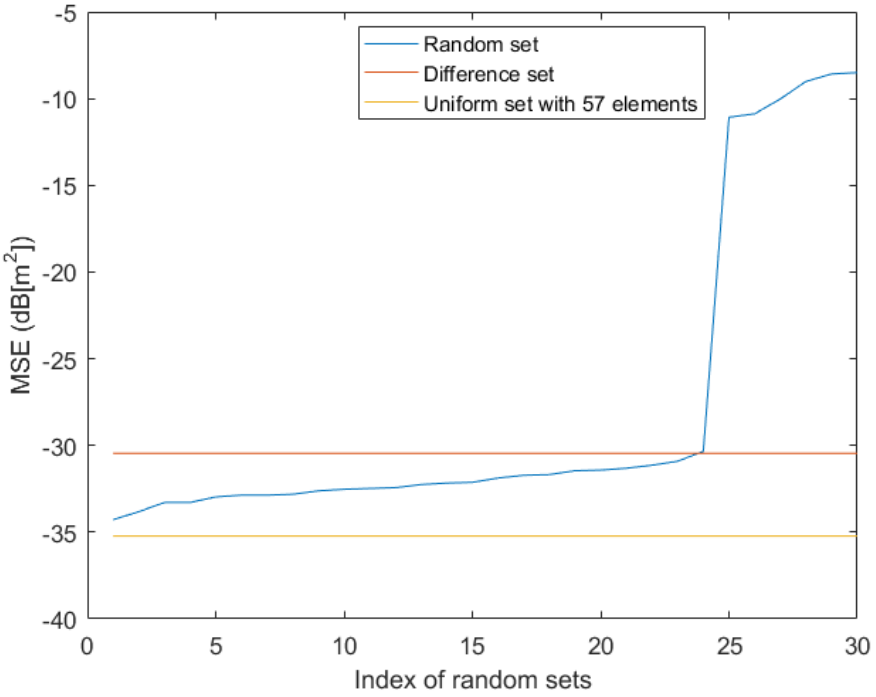

Figure 5.2: MSEs of estimated distance by NL-GMF for randomly chosen subsets with 57 elements, uniform distributed subsets with 57 elements and difference set (400,57,8).

compared its performance with the subset16. The uniform distributed subset is named the subset17. And the beampattern of the subset16 and the subset17 are presented in the figure 5.3.

By NL-GMF algorithm, the MSE of the estimated distance with subset17 is $0.0039(m^2)$ for $\mathbf{r}_N = [4, 9, 17]m$ which is lower than the subset16. And in the range of the beampattern, we can see that the beampattern of subset17 has higher sidelobes and mean coherence. Why would it have better accuracy and will uniform distributed subset always have the best accuracy?

To have a conclusion, we select subsets based on minimal mean coherence with different number of elements and compare them with uniform subsets which have corresponding number of elements in estimation accuracy. The number of iteration times for each random search algorithm is 10^7. For $\mathbf{r}_N = [4, 9, 17]m$, the MSEs of estimated distance using different subsets are obtained by using the NL-GMF algorithm which is repeated 100 times and by using ANM algorithm which is repeated 6 times. The desired accuracy is $0.3m$. The results are provided in the figure 5.4 and 5.5.

As shown in the figures, the subsets selected based on the minimal average coherence is not always bad in distance estimation. When using NL-GMF algorithm, the selected subset has similar accuracy with the uniform distribution subset but when using ANM algorithm the selected subset is always better. And for both reconstruction algorithm, the selected subset can reach the desired accuracy with fewer elements compared to the uniform subsets.

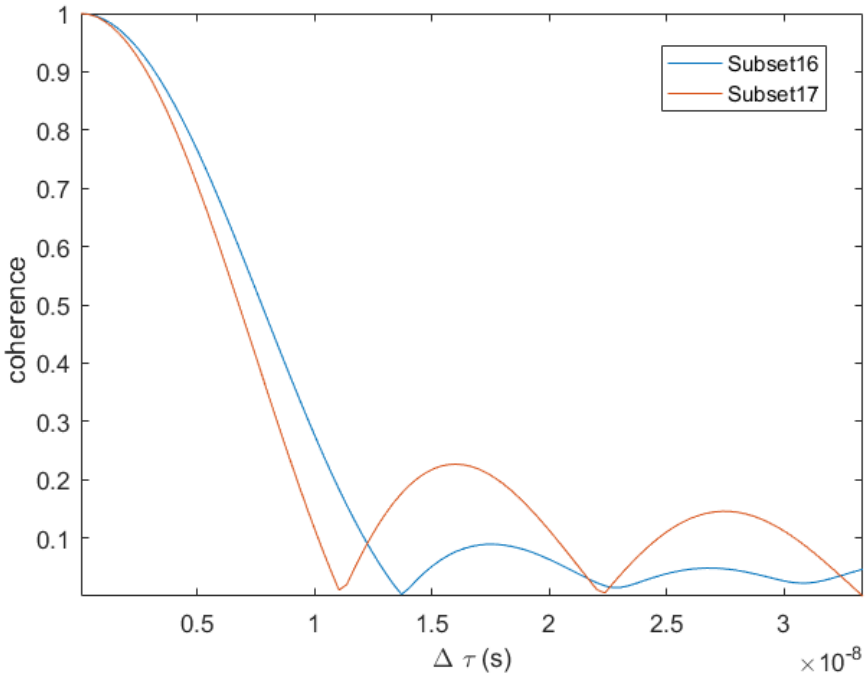

Figure 5.3: Beampattern of subset16 and subset17.

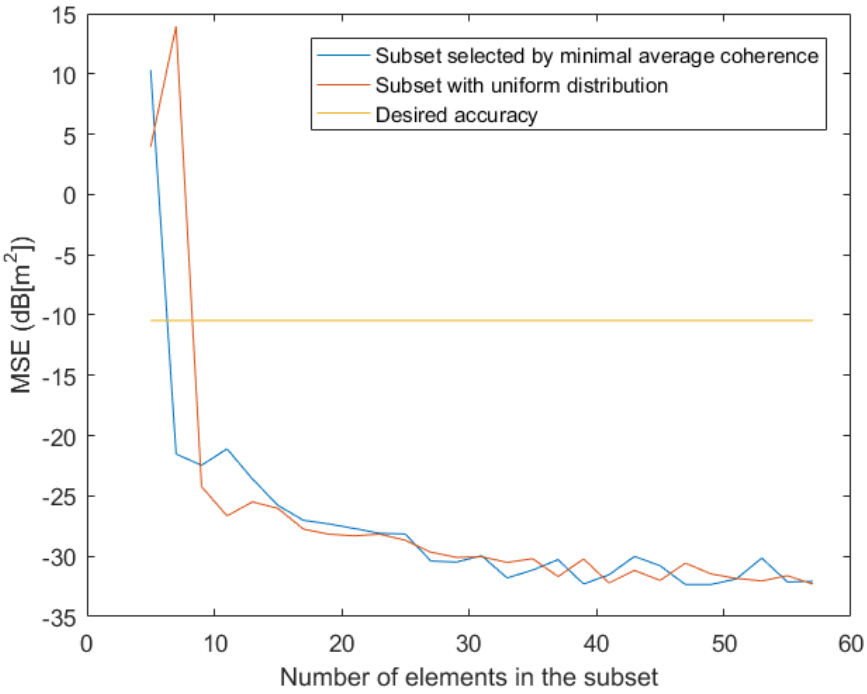

Figure 5.4: MSE comparison between subsets selected by minimal average coherence and uniform distributed subset with same number of elements using NL-GMF.

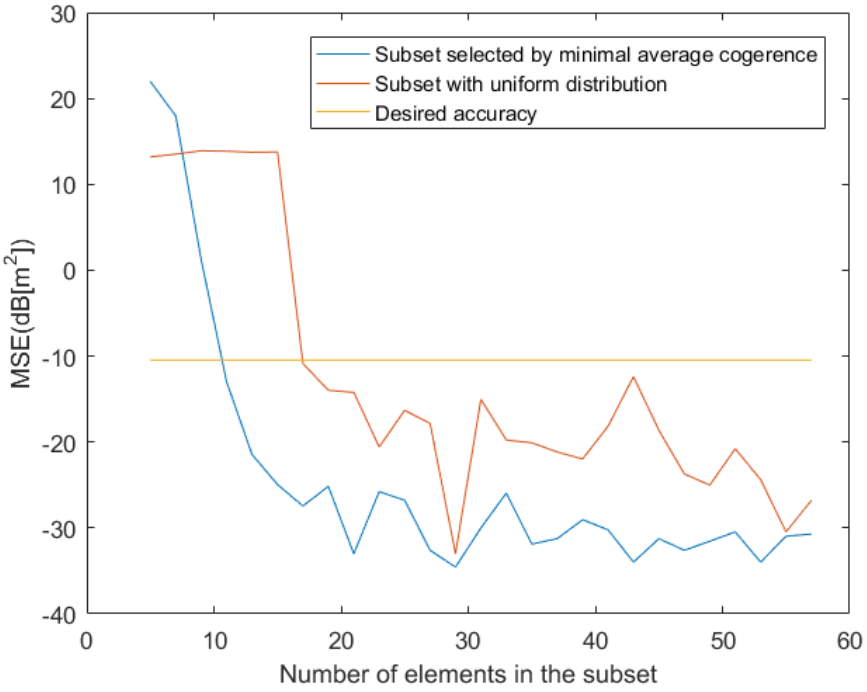

Figure 5.5: MSE comparison between subsets selected by minimal average coherence and uniform distributed subset with same number of elements using ANM.

v) Robustness of algorithms in noisy environment

Except the subset performance test, we would also like to see the difference between the two algorithms. Here, we use both algorithms, the NL-GMF and the ANM, to estimate the distance in different SNR values to see their difference. The subset used here is the difference set. The MSEs of estimated distance is provided in the figure 5.6.

Clearly, the NL-GMF algorithm is more sensitive to the environment condition. It can only estimate the distance more accurate than the ANM in high SNR condition as the algorithm is more suitable for noiseless condition. Compared to the NL-GMF, ANM method is less influence by the SNR and it has much exact results in low SNR condition. Except the accuracy, we would also like to mention that the ANM takes much longer time to output the result than NL-GMF does. Therefore, if the ranging procedure is carried out in good environment (high SNR), NL-GMF could be a good choice to save time. If we need high accuracy in noise environment, ANM algorithm should be chosen.

5.3 Test results in real data

In the above simulations, the selected subsets are all tested in simulated data which Gaussian white noise which is generated in ideal condition and may be different from the environment in practice. In this section, we test the subsets with real data provided

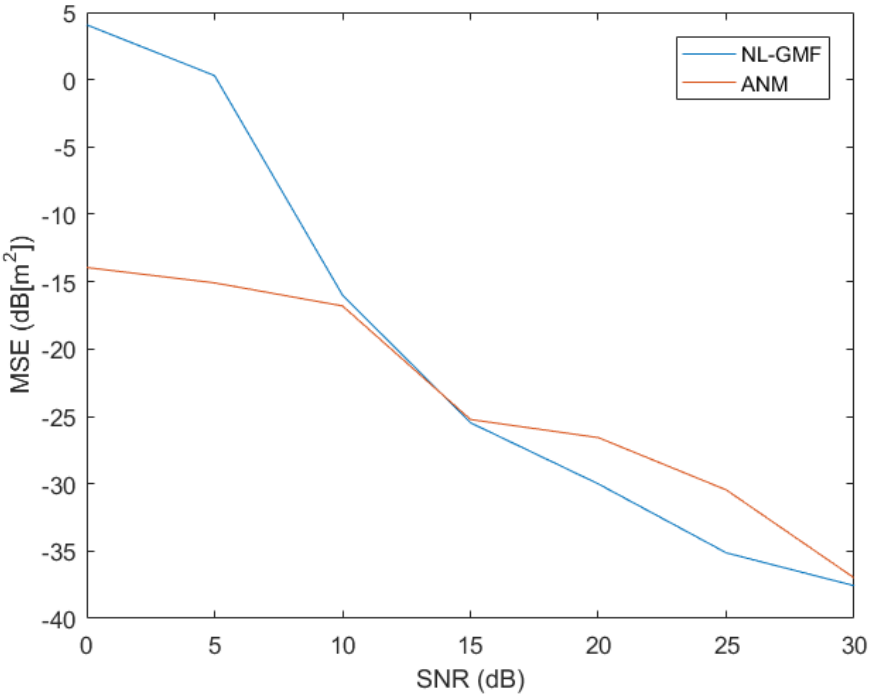

Figure 5.6: Average error of estimated distance by NL-GMF for $SNR = [0, 5, ..., 30]dB$ with difference set.

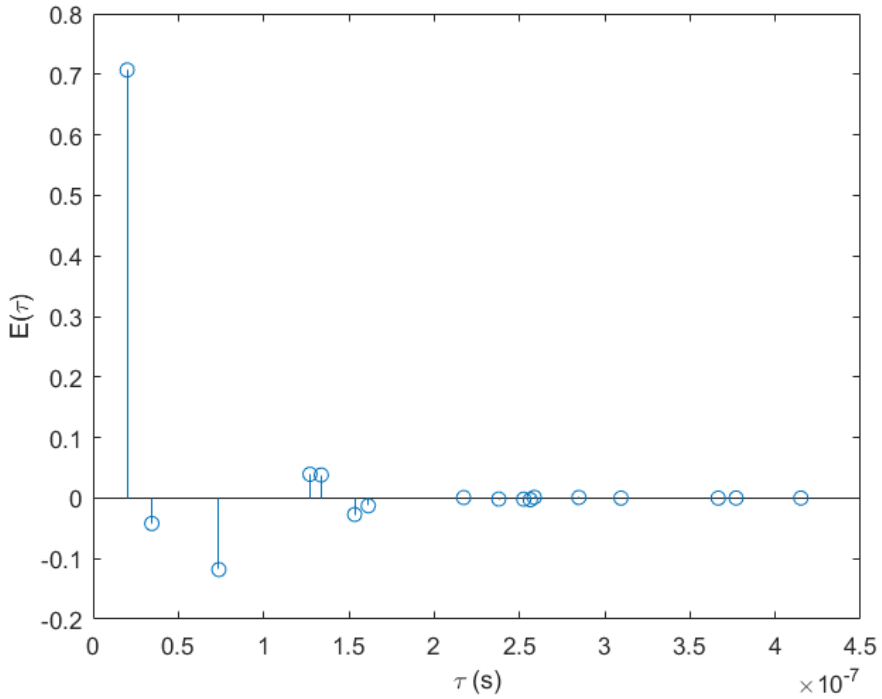

Figure 5.7: One generated multipath channel with practical conditions.

by imec company, compare their performance and study the influence of environment parameters. We generate one received channel with provided realistic parameters in more practical conditions. The parameters are set as: $K_f = 400$, $c = 299792458m/s$, $\Delta f = 200kHz$, $Band = 2.4GHz - 2.48Ghz$, the LOS path delay $\tau_0 = 2 \times 10^{-8}s$, the ray arrival rate $\eta = \frac{1}{25ns}$, the Ricean K factor $K = 1$ which indicates the ratio between LOS path energy and the NLOS path energy, the root mean square delay spread is $\tau_{rms-ds} = 20ns$ which can indicate the multipath richness of a communication channel. The generated multipath channel is a sparse channel and is shown in the figure 5.7. $E(\tau)$ indicates the energy of each path.

Then we use the subsets selected in the previous section to extract the original received data, apply NL-GMF and ANM algorithm to reconstruct the received data and estimate the target distance. The NL-GMF is repeated 100 times and the ANM is ran 6 times for each subset. Except the MSE and the $P_{suc-est}$, in this simulation we also count the number of estimations that can output an result to calculate the estimation probability P_{est}. The MSEs of the result, the P_{est} and the $P_{suc-est}$ are provided in the table 5.4.

Set number	M	NL-GMF			ANM		
		MSE(m^2)	P_{est}	$P_{suc-est}$	MSE(m^2)	P_{est}	$P_{suc-est}$
Full set	400	9.6102	100%	48%	0.0007	100%	100%
subset1	3	139.5441	100%	13%	31.9220	50%	0%
subset2	3	33.0822	8%	3%	0.0226	100%	100%
subset3	137	8.2733	100%	45%	1.2755	100%	33%
subset4	101	13.7764	100%	3%	2.5944	100%	17%
subset5	28	7.4485	100%	48%	1.9049	100%	83%
subset6	40	7.4519	100%	49%	12.8612	100%	17%
subset7	12	7.3472	100%	54%	8.4023	100%	50%
subset8	79	10.1907	100%	29%	5.0524	100%	50%
subset9	132	8.1972	100%	45%	0.6911	100%	17%
subset10	32	8.3308	100%	46%	6.5895	100%	50%
subset11	5	72.0111	87%	62%	1.9084	100%	67%
subset12	4	98.1793	48%	48%	1.1494	100%	50%
subset13	4	90.0812	97%	55%	1.5392	100%	50%
subset14	3	45.8175	3%	0%	28.6836	67%	0%
subset15	3	35.5903	1%	1%	24.5387	33%	17%
Difference set (400,57,8)	57	0.4699	100%	98%	0.0148	100%	100%
subset16	9	0.0468	100%	100%	0.0252	100%	100%
subset17	9	0.0368	100%	100%	3.8437	100%	50%

Table 5.4: Mean square error, estimation probability and successful estimation probability of estimated distances with different subsets for 1 channel.

In general, the MSEs of estimation result of ANM is lower than the MSE ofNL-GMF but ANM costs more time to calculate. The subset16 and the difference set are the only subsets that have good accuracy in both algorithms. And their successful estimation

probability is 100% which means we only need to measure the target distance for 1 time at most to get the true target distance if we use subset16 or difference set and the channel is similar with the one in figure 5.7.

But as shown in Figure 5.2 and 5.4, the subset16 and the difference set is not always optimal and the above conclusion is only in one channel. To show the general performance of all subsets, in same channel parameters, we test 100 generated channels by NL-GMF algorithm and test 18 generated channels by ANM algorithm. The MSEs, the P_{est} and the $P_{suc-est}$ are provided in the table 5.5.

Set number	M	NL-GMF			ANM		
		MSE(m^2)	P_{est}	$P_{suc-est}$	MSE(m^2)	P_{est}	$P_{suc-est}$
Full set	400	5.2799	100%	67%	0.0216	100%	89%
subset1	3	55.1448	14%	0%	27.0901	56%	0%
subset2	3	33.4576	13%	1%	9.6329	94%	16%
subset3	137	3.8355	100%	64%	1.7417	100%	50%
subset4	101	4.7537	100%	58%	3.4039	100%	50%
subset5	28	4.7323	100%	53%	11.5864	100%	39%
subset6	40	4.5327	100%	50%	13.5758	100%	33%
subset7	12	4.5681	100%	50%	10.3206	100%	39%
subset8	79	5.7795	100%	47%	3.5864	100%	50%
subset9	132	4.1402	100%	69%	3.4282	100%	61%
subset10	32	7.9713	100%	45%	4.7781	100%	28%
subset11	5	76.2420	65%	17%	3.1253	100%	22%
subset12	4	57.5224	24%	3%	28.1009	94%	17%
subset13	4	71.0863	27%	4%	16.9970	89%	17%
subset14	3	40.5450	12%	1%	21.4059	83%	17%
subset15	3	44.7242	7%	0%	21.5424	89%	17%
Difference set (400,57,8)	57	0.1200	100%	83%	0.2240	100%	83%
subset16	9	0.4245	100%	71%	0.5074	100%	33%
subset17	9	1.9492	100%	74%	2.6412	100%	67%

Table 5.5: Mean square error, estimation probability and successful estimation probability of estimated distances with different subsets for several channels.

As shown in the table 5.5, most of the subsets are able to output an estimation result but not able to estimate accurately. The full set, the difference set, the subset16 and subset17 are the only subsets that have good accuracy and high successful estimation probability. Compared to the subset17 which has uniform distribution, the subset 16 has lower MSE but lower $P_{suc-est}$ which means that the subset17 tend to produce few outliers.

In the next, we will study the influence of 3 essential parameters of the communication channel and show their impact on the estimation result.

i) Influence of ray arrival rate

The ray arrival rate η has been introduced in the Chapter3. It can influence the NLOS path dalay distribution. If η is high, the NLOS path delay will be more. In the test, we set the ray arrival rate as $\eta = \frac{1}{200}, \frac{1}{25}, \frac{1}{10}, \frac{1}{5}, \frac{2}{5}, \frac{3}{5}, \frac{4}{5}, 1$ and generate 20 channels for each η value. The subset16 and the NL-GMF is used to test the estimation result and the other parameters are the same with above. The mean MSE and the successful estimation probability among 20 channels of each η are provided in the Figure 5.8.

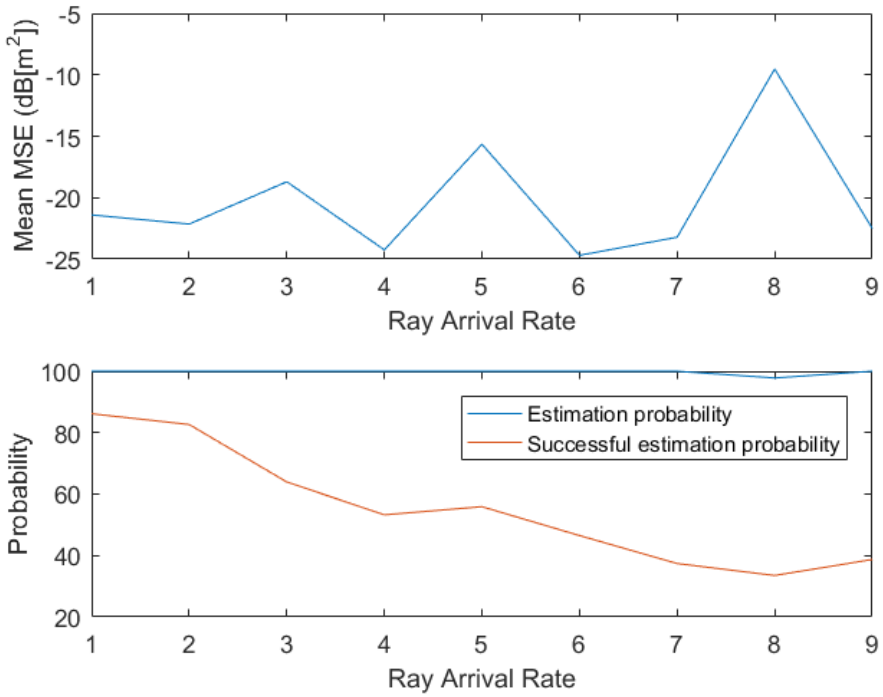

Figure 5.8: Mean MSE and the successful estimation probability among 20 channels of each η using subset16 and NL-GMF.

As shown in the Figure 5.8, if the ray arrival rate increases, the mean MSE of estimation result will be higher and we are less probable to obtain the true target distance with few measurement.

ii) Influence of root mean square delay spread

The root mean square delay spread τ_{rms-ds} is an important indicator of a wireless communication channel. It can represent the time difference between the LOS path and the latest NLOS path. If τ_{rms-ds} is high, the latest NLOS path dalay has larger time difference with the LOS path delay. In this test, we set $\tau_{rms-ds} = 5, 10, 15, 20, 25, 30, 35, 40$ and generate 20 channels for each τ_{rms-ds}. The subset16 and the NL-GMF is used to test the estimation result and the other parameters are the same with above. The mean MSE and the successful estimation probability among 20 channels of each τ_{rms-ds} are provided in the Figure 5.9.

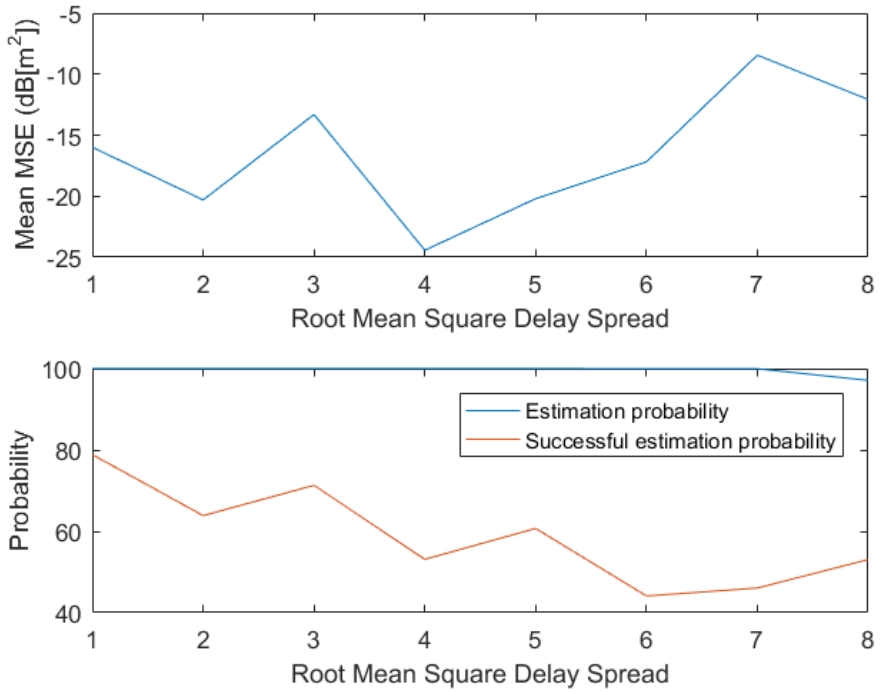

Figure 5.9: Mean MSE and the successful estimation probability among 20 channels of each τ_{rms-ds} using subset16 and NL-GMF.

As shown in the Figure 5.9, if the root mean square delay spread increases, the estimation result will be more inaccurate and we need to measure more data to get the target true distance.

iii) Influence of Ricean K factor

With higher Ricean K factor, the energy of NLOS path will has larger probability to be higher which may cause greater interference in the LOS delay estimation. In this test, we set the Ricean K factor as $\frac{1}{8}, \frac{1}{4}, \frac{1}{2}, 1234$ and generate 20 channels for each K. The subset16 and the NL-GMF is used to test the estimation result and the other parameters are the same with above. The mean MSE and the successful estimation probability among 20 channels of each energy ratio value are provided in the Figure 5.10.

As shown in the Figure 5.10, if the K increases, the estimation result will be more accurate and we can measure less times to obtain true target distance in acceptable error.

5.4 Conclusion

In this Chapter, we use two gridless reconstruction algorithms to test the performance of selected subsets in both simulated and real ranging procedure. We first introduce the

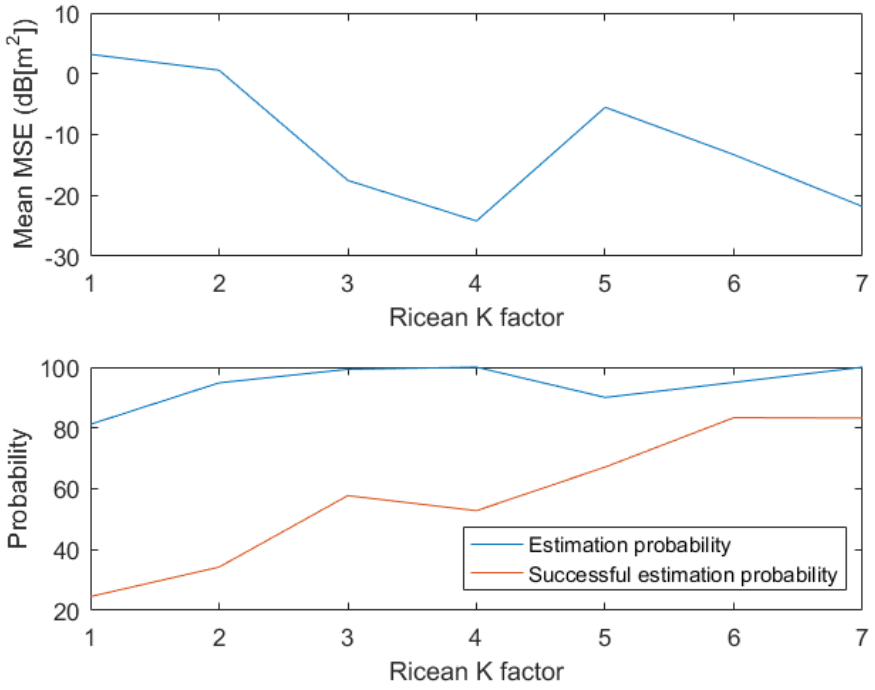

Figure 5.10: Mean MSE and the successful estimation probability among 20 channels of each K factor using subset16 and NL-GMF.

algorithms used, the noiseless global matched filter and the atomic norm minimization. Then we do the performance test and analyze the received result. The conclusion is listed in the follows:

i) For the subset performance test, the reconstruction algorithm used has influence on the estimation results. Same subset may have different MSE of result when using different algorithms to recover the data. As for the subset performance, the full set, the difference and the subsets selected in $\Delta d = 0.2 - 0.3m$, CRLB with $F_{mean}(\cdot)$, CRLB with $F_{expectation}(\cdot)$ and $G_{Co-mean}$ has small result MSE of at least one reconstruction algorithm.

ii) Compared to the case of the 3-path environment, the subsets selected based on 2-path CRLB have better performance in the case of 2-path environment. And as difference set has the best performance among all selected subset but has high CRLB value, it indicates that the 2-path CRLB may not be a good criterion in our case.

iii) The estimation results of NL-GMF algorithm are more influenced by the index beam pattern compared to the ANM algorithm.

iv) The uniform distribution subset and randomly chosen subset with 57 elements all have better performance than difference set which indicates that the maximum coherence may not be a good criterion in indoor ranging.

v) The uniform distribution subsets and subsets selected based on minimal average coherence with same number of elements have similar performance when using NL-GMF algorithm and the selected subsets has better performance when using ANM algorithm.

This indicates that minimal average coherence can be a good metric in subset selection compared to the other criteria we tested.

vi) In the comparison between two gridless CS algorithms, the ANM takes longer time to output the estimation result but it is robust in noise condition and has good accuracy in low SNR environment. The NL-GMF only perform better in high SNR environment but it can save time and provide estimated distance quickly.

vii) In the real data test, the subset16 has the best performance compared to the other subsets we tested which indicates that in practical, the metric $G_{Co-mean}$ is also suitable.

viii) Low ray arrival rate, low root mean square delay spread and high Ricean K factor between LOS path and NLOS path all have positive influence on indoor ranging when using NL-GMF.

Generally speaking, to achieve the goal of fewer tones used and good accuracy, we should use minimal average coherence as the criterion to achieve the optimal frequency selection and measure the target distance in conditions of low ray arrival rate, low root mean square delay spread and high energy ratio.

6 Conclusion and future workng

In the indoor ranging, a method using phase information with multiple frequencies is used to estimate the target distance. To save the measuring time and improve efficiency, in this thesis, we test several criteria and promote an optimal frequency selection. We at first build a signal model of our case and calculate the ambiguity range of our model to make sure all the estimations are carried within the ambiguity range. Then based on the concept of estimation theory and compressive sensing, we use 2-path CRLB and matrix coherence as the criteria to select suitable subsets of given tone set. The selected subsets are tested in both simulated and real ranging procedure using two gridless compressive sensing reconstruction algorithms, the NL-GMF and the ANM. The influences of communication channel parameters are also studied. Based on the above work, we can have the following conclusions:

i) The ambiguity range of our model is calculated by $\frac{c}{\Delta f}$ where c is the propagation speed and Δf is the frequency difference between two tones. And within the unambiguous range, wide bandwidth is the key point to have good accuracy in estimation procedure. The low noise variance also have positive impact on the estimation accuracy.

ii) Random selection on the tones will destroy the data structure which makes the MUSIC algorithm not applicable while uniform selection on the tones will not.

iii) The 2-path CRLB is correlated with the delay difference between two paths and the subset C_M. High SNR, high threshold and small step size of delay grid vector will reduce the number of tones selected. And the selected tones tend to locate at the both end of the bandwidth and are divided into blocks.

iv) Compared to the beam pattern of full set, selected subsets based on 2-path CRLB tend to have beam pattern with narrower mainlobe and higher sidelobes while difference set and subsets selected based on minimal mean coherence tend to have beam pattern with wider mainlobe and lower sidelobe.

v) For subset performance test, the reconstruction algorithm has influence on the estimation accuracy. The algorithm NL-GMF is more influenced by the beam pattern, tends to have larger estimation error and is not so robust in noisy environment. The algorithm ANM has better accuracy and is not influenced much by noise. But ANM takes much longer time to output the estimation result compared to NL-GMF.

vi) For subset performance test, the subset selected based on 2-path CRLB have better performance in 2-path case compared to 3-path case. But the subset with uniform distribution has better performance than subset selected by 2-path CRLB and difference set. Thus 2-path CRLB and maximal coherence of matrix are not good criteria for our case.

vii) For the subset selected based on minimal mean coherence, it only has better performance than uniform distribution subset when using ANM algorithm. But in real

data test, it has the best performance than all other subsets. It means that for practice, the criterion minimal mean coherence is a good choice in the tone selection problem.

viii) For the parameters of the communication channel, low ray arrival rate, low root mean square delay spread and high Ricean K factor have positive influence on indoor ranging when using NL-GMF algorithm.

From the above conclusions, we can say that for our case, the minimal average coherence is the best criterion that we tested and we can only use 9 tones instead of 400 to estimate indoor target accurately.

In the future, we are going to study more on this topic. The future work are mainly in three points. The first one is to consider the selection problem in other point views and test more criteria. The second one is to find other difference sets that meets our requirements and compare them with existing subsets to find the best one. The other point is to improve the accuracy and reduce the cost time of the reconstruction algorithms.

Part of Results in Chapter 3

A

In this appendix, Figure A.1, A.2 and A.3 present the element distributions in selected subsets. These subsets are selected based on 2-path CRLB with various time difference for different weighted mean function, Δds, desired range accuracy and SNRs.

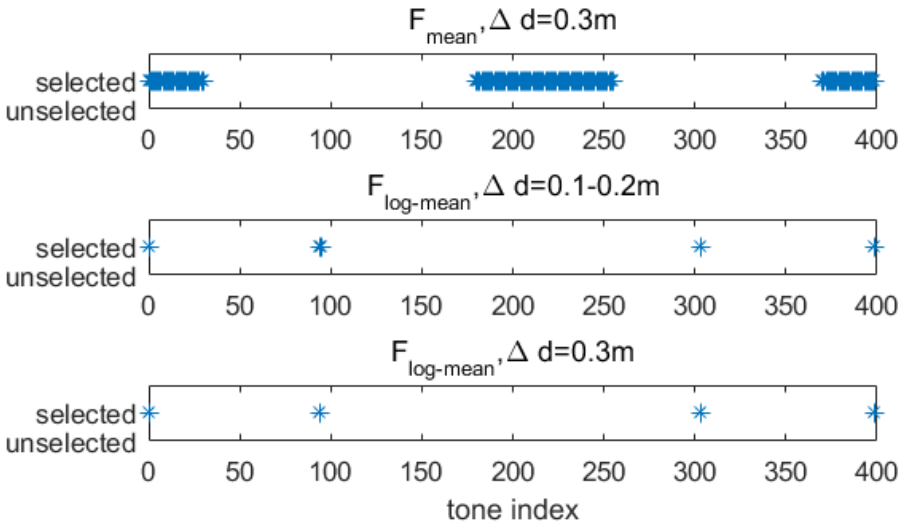

Figure A.1: Distribution of selected tone in two paths with various time difference for different weighted mean functions, Δds with desired range accuracy $0.1meter$ and SNR $20dB$.

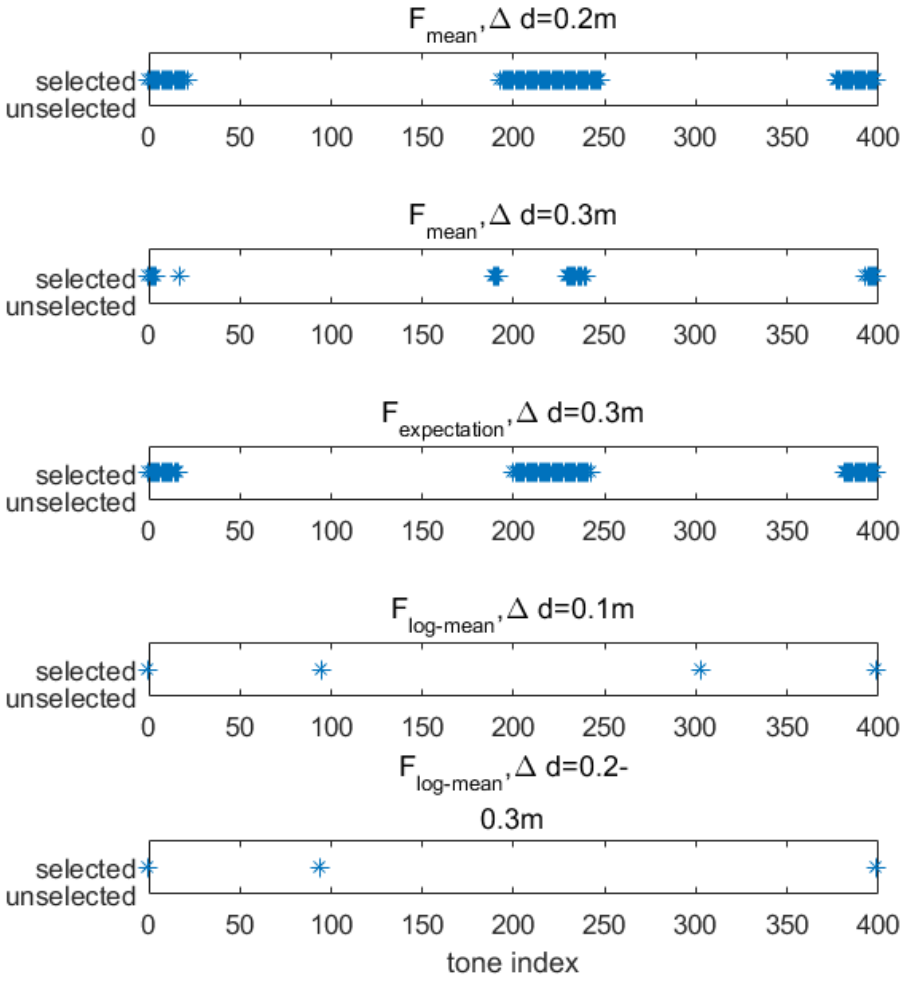

Figure A.2: Distribution of selected tone in two paths with various time difference for different weighted mean functions, Δds with desired range accuracy $0.2meter$ and SNR $20dB$.

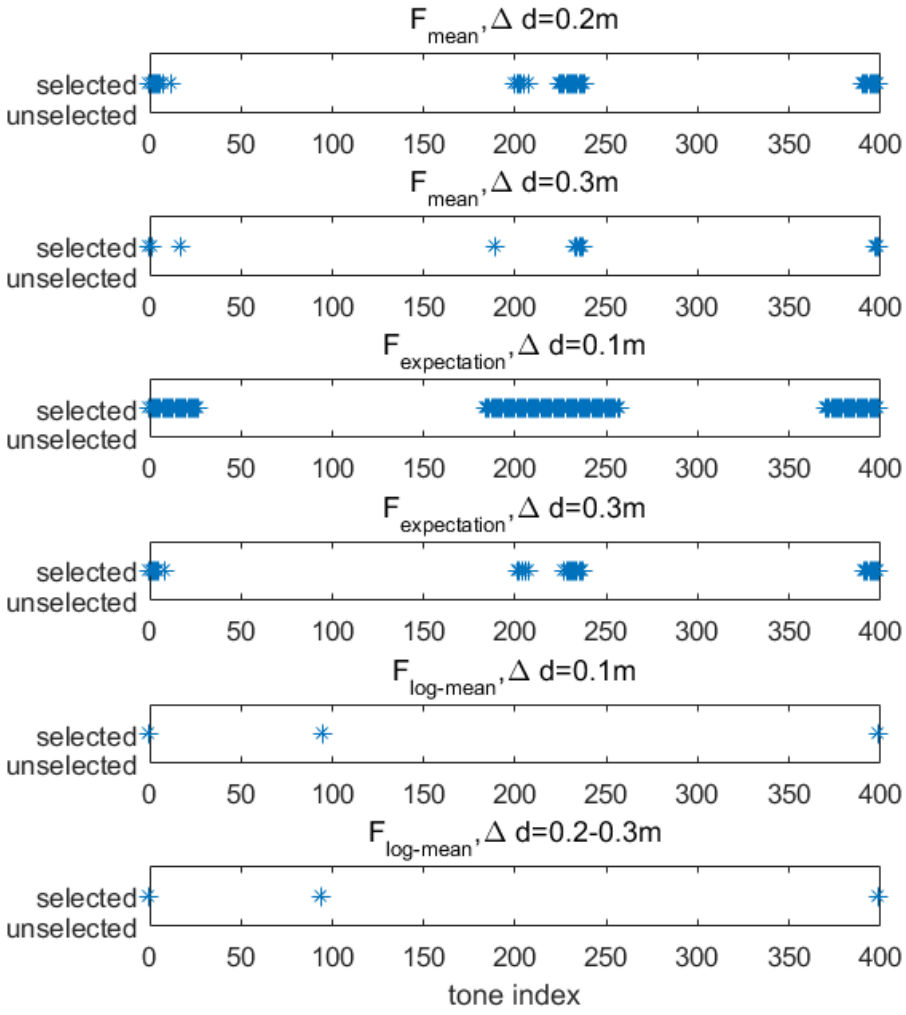

Figure A.3: Distribution of selected tone in two paths with various time difference for different weighted mean functions, Δds with desired range accuracy $0.3meter$ and SNR $20dB$.

Subset number and elements in Chapter 5

B

In this appendix, Table B.1 and B.2 provide the name and elements of selected subsets.

Set name	M	Selection criterion	threshold (m^2)	Δd(m)	CRLB (m^2)
Full set	400	-	-	0.1	0.1727 by $F_{mean}(\cdot)$ 1.998×10^{-4} by $F_{log-mean}(\cdot)$ 0.4869 by $F_{expectation}(\cdot)$
				0.2	0.0219 by $F_{mean}(\cdot)$ 1.854×10^{-4} by $F_{log-mean}(\cdot)$ 0.0605 by $F_{expectation}(\cdot)$
				0.3	0.0067 by $F_{mean}(\cdot)$ 1.764×10^{-4} by $F_{log-mean}(\cdot)$ 0.0180 by $F_{expectation}(\cdot)$
subset1	3	single path CRLB	-	-	2.6919×10^{-3}
subset2	3	2-path CRLB with fixed $\Delta\tau_1$	-	-	5.5719×10^{-3}
subset3	137	CRLB with $F_{mean}(\cdot)$	0.01	0.3	9.9846×10^{-3}
subset4	101	CRLB with $F_{mean}(\cdot)$	0.04	0.2	0.0397
subset5	28	CRLB with $F_{mean}(\cdot)$	0.04	0.3	0.0395
subset6	40	CRLB with $F_{mean}(\cdot)$	0.09	0.2	0.0881
subset7	12	CRLB with $F_{mean}(\cdot)$	0.09	0.3	0.0893
subset8	79	CRLB with $F_{expectation}(\cdot)$	0.04	0.3	0.0397
subset9	132	CRLB with $F_{expectation}(\cdot)$	0.09	0.2	0.0898
subset10	32	CRLB with $F_{expectation}(\cdot)$	0.09	0.3	0.0889
subset11	5	CRLB with $F_{log-mean}(\cdot)$	0.01	0.1 0.2	9.6021×10^{-3} 8.9253×10^{-3}
subset12	4	CRLB with $F_{log-mean}(\cdot)$	0.01	0.3	9.9774×10^{-3}
subset13	4	CRLB with $F_{log-mean}(\cdot)$	0.04	0.1	0.0113

Set name	M	Selection criterion	threshold (m^2)	Δd(m)	CRLB (m^2)
subset14	3	CRLB with $F_{log-mean}(\cdot)$	0.04 0.09	0.2 0.3	0.0375 0.0371
subset15	3	CRLB with $F_{log-mean}(\cdot)$	0.09	0.1	0.0445
Difference set (400,57,8)	57	$G_{Co-max}(\cdot)$	-	0.1	1.5560 by $F_{mean}(\cdot)$
subset16	9	$G_{Co-mean}(\cdot)$	-	0.1	5.1381 by $F_{mean}(\cdot)$
subset17	9	Uniform selection	-	0.1	5.7388 by $F_{mean}(\cdot)$

Table B.1: Subset's number

Set name	M	Elements
full set	400	[0 1 2 ... 398 399]
subset1	3	[0 398 399]
subset2	3	[86 349 399]
subset3	137	[0 1 2 3 4 5 6 7 8 9 10 11 12 13 14 15 16 17 18 19 20 21 22 23 24 25 26 27 28 29 30 180 181 182 183 184 185 186 187 188 189 190 191 192 193 194 195 196 197 198 199 200 201 202 203 204 205 206 207 208 209 210 211 212 213 214 215 216 217 218 219 220 221 222 223 224 225 226 227 228 229 230 231 232 233 234 235 236 237 238 239 240 241 242 243 244 245 246 247 248 249 250 251 252 253 254 255 370 371 372 373 374 375 376 377 378 379 380 381 382 383 384 385 386 387 388 389 390 391 392 393 394 395 396 397 398 399]
subset4	101	[0 1 2 3 4 5 6 7 8 9 10 11 12 13 14 15 16 17 18 19 20 21 193 194 195 196 197 198 199 200 201 202 203 204 205 206 207 208 209 210 211 212 213 214 215 216 217 218 219 220 221 222 223 224 225 226 227 228 229 230 231 232 233 234 235 236 237 238 239 240 241 242 243 244 245 246 247 248 377 378 379 380 381 382 383 384 385 386 387 388 389 390 391 392 393 394 395 396 397 398 399]
subset5	28	[0 1 2 3 4 17 189 190 191 192 229 230 231 232 233 234 235 236 237 239 240 393 394 395 396 397 398 399]
subset6	40	[0 1 2 3 4 5 6 7 12 200 201 202 203 205 207 224 225 226 227 228 229 230 231 232 233 234 235 236 237 238 390 391 392 393 394 395 396 397 398 399]
subset7	12	[0 1 17 189 233 234 235 236 237 397 398 399]
subset8	79	[0 1 2 3 4 5 6 7 8 9 10 11 12 13 14 15 16 200 201 202 203 204 205 206 207 208 209 210 211 212 213 214 215 216 217 218 219 220 221 222 223 224 225 226 227 228 229 230 231 232 233 234 235 236 237 238 239 240 241 242 381 382 383 384 385 386 387 388 389 390 391 392 393 394 395 396 397 398 399]

Set name	M	Elements
subset9	132	[0 1 2 3 4 5 6 7 8 9 10 11 12 13 14 15 16 17 18 19 20 21 22 23 24 25 26 27 184 185 186 187 188 189 190 191 192 193 194 195 196 197 198 199 200 201 202 203 204 205 206 207 208 209 210 211 212 213 214 215 216 217 218 219 220 221 222 223 224 225 226 227 228 229 230 231 232 233 234 235 236 237 238 239 240 241 242 243 244 245 246 247 248 249 250 251 252 253 254 255 256 257 370 371 372 373 374 375 376 377 378 379 380 381 382 383 384 385 386 387 388 389 390 391 392 393 394 395 396 397 398 399]
subset10	32	[0 1 2 3 4 5 8 201 202 204 206 207 227 228 229 230 231 232 233 234 235 236 237 391 392 393 394 395 396 397 398 399]
subset11	5	[0 94 95 303 399]
subset12	4	[0 94 303 399]
subset13	4	[0 95 303 399]
subset14	3	[0 94 399]
subset15	3	[0 95 399]
Difference set (400,57,8)	57	[0 1 2 9 27 36 37 41 46 49 50 69 70 72 85 93 98 100 105 118 123 138 150 157 160 164 165 175 176 179 181 182 200 203 211 213 217 224 230 233 240 242 244 250 254 258 284 300 316 328 339 345 347 350 356 362 371]
subset16	9	[8 86 109 164 215 219 294 311 394]
subset17	9	[0 50 100 150 200 250 300 350 399]

Table B.2: Subset's elements

C Nomenclature

$h(f,r)$	one received signal
$\mathbf{h}_{K_f}, \mathbf{h}_M$	received signals in vector form with K_f/M element according to C_{K_f}/C_M
f, f_n	radio channel frequency, $f_n = (n-1)\Delta f$
r, r_n	distance between devices in n-th path
$\mathbf{r}_N$	N path distances in vector form
$a(r)$	absolute amplitude of the signal which contains distance information
$\mathbf{a}(\mathbf{r}_N)$	absolute amplitude for N path distances in vector form
c	propagation velocity
K_f	the number of available frequencies
N	number of rays of the multi-path propagation
σ^2	noise variance
SNR	signal-to-noise ratio
Δf	the frequency step
τ, τ_n	delay in the n-th ray
$\boldsymbol{\tau}_N$	N path delays in vector form
$z(\tau_n)$	equals to $e^{-j2\pi\Delta f\tau_n}$, element in measurement matrix
C_{K_f}	full index set with K_f elements, equal to $[0, 1, ..., K_f - 1]$
C_M	selected frequency index set with M elements, $C_M \subset C_{K_f}$
$\mathbf{z}_{K_f}(\tau_n)$	column of measurement matrix with K_f elements according to C_{K_f}
$\mathbf{Z}_{K_f}$	measurement matrix with K_f rows according to C_{K_f}
$\mathbf{n}$	the environment noise
$G(\cdot)$	evaluation function of selected tone set
G_{Tr}	evaluation threshold
$\mathbf{S}$	covariance matrix of $\mathbf{h}_{K_f}$
$\mathbf{P}$	equal to $E\{\mathbf{a}(\mathbf{r}_N)\mathbf{a}^H(\mathbf{r}_N)\}$
$\mathbf{I}$	unit matrix
$\mathbf{v}_i$	i-th eigenvector of $\mathbf{S}$
λ_i	i-th eigenvalue of $\mathbf{S}$
$\hat{\mathbf{S}}$	covariance matrix of $\mathbf{H}_{K_f}$
$\mathbf{H}_{K_f}$	Hankel matrix based on $\mathbf{h}_{K_f}$
$J_{MUSIC}(\tau)$	cost function of delay τ used in MUSIC algorithm
$J_{MUSIC-max}$	Maximum in the inverse pseudo spectrum
$\hat{\mathbf{V}}_n$	null-subspace matrix of $\mathbf{H}\mathbf{H}^H$
τ_{unam}	unambiguous range in delay
$G_{CRLB}(\cdot), G_{Co}(\cdot)$	evaluation function of selected tone set regarding CRLB/RIP as the criterion
$G_{CRLB-Tr}, G_{Co-Tr}$	evaluation threshold regarding CRLB/RIP as the criterion

$d_{accuracy}$	estimation accuracy of distance
$p(\boldsymbol{\tau}_N \mid \mathbf{h}_{K_f})$	probability density function of unknown estimation targets $\boldsymbol{\tau}_N$ with full set measurements $\mathbf{h}_{K_f}$
$\boldsymbol{s}(\boldsymbol{\tau}_N \mid \mathbf{h}_{K_f})$	gradient of log-likelihood function of $p(\mathbf{h}_{K_f}, \boldsymbol{\tau}_N)$, also known as score function
$\boldsymbol{I}_{K_f}(\boldsymbol{\tau}_N \mid \mathbf{h}_{K_f})$	Fisher information matrix of unknown estimation targets $\boldsymbol{\tau}_N$ with full set measurements $\mathbf{h}_{K_f}$
$\hat{\boldsymbol{\tau}}_N$	estimation of delay vector $\boldsymbol{\tau}_N$
$var_{K_f}(\hat{\boldsymbol{\tau}}_N \mid \mathbf{h}_{K_f})$	variance of estimated delays compared to the $\boldsymbol{\tau}_N$
$\boldsymbol{\Lambda}$	$N \times N$matrix using $\mathbf{a}(\mathbf{r}_N)$ as the diagonal elements and zeros as the other elements
$\boldsymbol{\zeta}_{K_f}(\tau_n)$	consists of derivations of elements in $\mathbf{z}_{K_f}(\tau_n)$, $K_f \times 1$
$\boldsymbol{D}$	consists of $\zeta_{K_f}(\tau_n)$ for $n = 0, 1, ..., N-1$
l	equal to $(-j2\pi\Delta f)$
$\Delta\tau_{n0}$	time difference between LOS path and the other path, equal to $\tau_n - \tau_0$
$\boldsymbol{\tau}_{grid}$,$\boldsymbol{r}_{grid}$	delay grid vector, range grid vector
τ_{gn},r_{gn}	element in delay/range grid vector, $n \geq 1$
$\boldsymbol{G}_{CRLB}(\hat{\boldsymbol{\tau}}_N \mid \mathbf{h}_{K_f})$	CRLB of $\hat{\boldsymbol{\tau}}_N$ with full set C_{K_f} data $\mathbf{h}_{K_f}$
$\boldsymbol{G}_{CRLB,11}(\hat{\boldsymbol{\tau}}_N \mid \mathbf{h}_{K_f})$	first element of $\boldsymbol{G}_{CRLB}(\hat{\boldsymbol{\tau}}_N \mid \mathbf{h}_{K_f})$
$F(\cdot)$	weighted mean function used to calculate CRLB of τ_0 with different weights
N_{grid}	number of elements in delay grid vector
$p_{\Delta\tau}(\Delta\tau_{n0})$	probability of $\Delta\tau_n$ in multipath propagation environment
η	ray arrival rate used in $p_{\Delta\tau}(\Delta\tau_n)$
w	stage number in algorithm
E_s	signal energy, usually set as 1 in the report
$\mathbf{y}$	compressed signal in classical CS theory, $m \times 1$
$\mathbf{f}$	transmitted signal vector in classical CS theory, $q \times 1$
$\mathbf{R}(C_m)$, $\mathbf{R}(C_M)$	matrix extracting samples according to index set C_m/C_M, size $m \times q/M \times K_f$
C_m	a subset of $\{0, 1, \cdots, q-1\}$
Φ	measurement matrix in classical CS theory, $q \times q$
Ψ	sparse base in classical CS theory, $q \times p$
$\mathbf{x}$	k-th sparse signal in classical CS theory, $p \times 1$
$\mathbf{A}$	matrix equaling to $\Phi\Psi$, $q \times p$
$\mathbf{A'}(C_m)$	matrix equaling to $\mathbf{R}(C_m)\mathbf{A}$, $m \times p$
$\hat{\boldsymbol{h}}_{K_f}$	estimated complete received signal $\mathbf{h}_{K_f}$ by measurement $\mathbf{h}_M$
k	number of non-zero elements in k-sparse vector
δ_k	isometry constant
$\mu(C_M, n, n')$, $\mu(C_M, \Delta\tau_{gngn'})$	cross-correlation between n-th and n'-th column in $\mathbf{Z}_M$ matrix with index set C_M
$\mathbf{Z}'_{K_f}$, $\mathbf{Z}'_M$	grid dictionary
$\mathbf{z}'_{K_f}(\tau_{gn})$, $\mathbf{z}'_M(\tau_{gn})$	$n-th$ column of grid dictionary
b, b_n	$(n-th)$ element in subset C_M
λ	a parameter in difference set expression

$\hat{a}(r_n), \hat{\boldsymbol{a}}(\mathbf{r}_N)$	estimated amplitude value/vector
γ_n	equal to $\frac{\hat{a}(r_n)}{\lvert\hat{a}(r_n)\rvert}$
$\mathbf{g}$	a vector of dual parameters used in NL-GMF algorithm
w_{max}	maximal iteration number in algorithm
ϵ	step size used in NL-GMF algorithm
ξ	update direction used in NL-GMF algorithm
$J_{NL-GMF}(\tau)$	cost function of delay τ used in NL-GMF algorithm
$Toep(\mathbf{u})$	a Toeplitz matrix whose first column is vector $\mathbf{u}$
$\mathbf{u}$	an intermediate variable used in ANM algorithm
t	an intermediate variable used in ANM algorithm
τ_{rms-ds}	root mean square delay spread
P_{est}	estimation probability
$P_{est-suc}$	successful estimation probability

Bibliography

[1] W. Kluge and D. Eggert, "Ranging with ieee 802.15.4narrow-band phy," 2010.

[2] A. Basiri, E. S. Lohan, T. Moore, and et al, "Indoor location based services challenges, requirements and usability of current solutions," *Computer Science Review*, vol. 24, pp. 1–12, 2017.

[3] Bluetooth low energy. https://www.bluetooth.com/what-is-bluetooth-technology/how-it-works/low-energy. Accessed Septermber 14, 2018.

[4] Zigbee alliance. http://www.zigbee.org/. Accessed Septermber 14, 2018.

[5] R. Mautz, "Overview of current indoor positioning systems," *Geodezija ir kartografija*, vol. 35, no. 1, pp. 18–22, 2009.

[6] A. Goldsmith, *Wireless communications*. Cambridge university press, 2005.

[7] Y. Wang, X. Ma, and G. Leus, "Robust time-based localization for asynchronous networks," *IEEE Transactions on Signal Processing*, vol. 59, no. 9, pp. 4397–4410, 2011.

[8] Z. Sahinoglu, S. Gezici, and I. Guvenc, "Ultra-wideband positioning systems," *Cambridge, New York*, 2008.

[9] C. Zhang, M. J. Kuhn, B. C. Merkl, A. E. Fathy, and M. R. Mahfouz, "Real-time noncoherent uwb positioning radar with millimeter range accuracy: Theory and experiment," *IEEE Transactions on Microwave Theory and Techniques*, vol. 58, no. 1, pp. 9–20, 2010.

[10] S. Marano, W. M. Gifford, H. Wymeersch, and M. Z. Win, "Nlos identification and mitigation for localization based on uwb experimental data," *IEEE Journal on Selected Areas in Communications*, vol. 28, no. 7, 2010.

[11] C. Rohrig and M. Muller, "Localization of sensor nodes in a wireless sensor network using the nanoloc trx transceiver," in *Vehicular Technology Conference, 2009. VTC Spring 2009. IEEE 69th.* IEEE, 2009, pp. 1–5.

[12] K. Benkic, M. Malajner, P. Planinsic, and Z. Cucej, "Using rssi value for distance estimation in wireless sensor networks based on zigbee," in *Systems, signals and image processing, 2008. IWSSIP 2008. 15th international conference on.* IEEE, 2008, pp. 303–306.

[13] A. Faheem, R. Virrankoski, and M. Elmusrati, "Improving rssi based distance estimation for 802.15. 4 wireless sensor networks," in *Wireless Information Technology and Systems (ICWITS), 2010 IEEE International Conference on.* IEEE, 2010, pp. 1–4.

[14] H. Liu, H. Darabi, P. Banerjee, and J. Liu, "Survey of wireless indoor positioning techniques and systems," *IEEE Transactions on Systems, Man, and Cybernetics, Part C (Applications and Reviews)*, vol. 37, no. 6, pp. 1067–1080, 2007.

[15] M. Pelka, C. Bollmeyer, and H. Hellbrück, "Accurate radio distance estimation by phase measurements with multiple frequencies," in *Indoor Positioning and Indoor Navigation (IPIN), 2014 International Conference on*. IEEE, 2014, pp. 142–151.

[16] S. M. Kay, "Fundamentals of statistical signal processing, volume i: Estimation theory," *PTR Prentice-Hall, Englewood Cliffs*, 1993.

[17] E. J. Candès and M. B. Wakin, "An introduction to compressive sampling," *IEEE signal processing magazine*, vol. 25, no. 2, pp. 21–30, 2008.

[18] E. J. Candes and T. Tao, "Decoding by linear programming," *IEEE transactions on information theory*, vol. 51, no. 12, pp. 4203–4215, 2005.

[19] G. Tang, B. N. Bhaskar, P. Shah, and B. Recht, "Compressed sensing off the grid," *IEEE transactions on information theory*, vol. 59, no. 11, pp. 7465–7490, 2013.

[20] H. Zhu, G. Leus, and G. B. Giannakis, "Sparsity-cognizant total least-squares for perturbed compressive sampling," *IEEE Transactions on Signal Processing*, vol. 59, no. 5, pp. 2002–2016, 2011.

[21] C. Ekanadham, D. Tranchina, and E. P. Simoncelli, "Recovery of sparse translation-invariant signals with continuous basis pursuit," *IEEE transactions on signal processing*, vol. 59, no. 10, pp. 4735–4744, 2011.

[22] Z. Tan, P. Yang, and A. Nehorai, "Joint sparse recovery method for compressed sensing with structured dictionary mismatches," *IEEE Transactions on Signal Processing*, vol. 62, no. 19, pp. 4997–5008, 2014.

[23] A. Panahi and M. Viberg, "Gridless compressive sensing," in *Acoustics, Speech and Signal Processing (ICASSP), 2014 IEEE International Conference on*. IEEE, 2014, pp. 3385–3389.

[24] R. Schmidt, "Multiple emitter location and signal parameter estimation," *IEEE transactions on antennas and propagation*, vol. 34, no. 3, pp. 276–280, 1986.

[25] W. Liao and A. Fannjiang, "Music for single-snapshot spectral estimation: Stability and super-resolution," *Applied and Computational Harmonic Analysis*, vol. 40, no. 1, pp. 33–67, 2016.

[26] J. Han, J. Pei, and M. Kamber, *Data mining: concepts and techniques*. Elsevier, 2011.

[27] N. Levanon and E. Mozeson, *Radar signals*. John Wiley & Sons, 2004.

[28] H. Cramér, *Mathematical methods of statistics (PMS-9)*. Princeton university press, 2016, vol. 9.

[29] C. R. Rao, "Information and the accuracy attainable in the estimation of statistical parameters," in *Breakthroughs in statistics*. Springer, 1992, pp. 235–247.

[30] D. Rife and R. Boorstyn, "Single tone parameter estimation from discrete-time observations," *IEEE Transactions on information theory*, vol. 20, no. 5, pp. 591–598, 1974.

[31] P. Stoica and A. Nehorai, "Music, maximum likelihood, and cramer-rao bound," *IEEE Transactions on Acoustics, Speech, and Signal Processing*, vol. 37, no. 5, pp. 720–741, 1989.

[32] P. Stoica, E. G. Larsson, and A. B. Gershman, "The stochastic crb for array processing: A textbook derivation," *IEEE Signal Processing Letters*, vol. 8, no. 5, pp. 148–150, 2001.

[33] E. Tohidi, M. Coutino, S. P. Chepuri, H. Behroozi, M. M. Nayebi, and G. Leus, "Sparse antenna and pulse placement for colocated mimo radar," *arXiv preprint arXiv:1805.10641*, 2018.

[34] P. Pagani, F. T. Talom, P. Pajusco, and B. Uguen, *Ultra-wideband radio propagation channels: a practical approach*. John Wiley and Sons, 2013.

[35] L. Welch, "Lower bounds on the maximum cross correlation of signals (corresp.)," *IEEE Transactions on Information theory*, vol. 20, no. 3, pp. 397–399, 1974.

[36] P. Xia, S. Zhou, and G. B. Giannakis, "Achieving the welch bound with difference sets," *IEEE Transactions on Information Theory*, vol. 51, no. 5, pp. 1900–1907, 2005.

[37] S. S. Chen, D. L. Donoho, and M. A. Saunders, "Atomic decomposition by basis pursuit," *SIAM review*, vol. 43, no. 1, pp. 129–159, 2001.